

**CONFLICT DETECTION AND RESOLUTION  
FOR FUTURE  
AIR TRANSPORTATION MANAGEMENT**

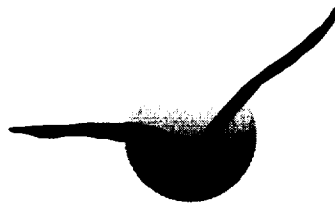
Jimmy Krozel, Ph.D., Mark. E. Peters, and  
George Hunter

Prepared for:

NASA Ames Research Center  
Moffett Field, CA 94035

Under Contract: NAS2-14285

April, 1997



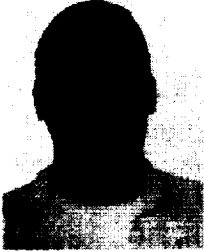
**SEAGULL TECHNOLOGY, INC.**  
16400 Lark Ave., Suite 100  
Los Gatos, CA 95032



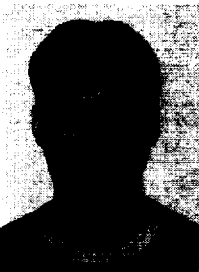
## ACKNOWLEDGMENTS

This research was funded by NASA Ames Research Center under contract NAS2-14285 for the AATT Advanced Air Transportation Technologies program; the authors appreciate the program support of Mr. Vern Battiste, Mr. Bill Kramer, and Dr. Dallas Denery at NASA. The authors acknowledge the various technical contributions and review from Ms. Susan Dorsky, Dr. Frank McLoughlin, Mr. Tysen Mueller, and Dr. John Sorensen at Seagull Technology, Inc. throughout this research. The authors enjoyed the collaborative efforts of Dr. Ron Azuma and Mr. Mike Daily at the Hughes Research Laboratories and thank them for their assistance in providing several three-dimensional visualization images for this report. Also, the permission of Dr. Ran Gazit of Stanford University is appreciated for allowing us to use results from his Ph.D. thesis. We also appreciate Dr. Gazit's research contributions to the stochastic analysis results in this report. Finally, we thank Prof. J. David Powell at Stanford University and Dr. Heinz Erzberger at the NASA Ames Research Center for their occasional discussions related to the approach taken in this research.

## ABOUT THE AUTHORS



**Jimmy Krozel, Senior Engineer** (Ph.D., Aeronautical and Astronautical Engineering, Purdue University, 1992). Since joining Seagull Technology in Aug., 1995, Dr. Krozel has worked on aircraft conflict detection and resolution for Free Flight and aircraft terminal area routing around heavy weather. His research interests are in the areas of air traffic control, Free Flight, route planning, terrain reasoning, autonomous vehicles, and intelligent path prediction. Dr. Krozel performed his M.S. thesis research under a fellowship at the NASA Ames Research Center, and performed his Ph.D. thesis as a Hughes Doctoral Fellow at the Hughes Research Laboratory. Dr. Krozel is a member of the American Institute of Aeronautics and Astronautics, American Association for Artificial Intelligence, Tau Beta Pi, Sigma Xi, and Sigma Gamma Rho. Dr. Krozel has a total of 17 technical publications.



**Mark E. Peters, Project Engineer** (M.S., Aeronautical and Astronautical Engineering, Purdue University, 1996) Mr. Peters joined Seagull Technology in June, 1996. He has interests in conflict detection and resolution for Free Flight, unmanned aerial vehicles, aircraft design, aircraft stability and control, and flight mechanics. Mr. Peters has designed and built 5 aircraft, and has co-authored 3 technical papers. Mr. Peters is a member of the American Institute of Aeronautics and Astronautics, the Experimental Aircraft Association, the Aircraft Owners and Pilots Association, and the Academy of Model Aeronautics.



**George Hunter, Program Manager** (M.S., Aerospace Engineering, University of Michigan, 1982) George Hunter joined Seagull Technology in May, 1990. Mr. Hunter has 15 years of experience involving (a) air traffic control system performance and automation, (b) optimal estimation and control system engineering, (c) aerospace vehicle performance and simulation, and (d) radar tracking and telemetry data. Mr. Hunter manages a variety of transportation-related projects underway at Seagull Technology.

# TABLE OF CONTENTS

<b>ABSTRACT .....</b>	<b>vii</b>
<b>1. INTRODUCTION .....</b>	<b>1</b>
1.1 Free Flight.....	1
1.2 A Review of Conflict Detection and Resolution Literature .....	2
1.3 Contributions and Report Organization .....	5
<b>2. SYSTEM ANALYSIS .....</b>	<b>7</b>
2.1 System Architecture.....	7
2.2 A Tactical/Strategic Decomposition.....	8
2.3 Cooperative and Non-Cooperative Cases.....	9
2.4 Horizontal, Vertical, Speed, and Combined Control.....	9
2.5 Equations of Relative Motion .....	10
<b>3. CONFLICT DETECTION.....</b>	<b>13</b>
3.1 Separation Requirements .....	13
3.2 Conflict Detection Criteria for Tactical Scenarios.....	15
3.3 Conflict Detection Criteria for Strategic Scenarios.....	21
3.4 Two-Dimensional Horizontal Deterministic Conflict Analysis.....	22
3.5 Two-Dimensional Horizontal Non-Deterministic Conflict Analysis.....	26
3.6 Three-Dimensional Deterministic Conflict Analysis.....	34
3.7 Applying Conflict Detection to Intent Data .....	39
3.8 Proximity Management for Multiple Aircraft.....	40
<b>4. TACTICAL CONFLICT RESOLUTION.....</b>	<b>45</b>
4.1 Tactical Heading Control Maneuvers .....	45
4.2 Tactical Speed Control Maneuvers .....	55
4.3 Tactical Altitude Control Maneuvers .....	63
4.4 Tactical Alert Zone Visualization.....	74
4.5 Multi-Aircraft Tactical Encounters.....	76

(continued)

<b>5. STRATEGIC CONFLICT RESOLUTION.....</b>	<b>83</b>
5.1 Strategic Heading Control Maneuvers .....	84
5.2 Strategic Speed Control Maneuvers .....	97
5.3 Strategic Altitude Control Maneuvers .....	98
5.4 Economics Analysis.....	98
5.5 Benefits of Reduced Separations Standards.....	110
5.6 Combined Tactical and Strategic Maneuver Charts.....	112
<b>6. SYSTEM MECHANIZATION ISSUES .....</b>	<b>113</b>
6.1 Mechanization Elements .....	113
6.2 System Sources of Errors and Uncertainties .....	116
6.3 Mechanization of Conflict Detection Logic .....	120
6.4 Coordination and Communications Requirements.....	122
6.5 Displays and Human Factors.....	124
6.6 Real-Time Testing .....	126
<b>7. SUMMARY, CONCLUSIONS, AND RECOMMENDATIONS .....</b>	<b>129</b>
7.1 Summary and Conclusions .....	129
7.2 Recommendations .....	131
<b>8. REFERENCES .....</b>	<b>135</b>

## ABSTRACT

With a Free Flight policy, the emphasis for air traffic control is shifting from active control to passive air traffic management with a policy of intervention by exception. Aircraft will be allowed to fly user preferred routes, as long as safety Alert Zones are not violated. If there is a potential conflict, two (or more) aircraft must be able to arrive at a solution for conflict resolution without controller intervention. Thus, decision aid tools are needed in Free Flight to detect and resolve conflicts, and several problems must be solved to develop such tools. In this report, we analyze and solve problems of proximity management, conflict detection, and conflict resolution under a Free Flight policy.

For proximity management, we establish a system based on Delaunay Triangulations of aircraft at constant flight levels. Such a system provides a means for analyzing the neighbor relationships between aircraft and the nearby free space around air traffic which can be utilized later in conflict resolution.

For conflict detection, we perform both 2-dimensional and 3-dimensional analyses based on the penetration of the Protected Airspace Zone. Both deterministic and non-deterministic analyses are performed. We investigate several types of conflict warnings including tactical warnings prior to penetrating the Protected Airspace Zone, methods based on the reachability overlap of both aircraft, and conflict probability maps to establish strategic Alert Zones around aircraft.

Conflict resolution maneuvers are investigated in the horizontal plane with heading or speed control, and in the vertical plane with altitude control. Conflict resolution maneuvers are studied for tactical close-range as well as strategic far-range cases. The tactical analysis maximizes safety. The tactical conflict resolution strategy is the result of an optimization problem: Determine the control as a function of the relative motion state such that the range at closest approach is maximized. The solution is arrived at by applying Euler-Lagrange equations for optimal control, and are best illustrated using maneuver charts. These maneuver charts concisely illustrate the tactical conflict avoidance “rules-of-the-road” indicating the turn directions, acceleration signs, or climb/descent rates that each aircraft should select for any arbitrary initial relative state. The strategic analysis optimizes economics while maintaining safety as the constraint. The strategic conflict resolution strategy analyzes the geometry of heading, speed, and altitude maneuvers and estimates the direct operating cost for these maneuvers. In general, altitude maneuvers are the most economical, followed by heading maneuvers, and finally speed change maneuvers. For non-cooperative heading maneuvers where only one aircraft maneuvers, it is generally more economical to turn the aircraft to the backside of the non-cooperating aircraft. For cooperative cases where both aircraft maneuver, it is generally better to let the faster aircraft bear more of the burden. The cost and range required for speed control maneuvers make this an ineffective means of conflict resolution.

Finally, the mechanization of a conflict detection and resolution system is analyzed. System sources of error and uncertainties are identified, including measurement and trajectory prediction uncertainties, actuation uncertainties, flight technical errors, and wind uncertainty. Performance metrics are also identified for the purpose of evaluating the safety, reliability, and efficiency of the system.

## LIST OF ACRONYMS

ADS .....	Automatic Dependent Surveillance
ADS-B .....	Automatic Dependent Surveillance - Broadcast
AERA .....	Automated En Route ATC system
AOC .....	Airline Operations Center
ATC .....	Air Traffic Control
ATM .....	Air Traffic Management
CRA .....	Conflict Resolution Advisory
CTAS .....	Center-TRACON Automation System
DA .....	Descent Advisor
DOC .....	Direct Operating Cost
FAA .....	Federal Aviation Administration
FAST .....	Final Approach Spacing Tool
FL .....	Flight Level
FMS .....	Flight Management System
FTE .....	Flight Technical Error
GPS .....	Global Positioning System
INS .....	Inertial Navigation System
LAAS .....	Local Area Augmentation System
NAS .....	National Airspace System
NASA .....	National Aeronautics and Space Administration
nmi .....	nautical mile
NRP .....	National Routing Program
ODAPS .....	Oceanic Display and Planning System
PAZ .....	Protected Airspace Zone
PCA .....	Point of Closest Approach
PVD .....	Plan View Display
RNP .....	Required Navigation Performance
RTCA .....	Radio Technical Commission for Aeronautics
SA .....	Selective Availability (for GPS)
SSR .....	Secondary Surveillance Radar
SUA .....	Special Use Airspace
TAZ .....	Tactical Alert Zone
TCAS .....	Traffic alert and Collision Avoidance System
TMA .....	Traffic Management Advisor
TRACON .....	Terminal Radar Approach CONTROL
URET .....	User Request Evaluation Tool
WAAS .....	Wide Area Augmentation System

# 1. INTRODUCTION

Aircraft conflict detection and resolution has a long history of investigation, but with emerging Free Flight policies, new technologies, and an increased emphasis on economic and market factors, conflict detection and resolution needs to be re-examined. New Free Flight policies include the removal of many constraints, such as airways, the reduction in required separations, and an emphasis on flight crews resolving conflicts without the assistance of air traffic controllers. New communications (*e.g.*, datalink), navigation (*e.g.*, GPS), and surveillance (*e.g.*, ADS, TCAS IV) technologies are becoming available. In the future, technological advancements will continue to shape tactical close range conflict avoidance, but strategic far range conflict avoidance will be reshaped by new procedures and flight operations economics as well as new technology. Additionally, increasing traffic levels challenge the air transportation system at all levels, including safety and capacity. Considering all these factors, the underlying guiding principle for today's conflict detection and resolution is improved flight economics, with the maintenance of today's level of safety as a constraint.

## 1.1 Free Flight

The FAA is shifting from the current air traffic control (ATC) system to an air traffic management (ATM) system with a policy referred to as *Free Flight* [A95, FF95, RTCA94]. In en route airspace, the emphasis will be shifted from active to passive ATM with an ATM policy of intervention by exception. Outside of congested airspace, an aircraft will be allowed to fly autonomously as long as no other traffic crosses an Alert Zone around the aircraft, as shown in Figure 1. If the Alert Zone is violated, either 1) an air traffic controller will intervene to assist in conflict avoidance, or 2) the flight crews will resolve the conflict autonomously while being monitored by the ATM system. The size and

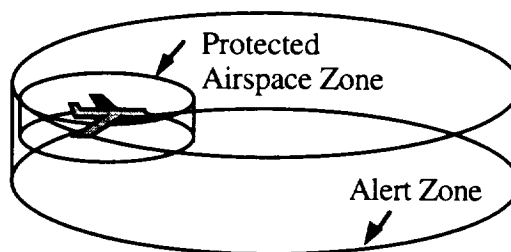


Figure 1. Free Flight zones around aircraft.

shape of the Alert Zone has yet to be determined. To ensure safety, no aircraft should penetrate another aircraft's Protected Airspace Zone. In Free Flight, expected aircraft trajectories will be optimal cost flights with adjustments to maintain reasonable time of arrivals consistent with operating schedules. These flights can be fuel efficient cruise-climb best wind route trajectories, rather than following the airways as constrained by current ATM/ATC.

Free Flight will enable greater traffic volume and complexity by distributing some of the functionality, including conflict detection and resolution, to airborne systems (including pilots). If there is a potential conflict, two (or more) aircraft must be able to arrive at a solution for conflict resolution with mutual gain (or mutual minimum loss) and without the need to contact an en route controller. Thus, decision aiding tools are needed in Free Flight to detect and resolve conflicts.

## **1.2 A Review of Conflict Detection and Resolution Literature**

Early collision avoidance investigators such as [Mo58, HM70, SM73] examined maneuvers analytically and developed conflict detection criteria. Most work involved encounters where only one aircraft maneuvers. A noteworthy early contribution was Morrel's [Mo58] predicted time-to-collision criteria,  $\tau$ , computed as range divided by range rate. Much of the past work dealt with the problem of incomplete tracking data which is rapidly becoming a non-issue. Nonetheless, this work should not be dismissed. Complex issues such as maneuver selection, false alarms resulting from measurement error, the definition of hazard regions, and the definition of "rules-of-the-road" were all addressed.

Today, traffic is strategically ordered to avoid conflicts. Such ordering is achieved via approach and departure routes, jet routes, the hemispherical altitude rule, step climbs, and so on. In Free Flight, much of this routing structure will become obsolete, but the need for conflict avoidance at the tactical and strategic levels will not; it will simply take on a new form.

Conflicts are currently automatically detected by ATC using a Conflict Alert on the Plan View Display (PVD) and with an Oceanic Display and Planning System (ODAPS) Conflict Probe. For the Conflict Alert [No94], lateral and vertical separation filters identify conflict conditions which alert the air traffic controller by blinking the conflicting pair of aircraft symbols and sounding an audible alert. ODAPS has a conflict probe that assists oceanic controllers by providing advance notification of conflicts detected from flight plan information [No94, FAA93]. The conflict probe first identifies candidate pairwise aircraft

conflicts using a coarse filter for proximity and time overlap. A fine filter is then applied for detailed calculations with respect to a given pair of aircraft. The fine filter outputs “conflict in” and “conflict out” data that identify the time and location where the conflict starts and ends, and the type of conflict, including trespassing over reserved airspace, head-on conflict, intersection conflict, overtaking conflict, or a bad data warning. No conflict resolution advisories are computed by either of these automation processes; rather, it is the role of the air traffic controller to solve the conflict resolution problem.

The Conflict Resolution Advisory (CRA) was designed to provide radar controllers with conflict resolution alternatives in a textual message format [HGT83, CBB92]. Resolutions were limited to vectoring left or right at a specified angle, or descending/climbing/holding for a specified altitude change. For complex scenarios, the CRA would not give an advisory. When evaluated by controllers [CBB92], most controllers used the CRA as a second-hand verification that they were making good conflict resolutions. Because the CRA could not be trusted for a solution for all cases, some controllers chose not to use the CRA. This experience demonstrates the need for complete solutions for conflict resolution, and ones with air traffic controller acceptance.

Close-proximity midair conflicts are currently detected by the Traffic alert and Collision Avoidance System (TCAS), an airborne based transponder/receiver system [F86, Ha89, WiS89, BAW94]. TCAS I simply alerts the pilot of an intruder aircraft. TCAS II is the current commercial transport version for TCAS; it provides resolution advisories for vertical avoidance maneuvers only. However, the fundamental  $\tau$  criterion defining the protected airspace zone for the current TCAS II is shown in Chapter 2 to be insufficient for the expected separation requirements for Free Flight. TCAS III incorporates horizontal maneuvers by exploiting bearing rate measurements, however, TCAS III was canceled by the FAA due to poor antenna performance results. Finally, TCAS IV, which is still being developed, exploits the precision of GPS and aircraft state information exchange via datalink. TCAS IV allows for the use of horizontal and vertical maneuvers. TCAS IV proceeds in the direction of Free Flight, and in the terms of this report, addresses the topic of tactical collision avoidance.

It is important to look at the current and future NASA and FAA research efforts in order to understand how any future Free Flight system might integrate into the National Airspace System (NAS). The trend with NASA and the FAA is to increase the degree of automation in ATM/ATC and to decrease the constraints imposed. As a step towards Free Flight, the FAA has established the National Route Program (NRP) [A95]. This program

currently involves over 100 city pairs, and includes a gradual adaptation of Free Flight concepts phased in at or above flight level FL390 and gradually including lower flight levels.

A Free Flight system may connect with future ATM by some extension of the Automated En Route ATC system (AERA) and Center-TRACON Automation System (CTAS). Higher capacities enabled by a Free Flight system may increase the density of traffic converging to arrival airports, and this will require such automated en route and TRACON systems [RTCA94].

The AERA project, developed by the MITRE Corporation, has progressed in stages [Ni89]. First, AERA 1 investigated conflict detection based on flight plans for pairs of aircraft with ultimate separation of aircraft remaining with the controller. Next, AERA 2 suggested resolution maneuvers generated through automation, but held the controller responsible for separation decisions. Finally, AERA 3 investigated fully automated algorithmic conflict detection and resolution. Multiple aircraft conflicts are handled by considering pairwise conflict resolutions. The controller performs planning functions but only participates in separation decisions in anomalous situations. While AERA was designed for today's ATC system, it may also provide some useful algorithmic background for Free Flight. As a result of the AERA project, the MITRE Corporation is currently developing the User Request Evaluation Tool (URET). URET is designed to be a monitoring tool that allows air traffic controllers to investigate potential conflicts that may occur with pilot requests for flight plan changes [SW95]. While this technology provides the air traffic controller a tool to investigate conflicts, it does not assist in suggesting conflict resolution strategies.

CTAS is an automation system for the management and control of arrival traffic developed by NASA and the FAA [DEG91, Er92, Er95]. CTAS is composed of a Traffic Management Advisor (TMA) that maintains sequencing and scheduling, a Descent Advisor (DA) that provides cruise speed and descent clearances, and a Final Approach Spacing Tool (FAST) that assists the TRACON controllers in spacing arrival aircraft on final approach. Extensive evaluations of CTAS have demonstrated controller acceptance, delay reductions, and fuel savings [BE96].

Other innovative approaches to conflict detection and resolution include knowledge-based system approaches [Da92, Cr83], self-organizing potential field approaches [Eb94], and agent-based negotiation or principled negotiation [Ste94, WaS94, WaS96]. For

further review of today's aircraft/airspace system and ATM/ATC, see [AIM95, No94, PM89, WaS95].

### 1.3 Contributions and Report Organization

The objective of this research effort is to examine the topic of conflict detection and resolution for Free Flight. Our contributions to this field include the following:

- Conflict detection schemes for 2-dimensional and 3-dimensional analysis, including deterministic and non-deterministic analysis,
- Optimal maneuver charts for heading, speed, and altitude maneuvers that maximize safety for tactical short range encounters,
- Short range tactical and far range strategic Alert Zone definitions to inform ATC or pilots of conflicts,
- Minimum cost heading, speed, and altitude control maneuvers for far range strategic encounters,
- Efficient proximity management of aircraft based on Delaunay Triangulations, and
- Examination of the implementation issues for a Free Flight conflict detection and resolution system.

The remainder of this report is organized as follows. Chapter 2 outlines the system analysis approach, including a tactical/strategic decomposition scheme, cooperative and non-cooperative scenarios, and cases for heading, speed, and altitude modes of control maneuvers. Chapter 3 presents the derivation of the equations for conflict detection criteria, both in two and three dimensions. Chapter 4 presents tactical conflict resolution strategies, and Chapter 5 presents strategic conflict resolution strategies. The treatment of measurement and trajectory actuation errors and implementation issues are discussed in Chapter 6; and conclusions and recommendations are stated in Chapter 7. References cited throughout this report are listed at the end.



## 2. SYSTEM ANALYSIS

In this chapter, an analysis of a conflict detection and resolution system is presented. This work includes the description of a candidate system architecture, a tactical/strategic problem decomposition, considerations of cooperative and non-cooperative cases, and a breakdown of different modes of control. Finally, the equations of relative motion for a two aircraft system are presented.

### 2.1 System Architecture

A candidate system architecture is proposed that is appropriate for Free Flight and recent technologies. This candidate system architecture is shown in Figure 2, and is composed of a proximity management system, a conflict detection system, a conflict resolution system, and a display management system. The proximity management system maintains aircraft identification and state information for a given sector of airspace. The conflict detection system identifies conflicts based on proximity data and computational analysis. The conflict resolution system uses both the proximity management system and conflict detection system to initialize conflict resolution, and analyzes the situation for a computed solution. The display management system communicates traffic information, conflicts, and conflict resolution advisories to the pilot and/or air traffic controller.

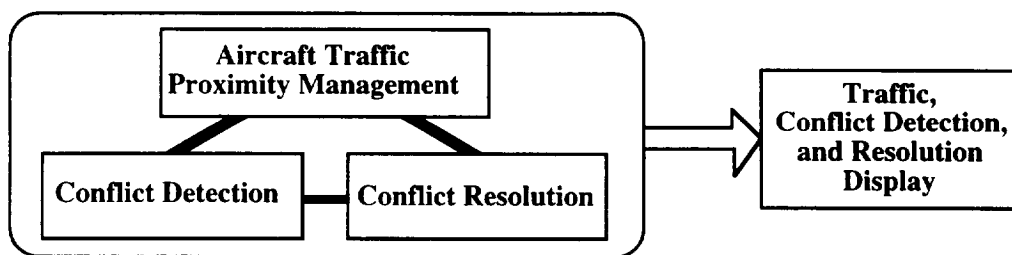


Figure 2. A top level description for a candidate conflict detection and resolution system.

The system architecture is not constrained to either an all-airborne system, mixed-airborne and ground-based system, or a ground-based system. We do not include any of these application specific considerations in our theoretical analysis until Chapter 6, which discusses implementation issues. However, in general, if the system is an all-airborne system, proximity management information will most likely be passed from aircraft to aircraft in an Automatic Dependent Surveillance - Broadcast (ADS-B) type datalink system.

With no ground-based component to compensate for unequipped aircraft, all aircraft would be required to possess datalink and Global Positioning System (GPS) capabilities to form the basis for aircraft proximity information. Conflict detection and resolution algorithms would be retained in flight management system (FMS) computers, and the display would be a pilot cockpit display.

If the system is a mixed or ground-based system, any or all of these components can be located on the ground. Ground-based radar could compensate for unequipped aircraft without datalink and GPS capabilities. Furthermore, ground-based systems could provide a proximity management system that links all aircraft to ATC as well as to Airline Operations Centers (AOCs).

Conflict detection and resolution analysis can be performed either on the ground or in the air, and communicated to the appropriate aircraft through today's radio communications techniques or datalink communications. In a mixed system, displays would exist for the pilot as well as for ground-based ATC/ATM/AOC.

## **2.2 A Tactical/Strategic Decomposition**

In our research, conflict scenarios are divided into two categories: near-range conflicts which cannot be avoided without immediate action and long-range conflicts which can be smoothly resolved so that they never become near-range threats. We refer to these as tactical and strategic encounters, respectively; we refer to the maneuvers that resolve them as conflict resolution maneuvers. In our technical approach, we first investigate how tactical encounters should be resolved, and then consider strategic encounters. There is considerable overlap between these two areas, but there are also important differences.

One difference between the tactical and strategic cases is that additional conflicts with neighboring traffic are more likely in strategic maneuvers. This is because strategic maneuvers take more time and airspace to perform. While the two-aircraft scenario can be used to approximate strategic maneuvers, they cannot be fully analyzed without looking at expected traffic patterns. This requires that strategic maneuvers be tested in a simulation to determine their true cost, and that traffic congestion problems for strategic maneuvers be sufficiently addressed. Our technical approach calls for both analysis and simulation.

Another significant difference between the tactical and strategic cases is that measurement and trajectory uncertainties become more important in the strategic case. For tactical cases, both aircraft are more likely to be experiencing the same wind conditions,

and the time required to resolve conflicts is small, thus allowing trajectory uncertainties less time to build up. In comparison, the strategic scenario occurs at far range when both aircraft may be experiencing different wind conditions and the time for trajectory uncertainties to propagate is much larger.

### **2.3 Cooperative and Non-Cooperative Cases**

The intruder aircraft may cooperatively maneuver to assist in increasing the miss distance, may be non-cooperative and execute no maneuver, or may blunder and execute a maneuver that reduces the miss distance. We investigate both cooperative maneuver and non-cooperative cases, and assume that the Alert Zone size and shape will provide a sufficient safety factor to account for the blundering intruder aircraft. For the non-cooperative case, we assume that the intruder has a constant-velocity vector. For the initial analysis, we assume that wind conditions are the same for both aircraft. This assumption is more appropriate for tactical situations; thus, wind variations are only considered for the analysis of missed and false alarms for strategic situations.

### **2.4 Horizontal, Vertical, Speed, and Combined Control**

Three fundamental controls for maneuvers can be used (alone or in combination) to avoid a conflict: turn (horizontal maneuvers), accelerate/decelerate (speed control maneuvers), and climb/descend (vertical maneuvers). In general, turns result in the greatest miss distance in the long term. For example, an aircraft maneuvering laterally with an acceleration of  $0.5g$  can achieve a turn displacement of approximately 3200 feet in 20 seconds. An aircraft with a maximum climb rate of 2400 feet per minute (typical of commercial jet transports) can attain a vertical displacement of only 800 feet in the same time period.

Vertical maneuvers do provide more separation than a turn, however, for a very short time period after the maneuver is initiated. More importantly, because vertical separation minimums are significantly less (currently by a factor of 15 for en route flight) than horizontal minimums, vertical maneuvers fare better when the basis of comparison is not absolute separation, but separation relative to the appropriate Protected Airspace Zone minimum. This vertical maneuver advantage will likely be reduced because horizontal minimums have more potential reduction than the vertical minimums – aircraft horizontal locations will be known more precisely in the future.

Of course, separation resulting from both turns and vertical maneuvers depend on the maneuver rates (lateral acceleration and altitude rate, respectively). But in general, a

vertical maneuver provides greater separation initially, and then the turn catches up and provides greater separation in the long term. Speed control provides the least separation over a given time span of the three maneuver types. A summary of the types of controls and generic initiation times is given in Figure 3. This report includes a complete analysis of conflict resolution strategies by considering all three control options.

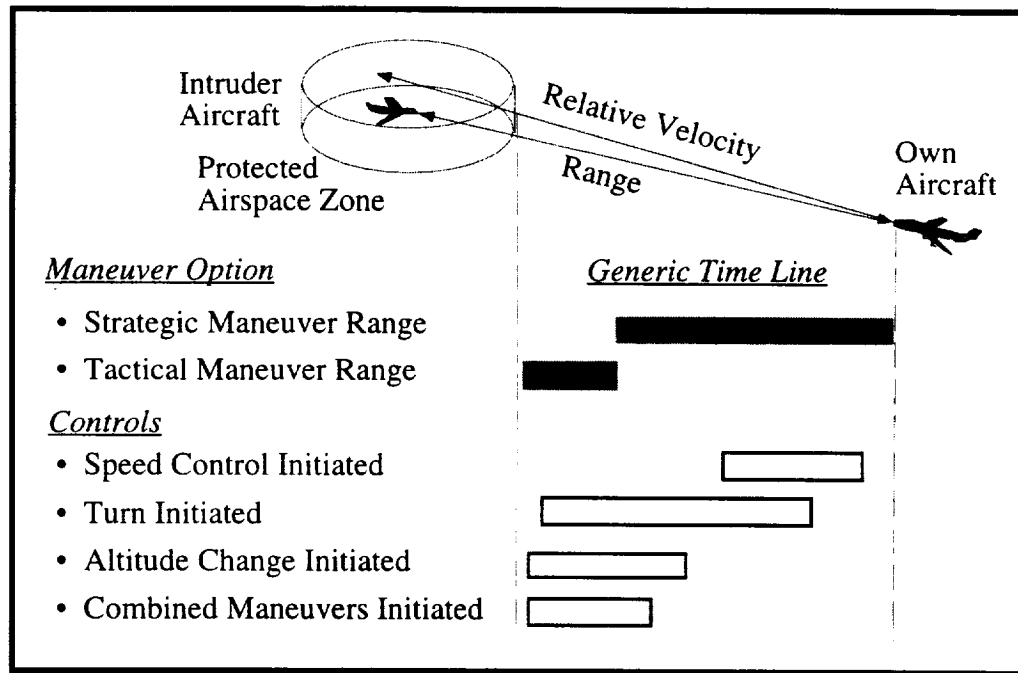


Figure 3. Comparison of effective initiation times for several modes of control.

## 2.5 Equations of Relative Motion

Relative to the own aircraft A, the equations of motion of the intruder aircraft B can be expressed in polar coordinates as [SM73]:

$$\text{Range Equation:} \quad \dot{r} = -v_A \cos \phi + v_B \cos(\theta - \phi) \quad (1)$$

$$\text{Bearing Equation:} \quad \dot{\phi} = -\omega_A + \frac{1}{r} [v_A \sin \phi + v_B \sin(\theta - \phi)] \quad (2)$$

$$\text{Relative Heading Equation:} \quad \dot{\theta} = \omega_B - \omega_A \quad (3)$$

$$\text{Relative Altitude Equation:} \quad \dot{z} = \delta v_B - \delta v_A \quad (4)$$

where, as shown in Figure 4,  $r$  is the range,  $v_A$  and  $v_B$  are the speeds of aircraft A and B relative to an inertially fixed reference,  $\theta$  is the heading of aircraft B relative to the heading of aircraft A,  $\phi$  is the angle-off from aircraft A to aircraft B,  $\omega_A$  and  $\omega_B$  are the turn rates of aircraft A and B, and  $\delta v_A$  and  $\delta v_B$  are the vertical speeds of aircraft A and B. Additionally,  $x$ ,  $y$ , and  $z$  locate the intruder aircraft B relative to the moving reference frame fixed in the own aircraft A, as shown in Figure 4. Throughout this report, the speed ratio parameter, defined as:

$$\gamma = v_B / v_A \quad (5)$$

is commonly used as a basis of comparing results.

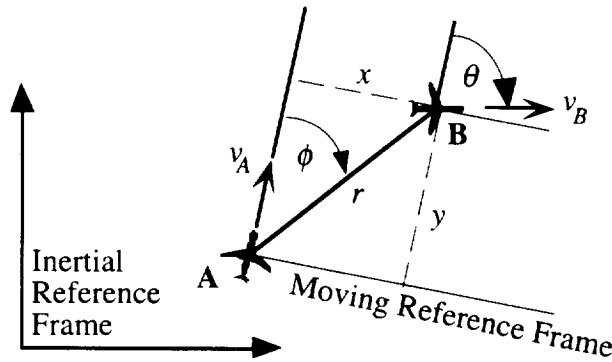


Figure 4. Relative geometry of two aircraft in a horizontal plane.



### 3. CONFLICT DETECTION

In this chapter, we discuss aircraft separation requirements, several candidate conflict detection criteria, and a method for aircraft proximity management.

#### 3.1 Separation Requirements

Today's separation standards are in part because of the accuracy of today's radar systems and displays. For domestic en route flight, current separation standards call for 5 nmi horizontal and 2000 ft vertical separation (1000 ft at or below FL290), as illustrated in Figure 5. Approach control standards are 3 nmi horizontal and 1000 ft vertical separation. Vertical separation standards today are influenced by the inherent errors in baro-altimeters. Domestic en route horizontal separations are set at 5 nmi because of worst case uncertainties of radar trackers where error grows with range from the tracker; this is reduced to 3 nmi inside the TRACON where range from the tracker is usually less than 50 nmi. In Free Flight, aircraft will be equipped with GPS navigation augmented by INS and WAAS or LAAS differential corrections. This will allow aircraft to operate at Required Navigation Performance (RNP) 5- $\sigma$  horizontal and vertical error limits of well below 1 nmi and 200 ft. This will also allow the implementation of Automatic Dependent Surveillance-Broadcast (ADS-B) where aircraft regularly report their position, velocity, and intent to other aircraft and to the ATM system. Thus, both navigation and surveillance errors that are

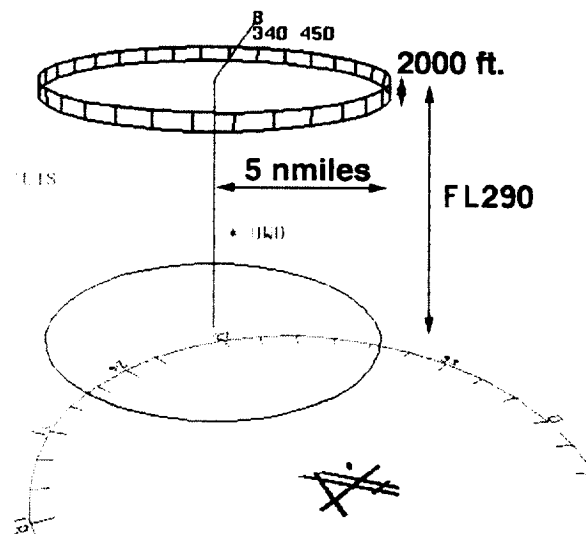


Figure 5. The current separation standards viewed as a Protected Airspace Zone for Free Flight (taken from [ADK96] with permission from the authors).

typical of today's flights will be greatly reduced leading to smaller separation constraints.

Today's separation standards are also established based on acceptable levels for the probability of unobserved close approach – a safety measure. As shown in Figure 6, today's Secondary Surveillance Radar (SSR) requires a 5 nmi horizontal separation to ensure a safe probability of no conflict between en route aircraft with crossing paths; the corresponding GPS-based system would require only 0.5 nmi separation for the same level of safety [Ga96]. The SSR used for today's terminal area requires a 3 nmi horizontal separation standard; the corresponding GPS-based system would require only 1 nmi separation for the same level of safety [Ga96]. With these reduced levels, the limiting factor is expected to be based on wake turbulence effects and flight technical errors more than on surveillance position uncertainty considerations. As GPS-based aircraft proliferate, separations standards will most likely be reduced in steps, perhaps from 5 nmi to 3 nmi to 1 nmi and then to 0.5 nmi. In [Ga96], it is shown that reduced separation standards can be implemented holding the current level of safety constant as long as the percentage of GPS-based aircraft increases accordingly. Finally, separation standards might also differ for aircraft that are radar-tracked versus aircraft that report GPS-based proximity information.

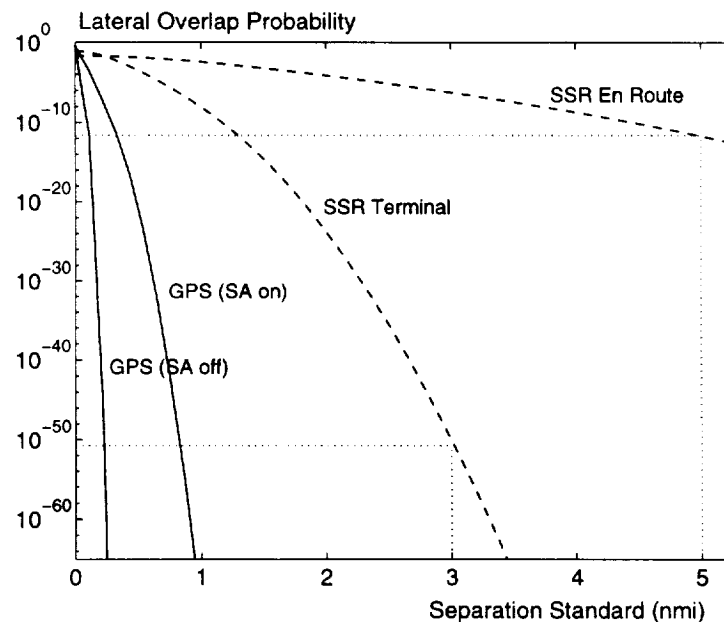


Figure 6. The probability of lateral overlap (unobserved close approach) as a function of horizontal separation standard; dotted lines represent today's separation standards for 5 nmi en route and 3 nmi terminal area (taken from [G96] with permission from the author).

### 3.2 Conflict Detection Criteria for Tactical Scenarios

Separation standards establish the size and shape of the Protected Airspace Zone and a conflict criterion for Free Flight. As shown in Figures 5 and 7, a constant horizontal and vertical separation standard establishes a cylindrical Protected Airspace Zone volume. To ensure safety, no aircraft should penetrate another aircraft's Protected Airspace Zone. Consider the situation when two aircraft traveling with constant speeds are oblivious of each other, and will engage in a crossing encounter. Figure 7 shows how the relative motion of the two aircraft can be analyzed by investigating the dynamics of the intruder aircraft B with respect to the own aircraft A. A conflict exists if an aircraft flies into the Protected Airspace Zone. A conflict detection mechanism should include an alert zone to warn of an impending conflict. The time-to-go for penetrating the Protected Airspace Zone volume, the time to closest approach, or other criteria may help define such an alert zone. Several candidate tactical conflict detection alert zones are next considered for Free Flight.

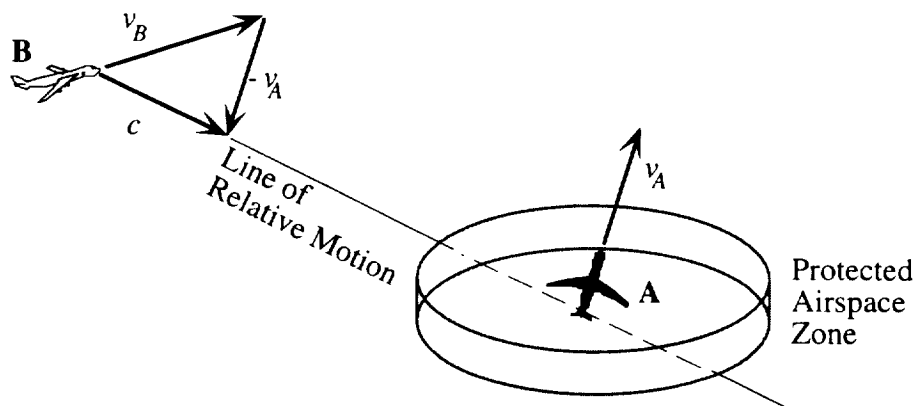


Figure 7. Conflict detection for Free Flight.

The first conflict detection criterion considered is based on a time-to-go alert zone around the Protected Airspace Zone. For comparison with other conflict detection criteria, Figure 8 illustrates the Protected Airspace Zone in the horizontal plane, and an alert zone. The alert zone identifies the location of the intruder 30 seconds or less from penetrating the Protected Airspace Zone of the own aircraft A. The alert zone is illustrated in a relative frame of reference with respect to the own aircraft A. By definition, this alert zone boundary resides outside the Protected Airspace Zone and is based on constant relative motion between the two aircraft. Thus, it makes a good candidate for a tactical conflict

detection mechanism for Free Flight, but has limitations for maneuvering or blundering aircraft – aircraft which happen to maneuver in a way that exacerbates the conflict. In the next section of this report, a two-dimensional analysis in the horizontal plane and a general three-dimensional analysis are performed for this conflict detection criterion.

Another alert zone can be based on the maneuver time required for conflict resolution. The time to the Protected Airspace Zone does not necessarily indicate if both aircraft can maneuver within the remaining time to avoid a conflict. In Chapter 4, we will determine a Tactical Alert Zone that indicates the last opportunity to start maneuvering to avoid a conflict. Since this is the last chance to maneuver, a conflict warning could be given  $T$  seconds prior to this last chance to maneuver. Figure 9 illustrates a 30 seconds or less alert zone warning before the last chance to maneuver. In general, this alert zone will be outside the 30 second warning for the Protected Airspace Zone. This conflict criterion makes a good candidate for a tactical conflict detection mechanism for Free Flight, assuming that both aircraft will cooperate in conflict resolution (neither aircraft will blunder).

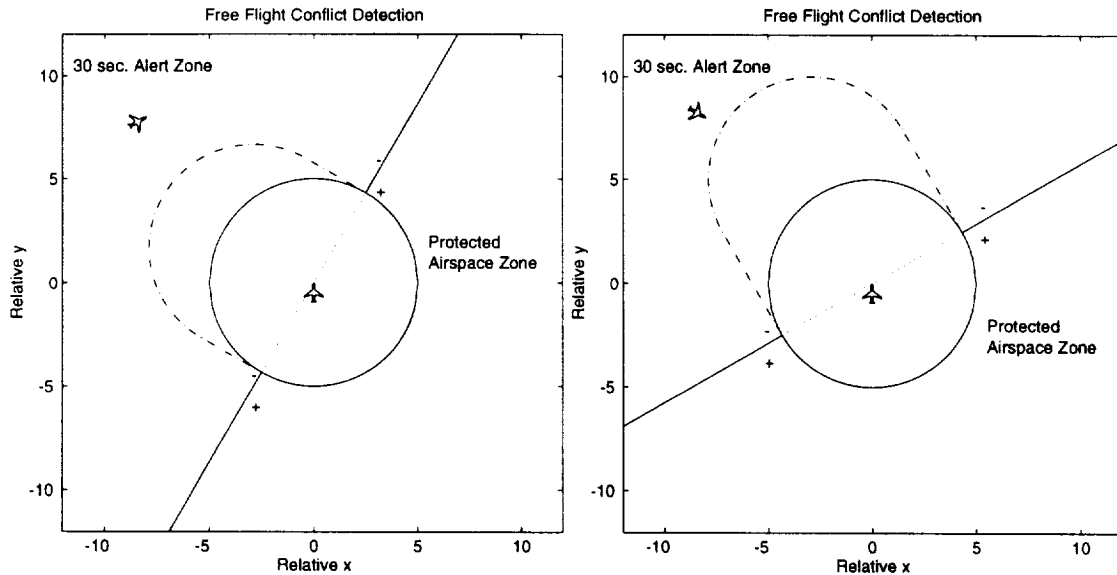


Figure 8. A horizontal Protected Airspace Zone conflict warning region for Free Flight. A  $\theta = 60^\circ$  heading difference (left) and a  $\theta = 120^\circ$  (right) heading difference is shown in a moving reference frame including the Protected Airspace Zone and zero range rate line (indicated by +/-).

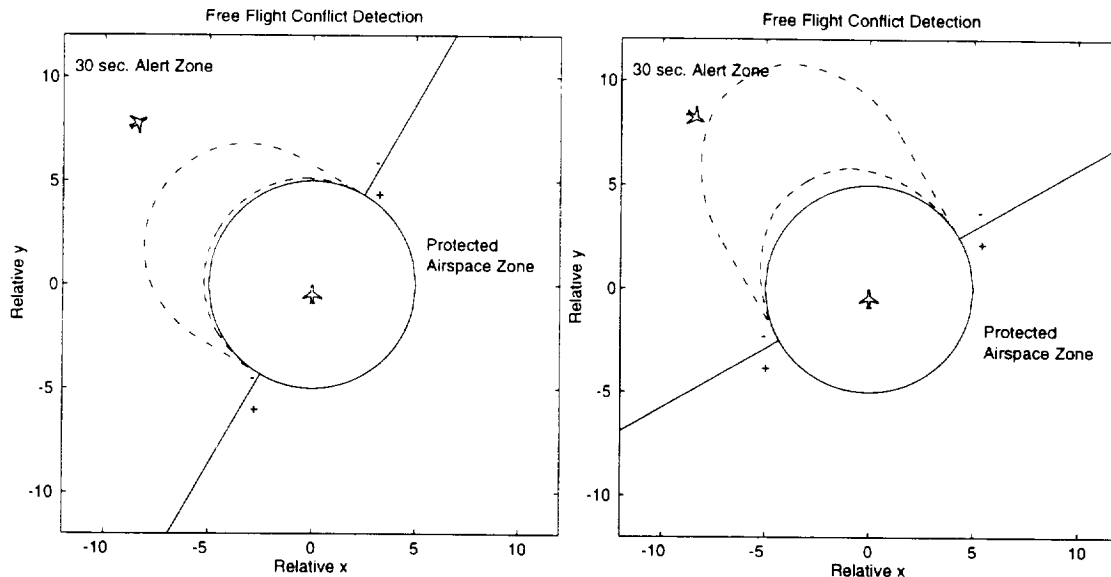


Figure 9. A horizontal Tactical Alert Zone conflict warning for Free Flight. The outer boundary identifies 30 seconds prior to the last chance to successfully maneuver around the Protected Airspace Zone – shown by the inner boundary. A  $\theta = 60^\circ$  heading difference (left) and a  $\theta = 120^\circ$  (right) heading difference is shown in a moving reference frame including the Protected Airspace Zone and zero range rate line (indicated by +/-).

For comparison, the TCAS II threat boundary is also examined. While the precise criterion for a conflict in TCAS II is multi-faceted (see [F86] for details), the basic “ $\tau$  criterion”, for which TCAS II logic is derived, can be readily depicted in the horizontal relative motion plane. Figure 10 illustrates the threat boundary for the  $\tau$  criterion based on a  $\tau = 30$  second warning. The  $\tau$  criterion, computed as range divided by range rate, does not incorporate bearing measurements nor does it incorporate the horizontal separation requirement. Notice that, depending on the relative motion, the TCAS II threat boundary may or may not reside outside the Protected Airspace Zone. Thus, it does not make a good criterion for tactical conflict detection for Free Flight.

Another alternative conflict detection criterion can be based on the time-to-go to the Point of Closest Approach (PCA). Figure 11 illustrates the alert zone boundary for a 30 seconds or less time-to-go to PCA criterion. Once again, notice that depending on the relative motion, the threat boundary may or may not reside outside the Protected Airspace Zone. This time-to-go criterion, like the  $\tau$  criterion, is a poor candidate for Free Flight because it does not directly incorporate the horizontal separation requirement.

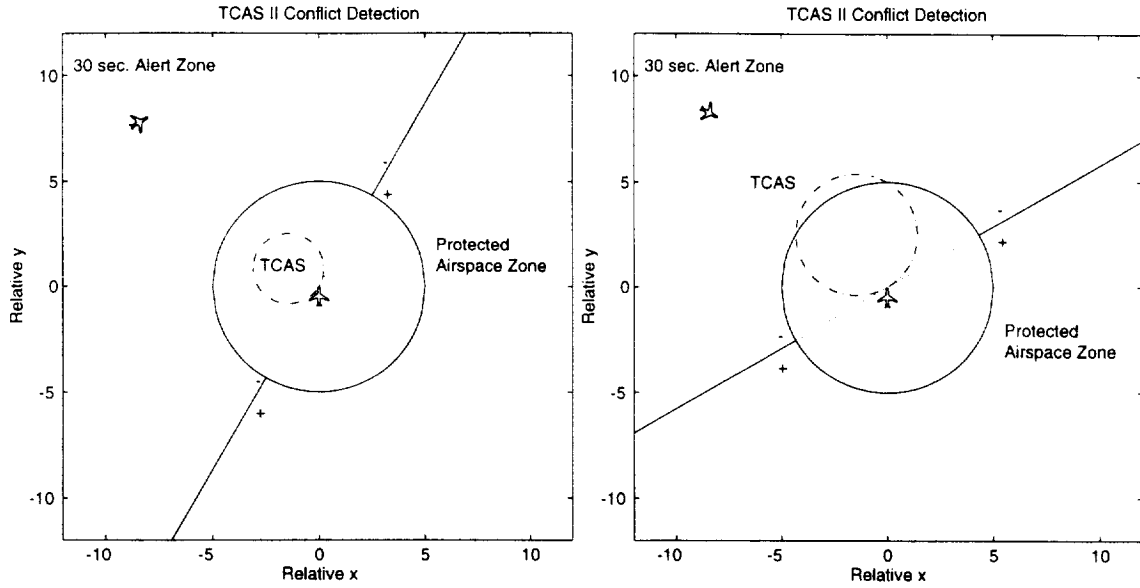


Figure 10. Horizontal conflict warning region for the  $\tau$  criterion in TCAS II. A  $\theta = 60^\circ$  heading difference (left) and a  $\theta = 120^\circ$  (right) heading difference is shown in a moving reference frame including the Protected Airspace Zone and zero range rate line (indicated by +/-).

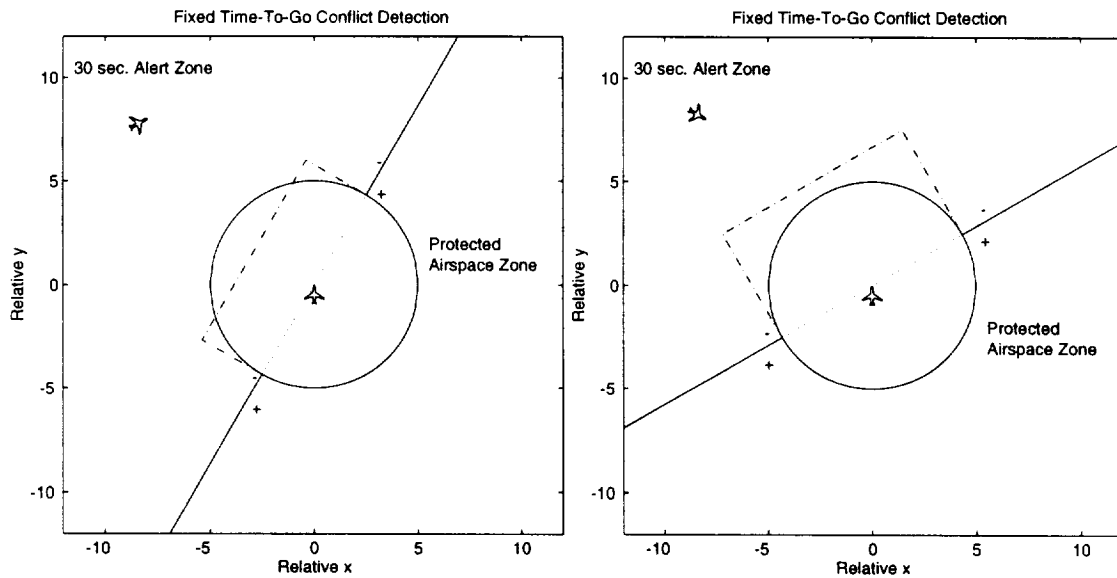


Figure 11. Horizontal conflict detection based on time-to-go to the point of closest approach. A  $\theta = 60^\circ$  heading difference (left) and a  $\theta = 120^\circ$  (right) heading difference is shown in a moving reference frame including the Protected Airspace Zone and zero range rate line (indicated by +/-).

A reachability criterion can also be used for tactical conflict detection. Several variations are possible. The first reachability criterion is based on checking the overlap between the locus of all possible points that each aircraft can be in the next  $T$  seconds, as shown in Figure 12. As shown later, this criterion is very conservative and has a high false alarm rate. Second, a reachability criterion which includes the Protected Airspace Zone (PAZ) is also a candidate conflict criterion. Consider the definition suggested by the RTCA Committee on Free Flight [RTCA94]:

“For a given look ahead time  $T$ , the Alert Zone is the locus of all possible Protected [Airspace] Zones of the aircraft at time  $T$ .”

If another aircraft crosses into this alert zone boundary, then a conflict occurs. This definition considers only the reachability of a single aircraft, and the intent of the aircraft is not considered. This definition may be slightly modified to account for intermediate locations of the aircraft by including the locus of all possible PAZ regions from any given time up to and including time  $T$  into the future. Figure 13 illustrates both this RTCA definition and this intermediate location definition. These two reachability definitions can be considered worst-case criteria, and may be applicable in situations where the intruder aircraft is non-cooperative, blundering, or is already engaged in a maneuver. Later, in Chapter 4, it is shown that such reachability conflict alert zone criteria could be useful in solving multiple aircraft conflict scenarios.

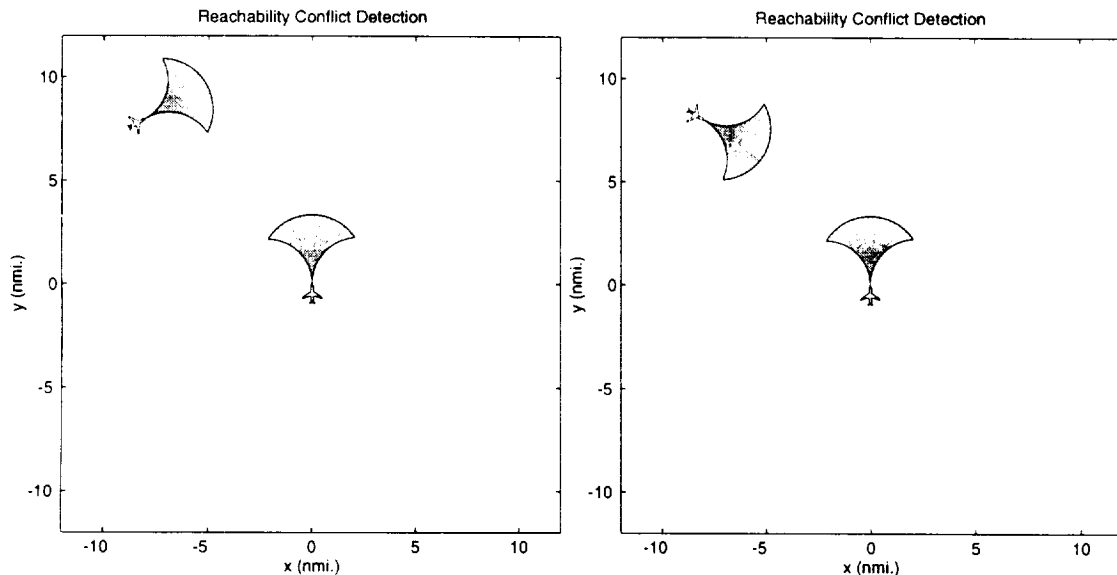


Figure 12. Horizontal conflict detection based on aircraft reachability. A  $\theta = 60^\circ$  heading difference (left) and a  $\theta = 120^\circ$  (right) heading difference is shown in an inertial reference frame identifying the locus of possible locations for each aircraft.

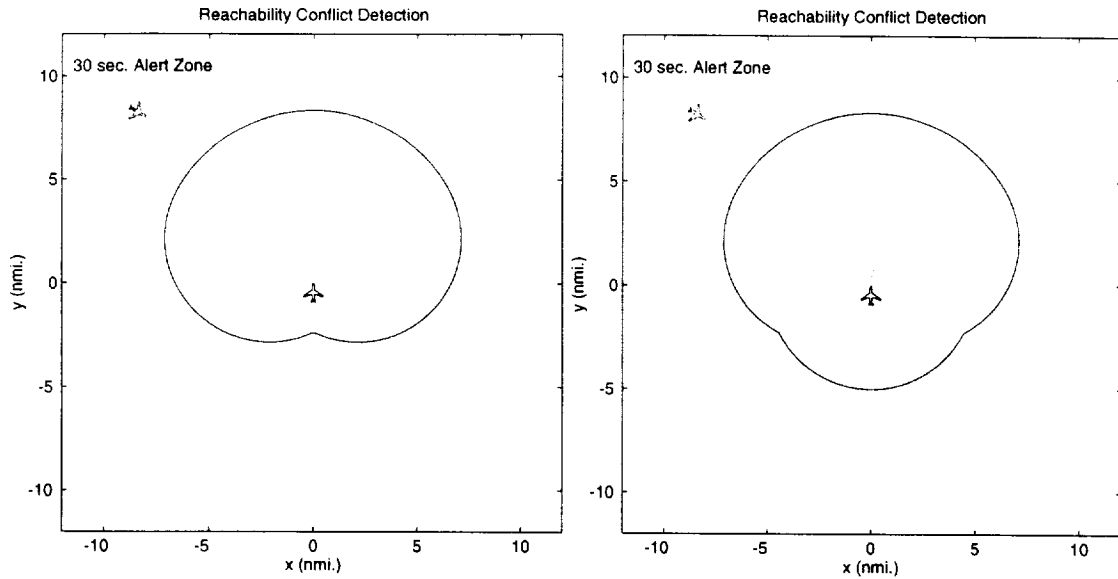


Figure 13. Horizontal conflict detection based on reachability of the Protected Airspace Zone. The locus of all Protected Airspace Zone volumes at time  $T=30$  seconds (left) and the locus of all Protected Airspace Zone volumes from time  $T=0$  seconds up to and including time  $T=30$  seconds (right) are compared.

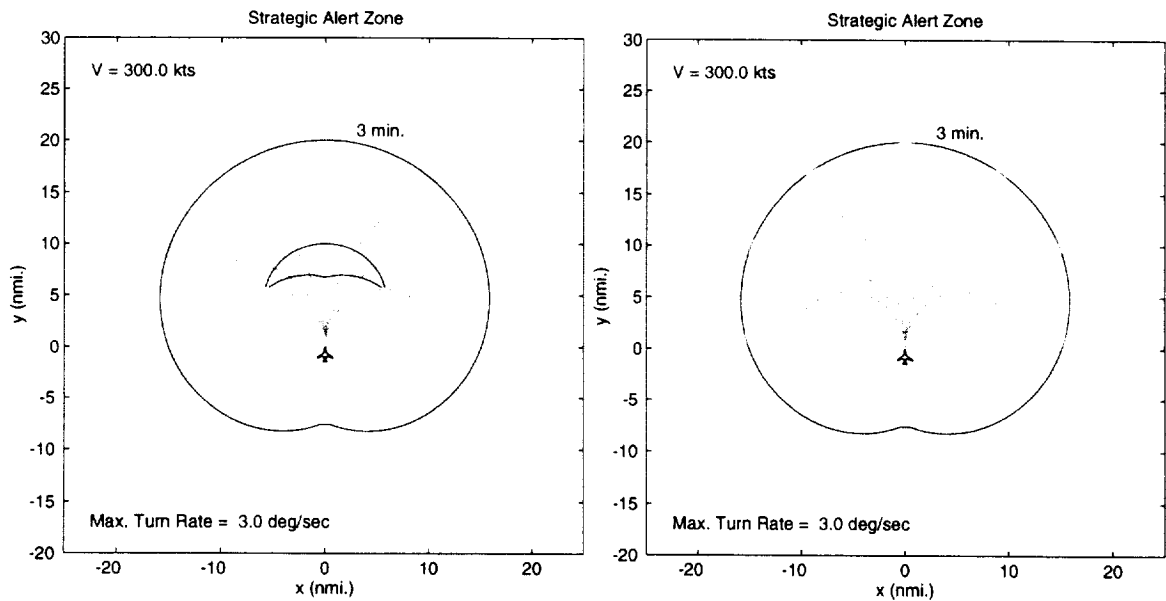


Figure 14. The locus of all possible Protected Airspace Zone locations after time  $T=3$  minutes (left) and up to and including time  $T=3$  minutes (right).

### 3.3 Conflict Detection Criteria for Strategic Scenarios

For strategic scenarios, the concept of a conflict detection should take into account separation standards as well as trajectory uncertainties due to wind variations, measurement errors, and actuation variations (flight technical errors). As shown in the example in Figure 15, if no errors were to occur, the relative motion of an aircraft far away in a strategic scenario can be classified as a conflict situation for a long narrow conflict region, the region thickness being equal to the diameter of the Protected Airspace Zone. However, when uncertainties are introduced in the initial relative position, velocity, and heading, the same relative aircraft geometry indicate a small 0.25 probability of a conflict. At a far range, there is a greater probability that the aircraft miss the Protected Airspace Zone than penetrate it. The development of such a non-deterministic analysis is presented later in Section 3.5.

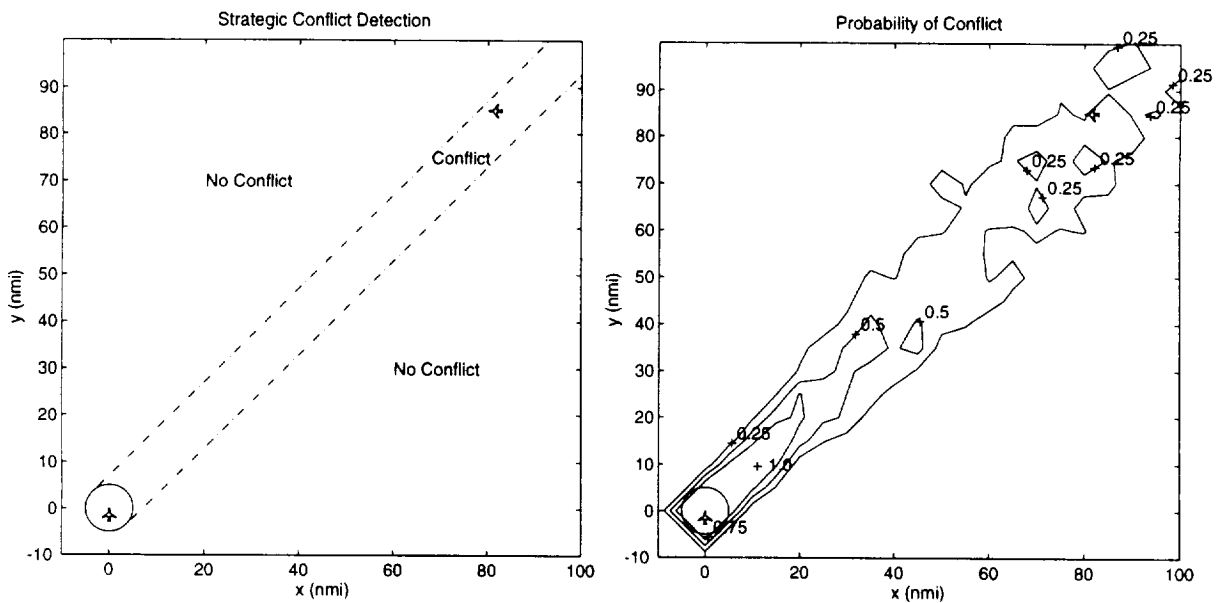


Figure 15. The deterministic strategic conflict region (left) for very large prediction times to closest approach and a non-deterministic strategic conflict region (right) based on the probability of a conflict given likely uncertainties in position ( $\sigma_p = 100$  m), speed ( $\sigma_v = 10$  m/sec), and heading ( $\sigma_\psi = 10^\circ$ ).

For strategic conflict detection, the avionics (or ATM ground system automation) must project the aircraft trajectories ahead in time out to, say, 20 minutes, where both aircraft may be experiencing vastly different wing conditions. At jet aircraft speeds, a 20 minute prediction could involve aircraft that are initially 400 nmi apart. The wind

variation over this range can be significant, especially in frontal conditions or near the jet stream. A 6 kt head wind error relative to the forecast in use for one aircraft could produce a 12 second error in the time to the point of closest approach or a range error of 2 nmi.

The second type of trajectory prediction error considered is due to navigation error. Even though augmented GPS will probably be used, there will still be error within the RNP equipment that is on each aircraft in the conflict. In particular, the measured velocity error has a significant effect on the projected crossing of two aircraft trajectories.

The third type of trajectory error is due the fact that the pilot (or autopilot) will not steer the aircraft perfectly along the intended flight plan; the variation between the state at which the navigation system depicts where the aircraft should be relative to the actual measured state is commonly referred to as flight technical error FTE. Lateral and vertical variations in position cause the aircraft to take longer to reach a certain point. Variations in airspeed, along with head wind variations from the wind forecast being used, affect arrival time at any future point. Thus, the strategic logic must be robust to errors in the wind field data, navigation state measurement, and FTE effects in terms of the dynamics used to project the trajectory outcomes.

### 3.4 Two-Dimensional Horizontal Deterministic Conflict Analysis

For the two-dimensional analysis, assume the motion of the two aircraft remains in a horizontal plane at a fixed altitude and that each aircraft flies without sideslip. The geometry is illustrated in Figure 16, where  $r$  is the range,  $v_A$  is the speed of the own aircraft A,  $v_B$  is the speed of the intruder aircraft B,  $\theta$  is the heading difference between

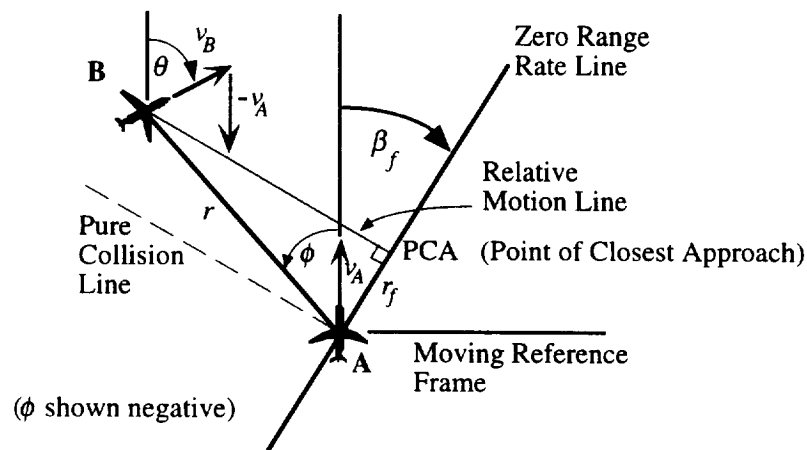


Figure 16. Relative motion of two oblivious aircraft in a horizontal plane.

aircraft B and aircraft A, and  $\phi$  is the angle-off from aircraft A's velocity vector to aircraft B. The heading of each aircraft is in the direction of the velocity vector, since the sideslip angle is assumed to be zero. The variables  $x$  and  $y$  locate the aircraft B relative to the moving reference frame fixed in aircraft A.

Depending on geometry, the situation may represent a pure collision, a near miss, or no conflict. Two critical factors to analyze are the zero range rate line where  $\dot{r} = 0$  and the range at closest approach. When the range rate is negative, future positions may lead the intruder aircraft closer to a conflict. In the moving reference frame, the zero range rate line is at a bearing angle  $\beta_f$  defined by the relation:

$$\cos \beta_f = \frac{v_B \sin \theta}{\sqrt{v_A^2 + v_B^2 - 2v_A v_B \cos \theta}} \quad (6)$$

where, as shown in Figure 16,  $v_A$  is the speed of the own aircraft A,  $v_B$  is the speed of the intruder aircraft B, and  $\theta$  is the heading difference between aircraft B and aircraft A. The relative motion of aircraft B will follow a trajectory perpendicular to the zero range rate line. A pure collision results if this trajectory is perpendicular to the zero range rate line at the origin, as shown in Figure 16. A conflict occurs if the miss distance  $r_f$ , occurring at the Point of Closest Approach (PCA), is less than the Protected Airspace Zone radius; the miss distance can be calculated from the equation:

$$r_f = r \cos(\beta_f - \phi) \quad (7)$$

where  $r$  is the initial range,  $\phi$  is the angle off, and  $\beta_f$  is the bearing angle. A definition for the miss distance as a vector  $\bar{r}_f$  is:

$$\bar{r}_f = \hat{c} \times (\bar{r} \times \hat{c}) \quad (8)$$

where  $\bar{r}$  is the vector locating aircraft B with respect to aircraft A, and  $\hat{c}$  is the unit vector in the direction of the relative motion vector  $\bar{c}$ :

$$\hat{c} = \frac{\bar{c}}{\|\bar{c}\|} \quad \text{where} \quad \bar{c} = \bar{v}_B - \bar{v}_A. \quad (9)$$

The time-to-closest-approach  $\tau$  is analyzed next. From analytic geometry:

$$\tau = \frac{r \sin(\beta_f - \phi)}{\sqrt{v_A^2 + v_B^2 - 2v_A v_B \cos \theta}}. \quad (10)$$

In vector notation, the time-to-closest-approach is equivalently defined:

$$\tau = -\frac{\bar{r} \cdot \hat{c}}{\|\bar{c}\|}. \quad (11)$$

The time-to-closest-approach is different from the classical definition of Morrel's [Mo58] predicted time-to-collision criteria, computed as simply range divided by range rate. To use a time-to-closest-approach criterion for conflict detection, accurate bearing measurements must exist and are available today with GPS and datalink technologies. In previous systems, accurate and timely bearing measurements were not available, leaving range and range rate for computing a time to a potential collision. Note that in comparison, the time-to-closest-approach becomes zero as the intruder aircraft crosses the zero range rate line, but the time-to-collision criteria approaches a singularity.

The relative motion of two aircraft may be analyzed by looking at relative motion charts for various heading differences, as shown in Figure 17. Relative motion charts become the basis for creating maneuver charts for conflict resolution, as developed later in Chapters 4 and 5. In Figure 17, neither aircraft performs a control action for conflict resolution; the notation  $A_0 B_0$  denotes that no control (0 turn rate and no speed change) is being performed by aircraft A and aircraft B.

The orientation of the zero range rate line can be examined for various heading differences as shown in Figure 18. Most aircraft speeds will be within the range:  $100 \leq v \leq 550$  kts, so throughout this report computations and examples are performed with the speed ratio in the range:  $\frac{1}{6} < \gamma < 6$ , with speed ratios near 1 being most typical. Finally, note that there is a singularity in the equation for the zero range rate line at zero heading difference  $\theta = 0$ , where the bearing is  $\beta_f = \pm \frac{\pi}{2}$ , unless  $\gamma = 1$ , where there is no solution (both aircraft are flying parallel to one another with the same velocity).

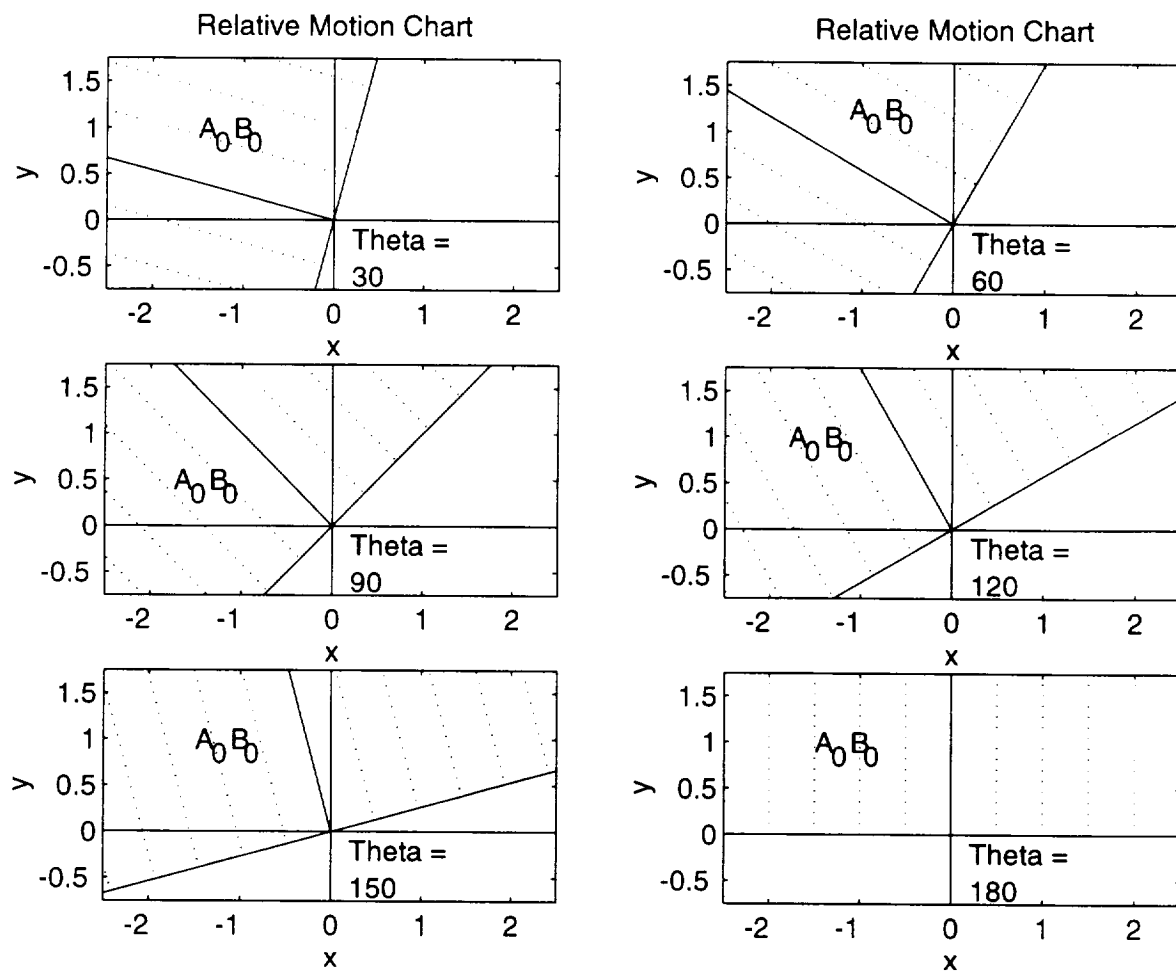


Figure 17. Relative Motion Charts for oblivious aircraft (speed ratio  $\gamma = 1$ ).

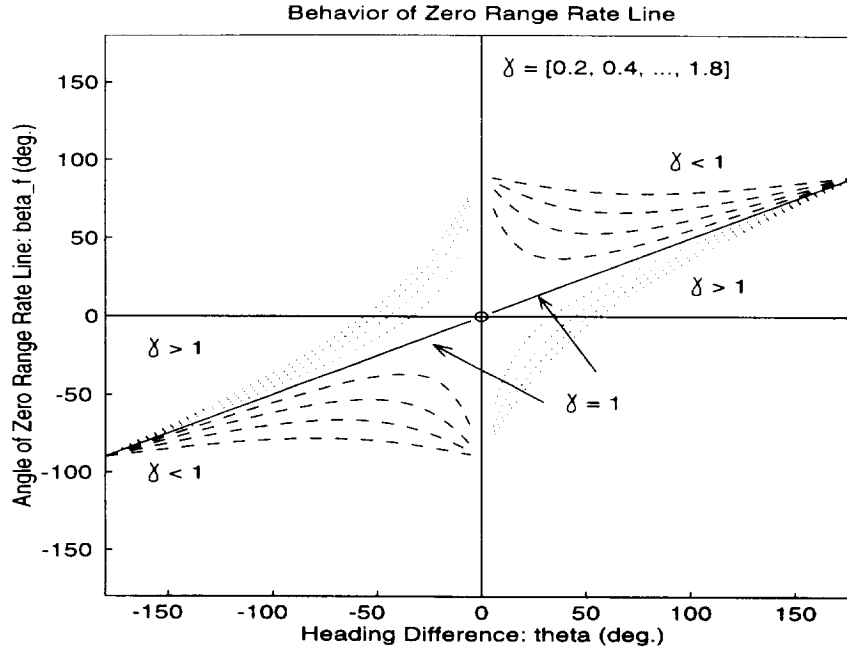


Figure 18. A plot showing the relationship from Equation (6) between the angle  $\beta_f$  of the zero range rate line and the heading difference angle  $\theta$ ; curves are shown for various speed ratios:  $\gamma = v_B/v_A$ .

### 3.5 Two-Dimensional Horizontal Non-Deterministic Conflict Analysis

As mentioned previously for the application of strategic scenarios, the concept of a conflict detection may also be modeled with a non-deterministic analysis. The implicit assumption is that a non-deterministic approach may be better than a deterministic approach when considering false alarm rates and missed detections. When the intruder aircraft is far away, the non-deterministic approach will identify that an actual conflict has a low probability, thus reducing the false alarm rate. When uncertainties are introduced in the initial relative position, velocity, and heading, the probability of a conflict can be considered in comparison to the precise geometric definition of a conflict from the deterministic approach.

The non-deterministic analysis assumes that the relative state information is known stochastically. The location, speed, and heading of aircraft are assumed to be normally distributed around measured or reported values, and these values are assumed to be held constant during the entire time of the encounter. The error sources are assumed to be independent, and the error characteristics of the two aircraft are assumed to be identical, to simplify the analysis.

As discussed with the deterministic approach, a conflict is defined for the two dimensional horizontal plane when the horizontal separation standard is violated. In a non-deterministic analysis, the probability of a conflict is determined by evaluating the probability  $P$  that the miss distance  $r_f$ , occurring at the Point of Closest Approach (PCA), is less than or equal to the Protected Airspace Zone radius  $R$ :

$$P(\text{conflict}) = P(r_f \leq R) \quad (12)$$

This probability can be computed for a range of initial conditions of aircraft B relative to aircraft A to form a conflict probability map.

One method for constructing a conflict probability map is to use Monte Carlo simulations. A grid is formed by discretizing the relative location  $(x,y)$  of the intruder aircraft B relative to aircraft A. Normal (Gaussian) distributions are used to model the position, velocity, and heading variables. A simulation propagates the motion of each vehicle to the point of closest approach and statistics can be enumerated for the probability of a conflict. An example is given in Figure 19, where the aircraft measurement

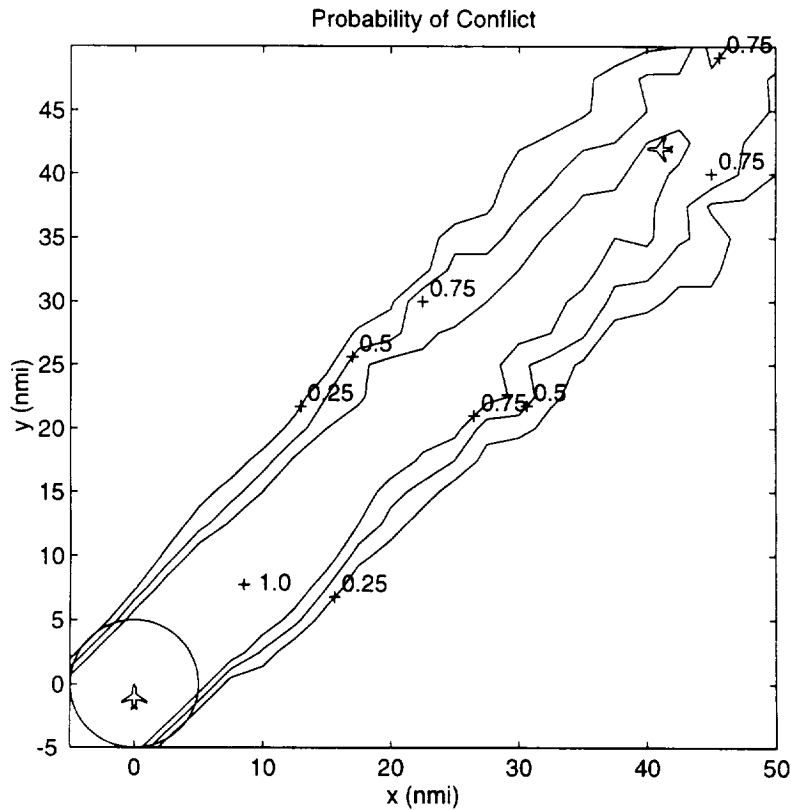


Figure 19. The conflict probability map derived from Monte Carlo simulations.

uncertainties for both aircraft are: the standard deviation on position  $\sigma_p = 100$  m, the standard deviation on speed  $\sigma_v = 10$  m/sec, and the standard deviation on heading  $\sigma_\psi = 5^\circ$ . This technique is used by Kuchar, *et al*, in conflict avoidance applications [Ku96, YaK97].

Alternatively, instead of using Monte Carlo simulations, analytic expressions can be used to establish probability maps. If one were to assume that the motion of each vehicle proceeds with a constant velocity, equation (7) or (8) can be applied to determine the point of closest approach, eliminating the need to propagate simulations. By mathematically analyzing a miss distance equation, the mean and error variance for the miss distance can be established. First, the miss distance is represented by taking the vector norm of equation (8):

$$r_f = \|\hat{c} \times (\bar{r} \times \hat{c})\| = r_x \hat{c}_y - r_y \hat{c}_x \quad (13)$$

where  $x$  and  $y$  subscripts represent the  $x$ -component and  $y$ -component of the relative position vector  $\bar{r}$  and relative motion unit vector  $\hat{c}$ . Furthermore, these vector components can be represented:

$$r_x = r_{x_B} - r_{x_A}, \quad (14)$$

$$r_y = r_{y_B} - r_{y_A}, \quad (15)$$

$$\hat{c}_x = \frac{v_{x_B} - v_{x_A}}{\sqrt{(v_{x_B} - v_{x_A})^2 + (v_{y_B} - v_{y_A})^2}}, \text{ and} \quad (16)$$

$$\hat{c}_y = \frac{v_{y_B} - v_{y_A}}{\sqrt{(v_{x_B} - v_{x_A})^2 + (v_{y_B} - v_{y_A})^2}}, \quad (17)$$

where subscripts  $A$  and  $B$  correspond to aircraft A and aircraft B. By substituting equations (14) through (17) into equation (13) the miss distance can be expressed in the form:

$$r_f = \frac{(r_{x_B} - r_{x_A})(v_{y_B} - v_{y_A}) - (r_{y_B} - r_{y_A})(v_{x_B} - v_{x_A})}{\sqrt{(v_{x_B} - v_{x_A})^2 + (v_{y_B} - v_{y_A})^2}}. \quad (18)$$

Next, the form of equation (18) is a non-linear function  $f$  of eight random variables:

$$r_f = f(r_{x_A}, r_{x_B}, r_{y_A}, r_{y_B}, v_{x_A}, v_{x_B}, v_{y_A}, v_{y_B}). \quad (19)$$

A general function of  $n$  random variables:

$$z = f(x_1, x_2, \dots, x_n) \quad (20)$$

can be approximated to the first order by expanding a Taylor's Series about the mean values of the random variables:

$$z = f(\bar{x}_1, \bar{x}_2, \dots, \bar{x}_n) + \sum_{i=1}^n \frac{\partial f}{\partial x_i} (x_i - \bar{x}_i) + H.O.T. \quad (21)$$

where *H.O.T.* stands for Higher Order Terms. Equation (21) can be approximated with the first order approximation:

$$z = f(\bar{x}_1, \bar{x}_2, \dots, \bar{x}_n) + \sum_{i=1}^n \frac{\partial f}{\partial x_i} \bar{x}_i + \sum_{i=1}^n \frac{\partial f}{\partial x_i} x_i \quad (22)$$

where the first two terms are composed of deterministic variables, and the last (summation) term is composed of random variables. Next, for a set of mutually independent random variables  $x_i$ :

$$Var(\sum_{i=1}^n a_i x_i) = \sum_{i=1}^n a_i^2 Var(x_i). \quad (23)$$

Applying equation (23) to the general expression of the miss distance, equation (19), gives the result:

$$\begin{aligned} Var(r_f) = & \left(\frac{\partial r_f}{\partial r_{x_A}}\right)^2 Var(r_{x_A}) + \left(\frac{\partial r_f}{\partial r_{y_A}}\right)^2 Var(r_{y_A}) \\ & + \left(\frac{\partial r_f}{\partial r_{x_B}}\right)^2 Var(r_{x_B}) + \left(\frac{\partial r_f}{\partial r_{y_B}}\right)^2 Var(r_{y_B}) \\ & + \left(\frac{\partial r_f}{\partial v_{x_A}}\right)^2 Var(v_{x_A}) + \left(\frac{\partial r_f}{\partial v_{y_A}}\right)^2 Var(v_{y_A}) \\ & + \left(\frac{\partial r_f}{\partial v_{x_B}}\right)^2 Var(v_{x_B}) + \left(\frac{\partial r_f}{\partial v_{y_B}}\right)^2 Var(v_{y_B}). \end{aligned} \quad (24)$$

The partial derivatives of equation (24) are determined from equation (18), for example:

$$\frac{\partial r_f}{\partial r_{x_A}} = \frac{-(v_{y_B} - v_{y_A})}{\sqrt{(v_{x_B} - v_{x_A})^2 + (v_{y_B} - v_{y_A})^2}}. \quad (25)$$

This equation (25) and the other partial derivatives in equation (24) further simplify to:

$$\frac{\partial r_f}{\partial r_{x_A}} = -\hat{c}_y; \quad \frac{\partial r_f}{\partial r_{y_A}} = \hat{c}_x; \quad \frac{\partial r_f}{\partial r_{x_B}} = \hat{c}_y; \quad \frac{\partial r_f}{\partial r_{y_B}} = -\hat{c}_x; \quad (26)$$

$$\frac{\partial r_f}{\partial v_{x_A}} = \hat{c}_x \tau; \quad \frac{\partial r_f}{\partial v_{y_A}} = -\hat{c}_y \tau; \quad \frac{\partial r_f}{\partial v_{x_B}} = -\hat{c}_x \tau; \quad \frac{\partial r_f}{\partial v_{y_B}} = \hat{c}_y \tau; \quad (27)$$

where  $\tau$  is the time-to-closest-approach, defined earlier by equation (10) or (11).

The variances of the random variables are determined next. Assume, for convenience, that the  $x$  and  $y$ -components of the GPS horizontal position, and similarly velocity, are independent. In reality, their independence is a function of the number and geometry of the visible GPS satellites (even when it is assumed that the pseudorange measurements and range rate measurements are separately (approximately) independent). Also assume that both aircraft will use the same type of receiver (such as a six-channel receiver) and are relatively close (within several hundred miles). Then it is also reasonable to assume that both aircraft will see the same GPS satellites and experience the same GPS position and velocity accuracy. Then, the standard deviation of the position measurement error  $\sigma_p$  is the same for both aircraft:

$$\text{Var}(r_x) = \text{Var}(r_y) = \sigma_p^2. \quad (28)$$

If the velocity measurements are provided in the form of velocity vector components, then assuming the same accuracy in both component axes, the standard deviation of the velocity measurement error  $\sigma_v$  is the same for both aircraft:

$$\text{Var}(v_x) = \text{Var}(v_y) = \sigma_v^2. \quad (29)$$

Using equations (28) and (29) and substituting the equations for the partial derivatives in equation (26) and (27) into equation (24) gives a simple equation for the variance of the miss distance:

$$\text{Var}(r_f) = 2\sigma_p^2 + 2\sigma_v^2\tau^2. \quad (30)$$

However, if the velocity vector measurements are given in terms of speed and heading, then the analysis is different. Given the velocity vector of aircraft A or B is in the form:

$$\vec{v} = v_x \hat{x} + v_y \hat{y} = v \sin \psi \hat{x} + v \cos \psi \hat{y}, \quad (31)$$

then the variance of the  $x$ -component of velocity is:

$$Var(v_x) = \left(\frac{\partial v_x}{\partial v}\right)^2 Var(v) + \left(\frac{\partial v_x}{\partial \psi}\right)^2 Var(\psi), \quad (32)$$

and after evaluating the partial derivatives in equation (32), the expression simplifies to:

$$Var(v_x) = (\sin \psi)^2 \sigma_v^2 + (v \cos \psi)^2 \sigma_\psi^2 \equiv \sigma_{v_x}^2, \quad (33)$$

where  $\sigma_v$  and  $\sigma_\psi$  are the standard deviations of the aircraft speed and heading measurement errors. In a similar manner, the variance of the y-component can be shown to be:

$$Var(v_y) = (\cos \psi)^2 \sigma_v^2 + (-v \sin \psi)^2 \sigma_\psi^2 \equiv \sigma_{v_y}^2. \quad (34)$$

Finally, the variance of the miss distance using equations (33) and (34) for both aircraft A and B results in:

$$Var(r_f) = 2\sigma_p^2 + \hat{c}_x^2 \tau^2 (\sigma_{Av_x}^2 + \sigma_{Bv_x}^2) + \hat{c}_y^2 \tau^2 (\sigma_{Av_y}^2 + \sigma_{Bv_y}^2), \quad (35)$$

where the subscripts A and B are important to note since different speeds and heading angles  $\psi_A$  and  $\psi_B$  will most likely exist in equations (33) and (34) when applied to both aircraft.

The probability of a conflict is determined next. Given the mean of the miss distance  $\bar{r}_f$  and the variance of the miss distance  $Var(r_f) = \sigma_{r_f}^2$ , the probability of a conflict is determined by integrating the area under the probability distribution function between the locations that correspond to  $-R$  and  $R$ :

$$P(\text{conflict}) = \frac{1}{\sigma\sqrt{2\pi}} \int_{-R}^R e^{-\frac{(x-\bar{r}_f)^2}{2\sigma^2}} dx. \quad (36)$$

Figure 20 shows an example. Next, using a change of variable  $u = \frac{x - \bar{r}_f}{\sqrt{2}\sigma}$  and the Gaussian error function  $erf(x)$ :

$$erf(x) = \frac{2}{\sqrt{\pi}} \int_0^x e^{-u^2} du, \quad (37)$$

the probability of a conflict is given by:

$$P(\text{conflict}) = \frac{1}{2} erf\left(\frac{R + \bar{r}_f}{\sqrt{2}\sigma_{r_f}}\right) + \frac{1}{2} erf\left(\frac{R - \bar{r}_f}{\sqrt{2}\sigma_{r_f}}\right). \quad (38)$$

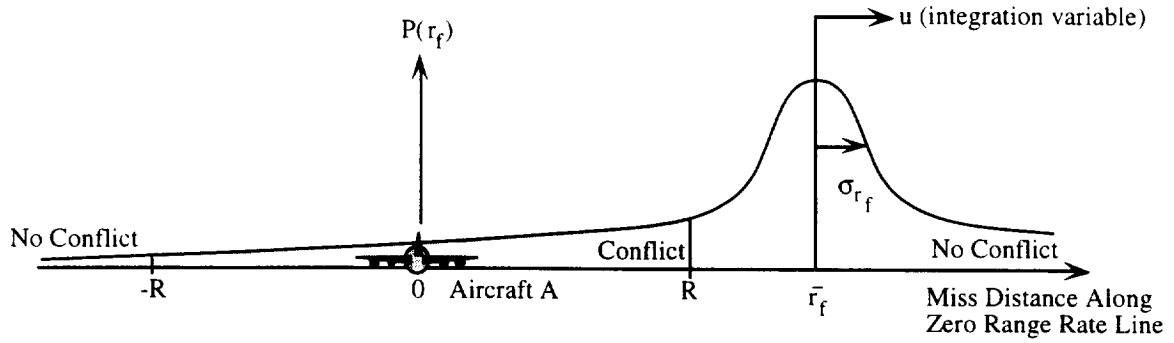


Figure 20. The miss distance probability distribution function is used to determine the probability of a conflict (shaded area) compared to the probability of a non-conflict (non-shaded area).

An example using this analytical method for determining non-deterministic conflicts is given in Figure 21. In this example, the aircraft measurement uncertainties for both aircraft are: the standard deviation on position  $\sigma_p = 100$  m, the standard deviation on speed  $\sigma_v = 10$  m/sec, and the standard deviation on heading  $\sigma_\psi = 5^\circ$ . Note the similarity between the Monte Carlo simulation results in Figure 19 and the analytic method in

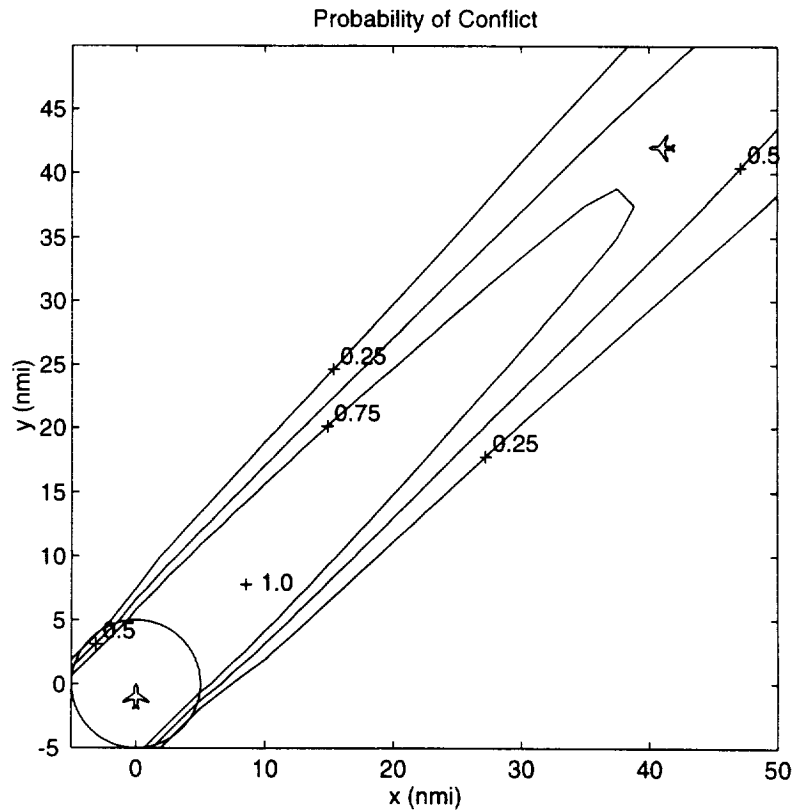


Figure 21. The conflict probability map using the analytic analysis.

Figure 21. The benefit of the analytic method is that it does not require repeated simulations to establish statistics for the probability of a conflict.

The analytic method for establishing the conflict probability map may also be used to establish Strategic Alert Zones. The notion of an Alert Zone was first introduced in Chapter 1 and an example was shown in Figure 1. For an airline, a Strategic Alert Zone may determine when the probability of a conflict is high enough for the airline to initiate a strategic maneuver. For the Alert Zone as defined by Free Flight air traffic controller intervention, there may be yet another probability of conflict which is sufficiently high that air traffic controllers may want to intervene. The research necessary to determine what these probabilities should be is not covered in this report. However, for an example, if an airline were to establish that no action should be taken by one of their pilots unless the probability of a conflict is greater than 50%, then the Strategic Alert Zone in Figure 22 would result for the given measurement uncertainties described previously for Figure 21. Such a Strategic Alert Zone may also be interpreted as a strategic conflict detection mechanism.

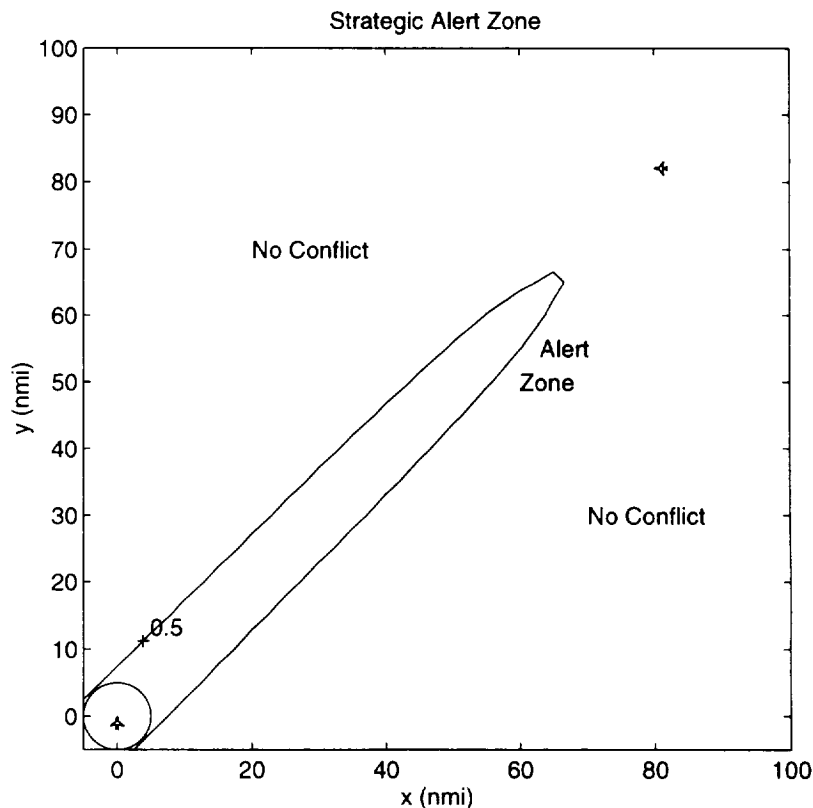


Figure 22. A Strategic Alert Zone defined by a 50% probability of conflict.

### 3.6 Three-Dimensional Deterministic Conflict Analysis

For the three-dimensional analysis, any arbitrary relative motion may exist for the two aircraft. The geometry for the three-dimensional relative motion is illustrated in Figure 23. Two geometric planes are described. First, a horizontal plane  $A$  passes through aircraft  $A$ ; this plane bisects the Protected Airspace Zone cylinder and is perpendicular to the cylinder axis. A second plane is a skewed relative motion plane  $AB$  defined by the two aircraft velocity vectors  $\bar{v}_A$  and  $\bar{v}_B$ . The surface normal for the relative motion plane  $AB$  is defined by the vector cross product  $\bar{v}_A \times \bar{v}_B$ . The relative motion remains in the relative motion plane since conflict detection analysis assumes that both aircraft hold their velocity vectors constant.

Variables defined in the moving reference frame locate the intruder aircraft  $B$  relative to aircraft  $A$ . A moving reference frame is fixed to aircraft  $A$  with the  $\hat{x}$ -axis and  $\hat{y}$ -axis residing in the horizontal plane  $A$ . If the velocity of aircraft  $A$  were to reside in the horizontal plane  $A$ , then the  $\hat{x}$ -axis would be directed toward the right wing, and the  $\hat{y}$ -axis would be directed from the aircraft center out the aircraft nose. However, the aircraft  $A$  may have a velocity vector that pitches out of the horizontal plane  $A$ ; so the  $\hat{y}$ -axis and the velocity vector may not necessarily align. It is assumed that neither aircraft is banked from horizontal before a conflict resolution maneuver, so the  $\hat{x}$ -axis should always align with the direction of the right wing of aircraft  $A$ . The  $\hat{z}$ -axis is defined such that  $\hat{x}$ ,

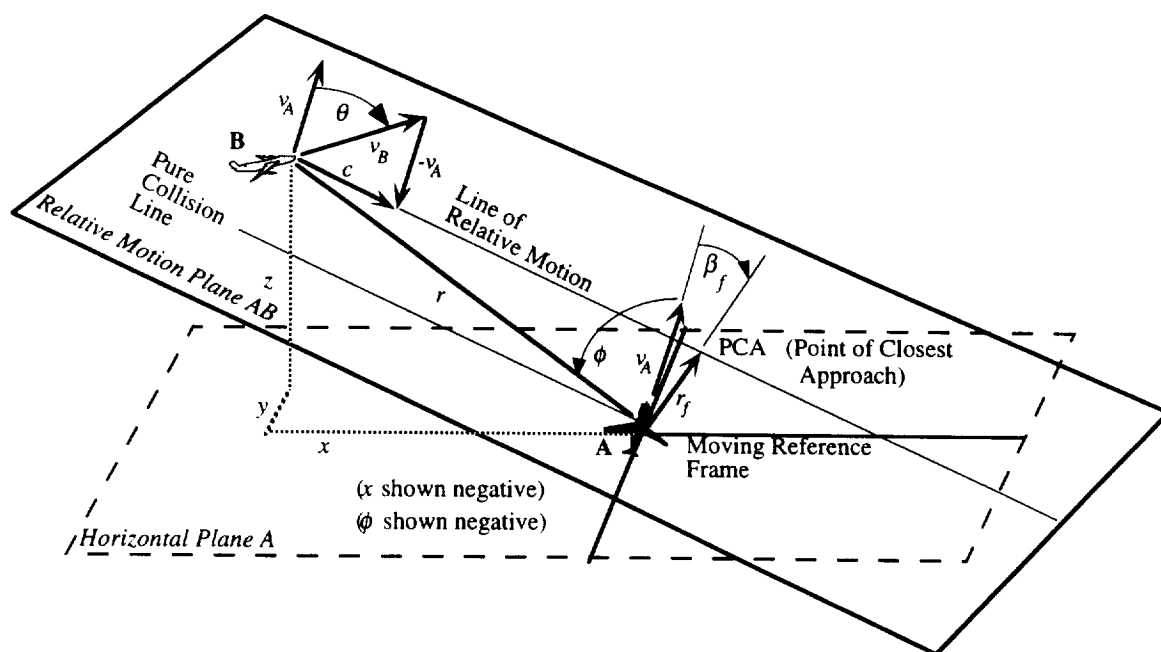


Figure 23. Relative motion of two oblivious aircraft in three-dimensions.

$\hat{y}$ , and  $\hat{z}$  axes form a right hand system, thus,  $\hat{z} = \hat{x} \times \hat{y}$ , and the  $\hat{z}$ -axis always points in the vertical direction. In the moving reference frame, the variables  $x$ ,  $y$ , and  $z$  locate the intruder aircraft B relative to aircraft A.

Variables defined in the relative motion plane are described as follows;  $\bar{r}$  is the Euclidean range vector locating aircraft B relative to aircraft A, defined by:

$$\bar{r} = x\hat{x} + y\hat{y} + z\hat{z}, \quad (39)$$

$\theta$  is the angle between the vectors  $\bar{v}_A$  and  $\bar{v}_B$ , determined from the dot product:

$$\bar{v}_A \cdot \bar{v}_B = |\bar{v}_A| |\bar{v}_B| \cos \theta \quad (40)$$

(which is not necessarily the heading difference, as for the two-dimensional analysis),  $\bar{r}_f$  is the miss vector (defined later) locating the Point of Closest Approach PCA,  $\phi$  is the angle-off in the relative motion plane  $AB$  from the velocity vector  $\bar{v}_A$  of aircraft A to aircraft B, and  $\beta_f$  is the angle between the velocity vector  $\bar{v}_A$  and the miss vector  $\bar{r}_f$ , determined by the dot product:

$$\bar{v}_A \cdot \bar{r}_f = |\bar{v}_A| |\bar{r}_f| \cos \beta_f. \quad (41)$$

The zero range rate line is defined to be the locus of points along the miss vector  $\bar{r}_f$ . While some of these variables are defined differently from the two-dimensional analysis, the objective of defining them in this manner allows equations (6) through (11) to directly apply to the motion in the relative motion plane.

The miss vector  $\bar{r}_f$ , as well as the time-to-closest-approach  $\tau$ , may be found as follows. At the Point of Closest Approach, the miss vector  $\bar{r}_f$  and the relative motion vector  $\bar{c}$  are orthogonal:

$$\bar{r}_f \cdot \bar{c} = 0. \quad (42)$$

Also, the motion of aircraft B relative to aircraft A will follow in the direction of  $\bar{c}$ , and will be located at the vector location  $\bar{r}_f$  at the time-to-closest-approach  $\tau$ :

$$\bar{r}_f = \bar{r} + \bar{c} \tau. \quad (43)$$

Solving equations (42) and (43) simultaneously yields the time-to-closest-approach  $\tau$ :

$$\tau = -\frac{\bar{r} \cdot \bar{c}}{\bar{c} \cdot \bar{c}} \quad (44)$$

which may be substituted into equation (43) to evaluate the miss vector  $\bar{r}_f$ .

Depending on geometry, the situation may represent a pure collision, a near miss, or no conflict. Two critical factors to examine are the zero range rate line where  $\dot{r} = 0$  and the range at closest approach. The motion of aircraft B relative to aircraft A will follow a trajectory in the relative motion plane perpendicular to the zero range rate line. A pure collision results if this trajectory is perpendicular to the zero range rate line at the origin, as shown in Figure 23. A conflict occurs if the miss vector  $\bar{r}_f$ , occurring at the Point of Closest Approach (PCA), falls within the Protected Airspace Zone (PAZ). The PAZ is defined by a cylinder with radius  $R$  and height  $h$ , centered around aircraft A. The miss vector  $\bar{r}_f$  can be expressed in the moving reference frame of aircraft A as:

$$\bar{r}_f = r_{f_x} \hat{x} + r_{f_y} \hat{y} + r_{f_z} \hat{z}. \quad (45)$$

A Protected Airspace Zone conflict exists if:

$$i) \quad r_{f_z} \leq h/2 \quad (\text{below the upper PAZ limit}), \quad (46)$$

$$ii) \quad r_{f_z} \geq -h/2 \quad (\text{above the lower PAZ limit}), \text{ and} \quad (47)$$

$$iii) \quad r_{f_x}^2 + r_{f_y}^2 \leq R^2 \quad (\text{within the PAZ radius limit}). \quad (48)$$

While this criterion is a sufficient condition for a conflict, it is not a necessary condition. As shown in Figure 24, the PCA may not in itself identify a conflict, but some other portion of the line of relative motion may pass through the PAZ and cause a conflict.

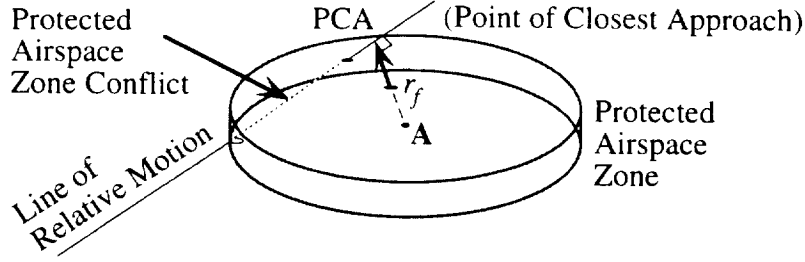


Figure 24. The Point of Closest Approach PCA may reside outside the Protected Airspace Zone even though a conflict exists.

A necessary and sufficient condition for a conflict involves checking three specific point locations derived from the Protected Airspace Zone and the line of relative motion. First, let  $\vec{l}$  be the line of relative motion, defined by the vector equation:

$$\vec{l} = \vec{r} + \vec{c}t \quad (49)$$

for all time  $t$ . Next, define a projection operator,  $P$ , which projects a vector onto the horizontal  $\hat{x}$ - $\hat{y}$ -plane (plane A), thus, for the vector  $\vec{r} = [x \ y \ z]$ ,

$$P(\vec{r}) = \vec{r} - \vec{r} \cdot \hat{z} = [x \ y \ 0]. \quad (50)$$

Let the under-bar notation  $\bar{r}$  identify the projection of  $\vec{r}$ , written  $P(\vec{r}) = \bar{r}$ . For conflict detection, the segment  $s$  of the line of relative motion  $\vec{l}$  between the altitudes of  $-h/2 \hat{z}$  and  $+h/2 \hat{z}$  is investigated to identify if any part of this segment is within the distance  $R$  from the  $\hat{z}$ -axis. In general, the line of relative motion  $\vec{l}$  is not parallel to the  $\hat{x}$ - $\hat{y}$ -plane, but when it is, the previously stated two-dimensional analysis applies. The endpoints of segment  $s$  are located at  $\bar{r}_L$  and  $\bar{r}_U$ , where:

$$\bar{r}_L = \vec{r} + \vec{c} \tau_L \quad (51)$$

with  $\tau_L$  defined by

$$(\vec{r} + \vec{c} \tau_L) \cdot \hat{z} = -h/2, \quad (52)$$

and

$$\bar{r}_U = \vec{r} + \vec{c} \tau_U \quad (53)$$

with  $\tau_U$  defined by

$$(\bar{r} + \bar{c}\tau_U) \cdot \hat{z} = h/2. \quad (54)$$

Here,  $\tau_L$  is the time to reach the lower altitude  $-h/2 \hat{z}$  and  $\tau_U$  is the time to reach the upper altitude  $+h/2 \hat{z}$ . Note that  $\tau_L > \tau_U$  if aircraft B approaches aircraft A from above, and  $\tau_L < \tau_U$  if aircraft B approaches aircraft A from below. Using the projection operator  $P$ , the two vectors:

$$\underline{\bar{r}}_L = P(\bar{r}_L) \quad (55)$$

and

$$\underline{\bar{r}}_U = P(\bar{r}_U) \quad (56)$$

are identified. Next, identify the vector location  $\underline{\bar{r}}_*$  on the projected line that is closest to the origin:

$$\underline{\bar{l}} = \underline{\bar{r}} + \underline{\bar{c}}t. \quad (57)$$

This is achieved by solving the scalar equation:

$$(\underline{\bar{r}} + \underline{\bar{c}}\tau_*) \cdot \underline{\bar{c}} = 0 \quad (58)$$

for  $\tau_*$ :

$$\tau_* = -\frac{\underline{\bar{r}} \cdot \underline{\bar{c}}}{\underline{\bar{c}} \cdot \underline{\bar{c}}}. \quad (59)$$

This defines the location:

$$\underline{\bar{r}}_* = \underline{\bar{r}} + \underline{\bar{c}}\tau_*. \quad (60)$$

The three points needed to detect a conflict are  $\underline{\bar{r}}_L$  from equation (55),  $\underline{\bar{r}}_U$  from equation (56), and  $\underline{\bar{r}}_*$  from equation (60). The necessary and sufficient conditions for a Protected Airspace Zone PAZ conflict are:

$$i) \text{ if } \underline{\bar{r}}_L \cdot \underline{\bar{r}}_L \leq R^2, \text{ or} \quad (61)$$

$$ii) \text{ if } \underline{\bar{r}}_U \cdot \underline{\bar{r}}_U \leq R^2, \text{ or} \quad (62)$$

$$iii) \text{ if } \underline{\bar{r}}_* \cdot \underline{\bar{r}}_* \leq R^2 \text{ and } (\tau_L < \tau_* < \tau_U \text{ or } \tau_U < \tau_* < \tau_L). \quad (63)$$

Figure 25 illustrates the application of these conflict detection rules to identify a no conflict and a Protected Airspace Zone conflict situation. In this example, one aircraft is climbing near another aircraft. In the situation shown on the left plot, the relative motion passes behind the climbing aircraft, and no conflict results. In the situation on the right plot, the line of relative motion passes through the Protected Airspace Zone, and a violation of conditions i) and ii) identifies a conflict.

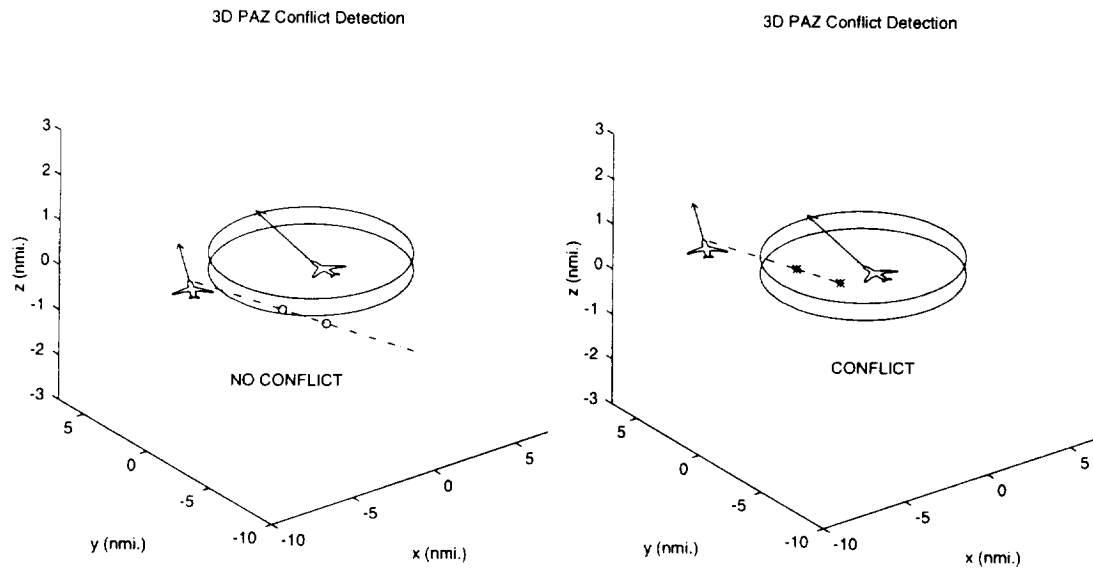


Figure 25. Conflict detection for a climbing aircraft (located at the origin) and a level aircraft (located to the upper left of the center aircraft). The intercept location of the line of relative motion with the Protected Airspace Zone is identified with a (○) if there is no conflict (left figure) or with a (\*) if there is a conflict (right figure) at the upper and lower separation standard altitudes.

### 3.7 Applying Conflict Detection to Intent Data

In general, Free Flight policy will not require a full flight plan that indicates all the waypoints to a destination, but may require a shorter list of waypoints describing intent data. Intent data may include a single waypoint or several waypoints (if known) extending perhaps 10 to 20 minutes into the future from an aircraft's current state. Assuming that the waypoints describe a piecewise linear description of the intent of each aircraft for the immediate future, the two-dimensional or three-dimensional conflict detection criteria can be applied to segments connecting waypoints that correspond to overlapping time intervals. Starting with the first segment of each aircraft defined by the current position and the first waypoint, conflict detection is performed. If a conflict occurs with a time to conflict  $\tau$  before each aircraft reaches their first waypoint, then conflict resolution advisories are

given. If the time to conflict  $\tau$  occurs after either of the first waypoints, the conflict may not occur, since the change in flight paths may resolve the conflict. In this case, the next segment in between waypoints of intent data is considered. Waypoint arrival times may not be synchronized between aircraft, so segments between waypoints may represent different time intervals. Only segments with overlapping time intervals are compared.

Note that this is a deterministic approach. To account for increasing uncertainty of aircraft positions with time, a growing position error covariance envelope may be applied to each aircraft's nominal position, as projected by the intent data. This is discussed further in the implementation issues in Chapter 6.

### 3.8 Proximity Management for Multiple Aircraft

As alluded to in Chapter 2, a proximity management system for aircraft is likely to play an important role in the system architecture. A proximity management system maintains spatial-temporal information for all aircraft. As shown in Figure 26, a Proximity Management system can use navigation data based on radar, FMS outputs, and GPS to establish the location of nearby aircraft. Intent information may be derived from flight plan data for the far term and FMS, radar, or GPS data for the near term. The size and shape of the sector considered may be determined through either range criteria or from dynamic density criteria. Two proximity management methods are considered: a horizontal decomposition method based on two-dimensional Delaunay Triangulations for aircraft at the same flight level, and a three-dimensional Delaunay Triangulation method covering all flight levels. Delaunay Triangulations [PS85, OBS92] are spatial data structures from computational geometry that allow for rapid identification of nearest neighbors. For nearby air traffic, aircraft are represented as points in the triangulation, and edges identify nearest neighbors, as shown in Figure 27.

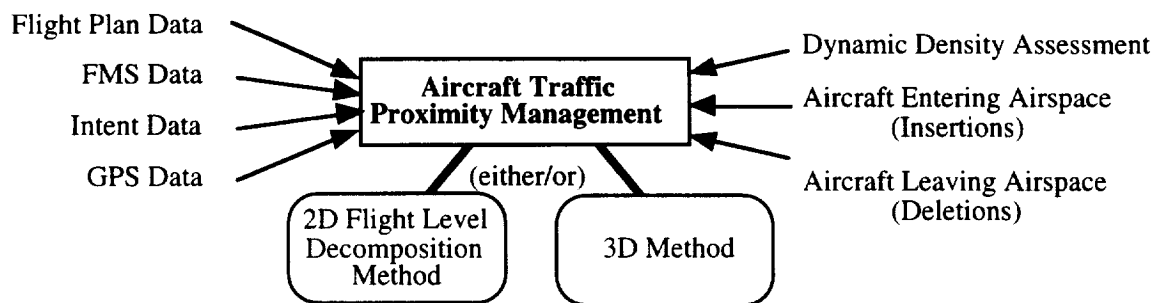


Figure 26. A Proximity Management System.

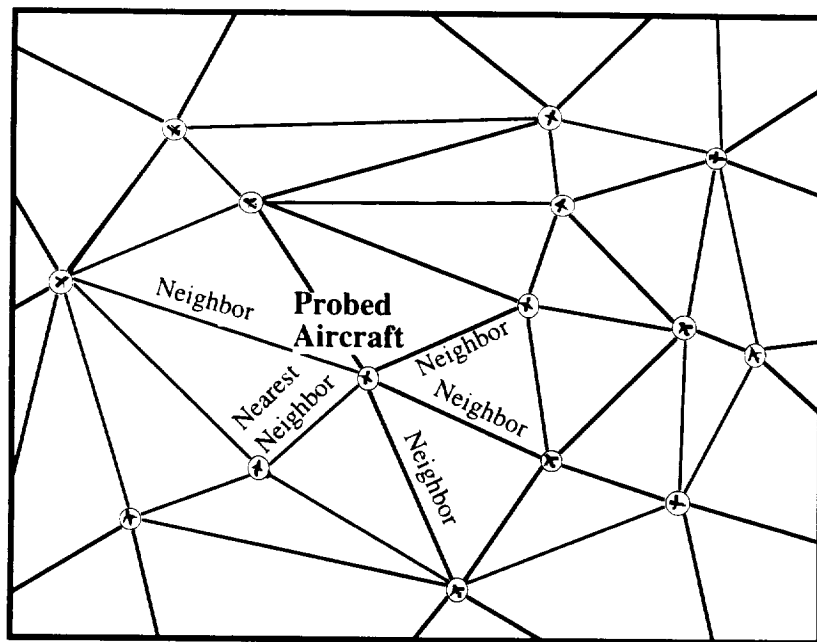


Figure 27. A Delaunay Triangulation of  $N$  aircraft at a constant flight level.

A Conflict Detection system works with Proximity Management to identify conflicts based on future Alert Zone and Protected Airspace Zone overlaps, and can be used to determine the effects of conflict resolution strategies on neighboring aircraft. For tactical conflict detection, the Delaunay Triangulation can be used to detect future Protected Airspace Zone overlaps by identifying future Delaunay Triangulation edges that will be shorter than the horizontal separation standard length. For Alert Zone overlaps, further conditions are applied due to the dependence of the Alert Zone on speed, heading difference, and range (discussed in detail in Chapter 4). For the future time analysis, the Delaunay Triangulation is advanced forward in time to detect future conflicts by looking at projected future positions from tracking data, flight plans, and aircraft intent data.

One appropriate proximity management method is based on the Delaunay Triangulation for points in a two-dimensional geometric plane. A triangulation is a straight line graph partitioning of a set of  $N$  points such that no two edges intersect at any point other than the  $N$  data points. The Delaunay Triangulation has the additional property that the circumcircle of any triangle in the triangulation contains no point (in the set of  $N$  points) in its interior. Given four points  $A$  located at  $(x_A, y_A)$ ,  $B$  located at  $(x_B, y_B)$ ,  $C$  located at  $(x_C, y_C)$ , and  $D$  located at  $(x_D, y_D)$ , the test to identify if point  $D$  is within the circumcircle defined by points  $A$ ,  $B$ , and  $C$  is determined by the criterion [GS85]:

$$\begin{vmatrix} x_A & y_A & x_A^2 + y_A^2 & 1 \\ x_B & y_B & x_B^2 + y_B^2 & 1 \\ x_C & y_C & x_C^2 + y_C^2 & 1 \\ x_D & y_D & x_D^2 + y_D^2 & 1 \end{vmatrix} > 0. \quad (64)$$

Equation (64) must hold for all triangles defined by the points  $A$ ,  $B$ , and  $C$  in the Delaunay Triangulation.

Several algorithms exist for constructing Delaunay Triangulations. When considering a set of aircraft at a constant flight level, the Delaunay Triangulation of a set of points in the (geometric) plane is applicable [FP93, LS80, OBS92]. The iterative solution of [LS80] provides a means for introducing new aircraft to (or removing existing aircraft from) an already existing triangulation, say for instance when an aircraft step climbs to a new flight level.

An example of how the Delaunay Triangulation provides proximity management for a set of aircraft within a constant flight level follows. Figure 28 illustrates the Delaunay Triangulation for a set of aircraft composed of two streams of traffic. In addition to the aircraft, four sector corners are used as stationary points in the Delaunay Triangulation to identify the proximity of the aircraft to the sector boundaries. As the aircraft progress forward, the Delaunay Triangulation changes. At any given instant, though, the nearest neighbors of any aircraft can be identified by the edges in the Delaunay Triangulation. If a conflict occurs, the effect a conflict resolution maneuver has on neighboring aircraft can be evaluated, as discussed in Chapter 4 and 5.

A second appropriate proximity management method is based on the Delaunay Triangulation defined for points in a three-dimensional Euclidean space. Delaunay Triangulation algorithms for three dimensions are described in [OBS92]. For dynamic data, the method of [AMGR91] applies. At the extreme, the Delaunay Triangulation of a million points may be computed, as claimed by [SuI92]. However, a practical partitioning of a flight level into dynamic sectors may break down the set of aircraft to orders of tens to hundreds.

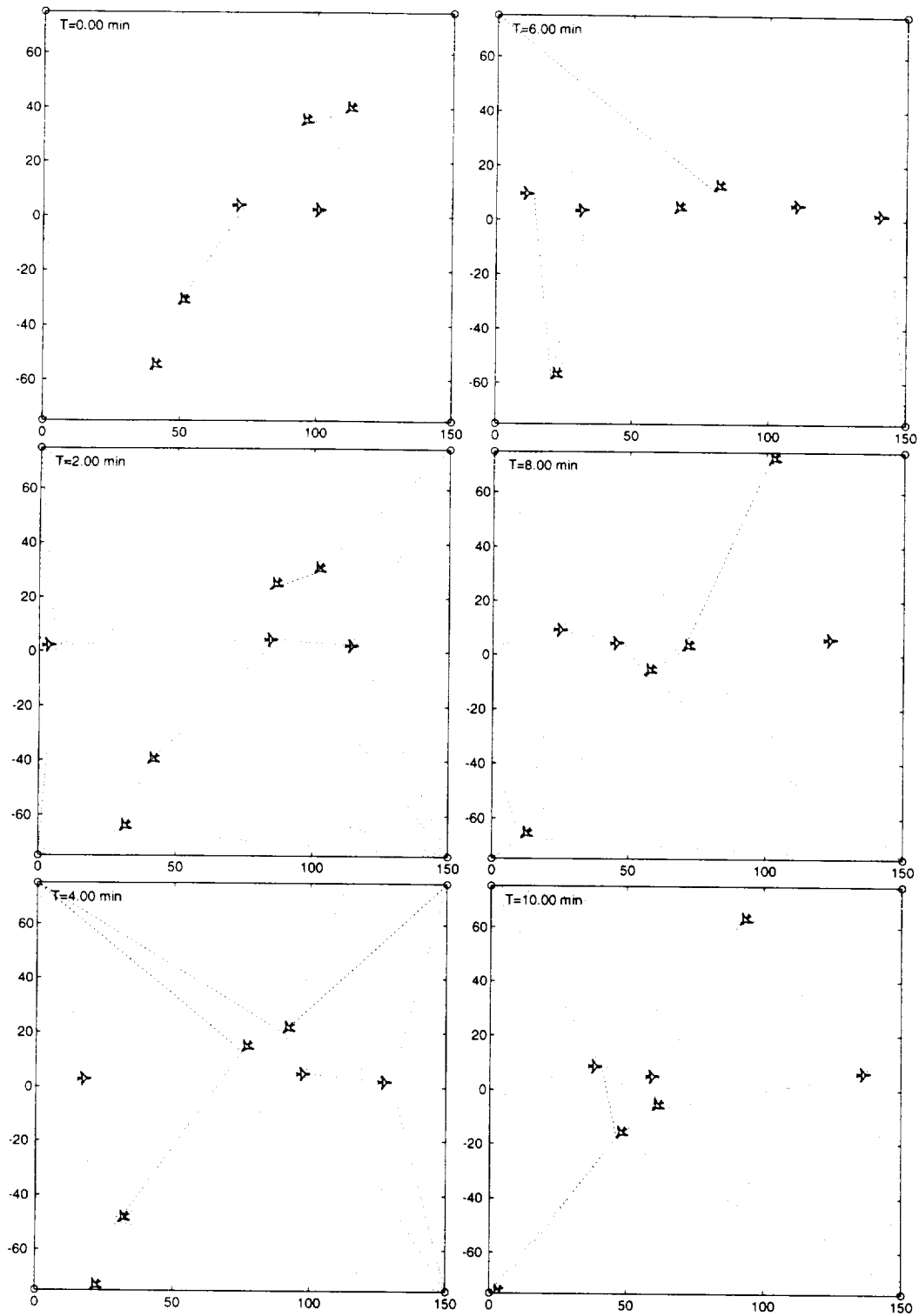


Figure 28. Proximity management of aircraft at a constant flight level. Each window depicts a snapshot of the Delaunay Triangulation at 2 minute intervals.



## 4. TACTICAL CONFLICT RESOLUTION

In this chapter, tactical conflict resolution strategies are investigated. A tactical encounter uses safety as the primary criterion for trajectory synthesis. Tactical maneuvers are derived so that the range at the point of closest approach is maximized by using heading, speed, or altitude maneuvers. In Free Flight, datalink will allow complete state information about nearby aircraft to be used in the execution of optimal tactical maneuvers without knowledge constraints. The need for tactical maneuvers should be limited to instances of hardware failure or procedural non-adherence. This is because precautionary actions should be taken to resolve the potential conflict long before the tactical maneuver envelope is encroached, at a time where decisions are considered to be strategic.

The objectives of our tactical encounter research are: to evaluate different tactical maneuvers for arbitrary initial orientations, to define a logical set of “rules-of-the-road” for conflict resolution, to identify a tactical alert zone definition, and to evaluate how reduced separation requirements affect the tactical maneuvers.

### 4.1 Tactical Heading Control Maneuvers

For horizontal maneuvers, we consider the problem of maximizing the range at the point of closest approach, where both aircraft may execute maximum turn rate heading maneuvers. Coordinated turns are used for heading maneuvers. In a coordinated turn, the motion remains in the horizontal plane, with no descent rate; the steady turn rate  $\omega$  is defined by the relationship:

$$\omega = \dot{\Psi} = \frac{g}{v} \tan \Phi \quad (65)$$

where  $\dot{\Psi}$  is the rate of change of the heading  $\Psi$ ,  $g$  is the gravitational acceleration,  $v$  is the airspeed, and  $\Phi$  is the bank angle relative to the horizontal plane. The maximum bank angle is determined by either the maximum acceptable load factor for passenger comfort or the maximum lift:

$$L_{\max} = \frac{1}{2} \rho v^2 S C_{L_{\max}} \quad (66)$$

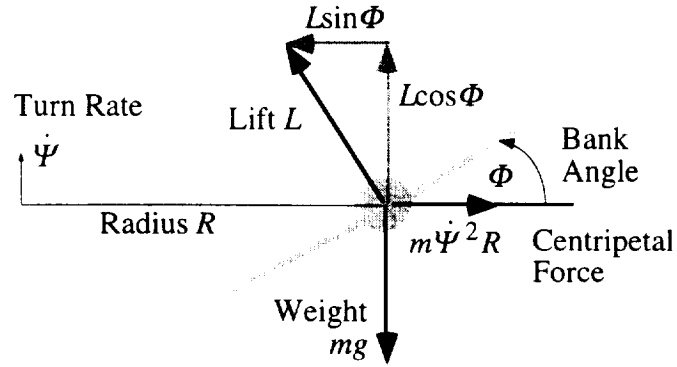


Figure 29. The geometry and forces of the coordinated turn.

where  $\rho$  is the atmospheric density,  $S$  is the wing planform area, and  $C_{L_{\max}}$  is the maximum lift coefficient. In a coordinated turn, the weight of the aircraft balances the lift as shown in Figure 29. The relationship between the weight  $mg$  and lift  $L$  is:

$$mg = L \cos \Phi \quad (67)$$

where  $m$  is the total mass of the aircraft. Combining equations (66) and (67) gives the maximum bank angle:

$$|\Phi_{\max}| = \cos^{-1} \left\{ \frac{2mg}{\rho v^2 S C_{L_{\max}}} \right\} \quad (68)$$

which, when used in equation (65), determines the maximum turn rate for a maximum bank maneuver. Additionally, in a coordinated turn the centripetal acceleration results from the horizontal component of lift:

$$m\dot{\Psi}^2 R = L \sin \Phi \quad (69)$$

where  $R$  is the turn radius. By combining equations (65), (67), and (69), the turn radius  $R$  can be expressed as:

$$R = \frac{v^2}{g \tan \Phi}. \quad (70)$$

Finally, the minimum turning radius  $R_{\min}$  is obtained from equation (70) when flying at the maximum bank angle  $\Phi_{\max}$ .

The role response for commanded bank angles has fairly quick dynamics for most aircraft. For most commercial aircraft, a 2 to 5 second rise time (time to reach 90% of maximum) can be realized for roll (bank) maneuvers. For example, in Figure 30 an investigation of the dynamics of the Boeing 737 aircraft indicates that the rise time is roughly 3.7 seconds to bank from steady level flight to a 45° bank angle. In general, individual pilots will maneuver to different maximum bank angles based on the conflict situation and level of experience. Additionally, the level of comfort for the passengers degrades as higher bank angles are commanded, so there is a tendency to limit bank angles to no more than 40° to 45° under tactical maneuvers or from 20° to 30° for strategic maneuvers. A turn rate of 3°/sec is typical in the terminal area. In terms of modeling heading maneuvers, quick changes in bank angle may be approximated as step changes. Transients in the bank angle step response can be accounted for by considering at least a 2 to 5 second lead time prior to initiating a maneuver. For the Boeing 737 example, Figure 31 compares the trajectory resulting from a step change in bank angle to a trajectory with simulated aircraft dynamics. When the maneuver is initiated with sufficient lead time, the resultant dynamics matches the instant bank maneuver quite well. Conflict advisories can be given with sufficient lead times to account for these transients.

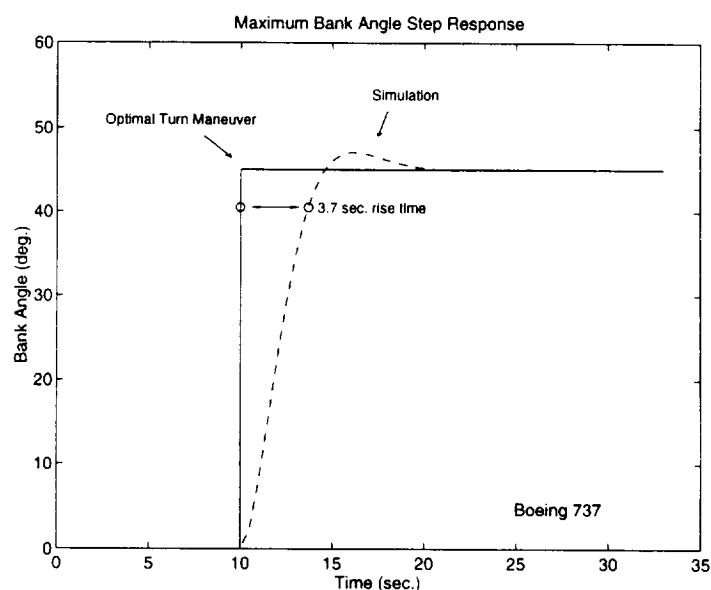


Figure 30. Maximum bank angle step response for a Boeing 737 aircraft.

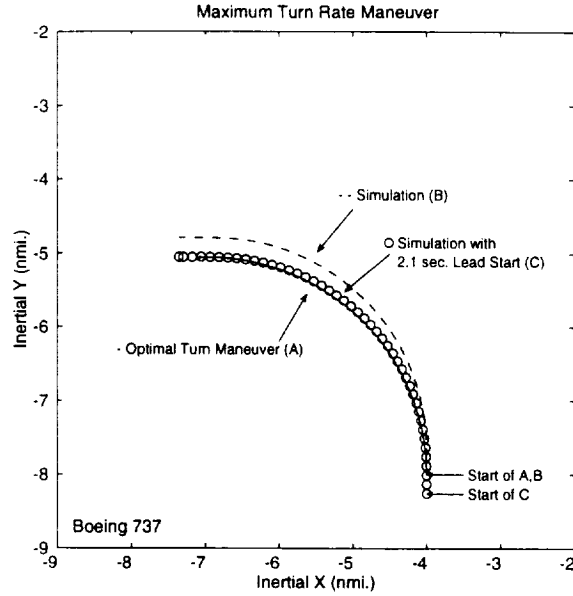


Figure 31. A comparison between the modeled optimal maneuver and a simulation for a Boeing 737 aircraft, and the effects of starting the maneuver with sufficient lead time to offset the dynamics transients.

The tactical conflict resolution strategy is the result of an optimization problem: Determine the turn rates  $\omega_A$  and  $\omega_B$  as functions of the relative motion state  $(r, \phi, \theta)$  such that the minimum range distance is maximized. The cost function  $J = r(t_f)$  is simply the range  $r$  at the point of closest approach, occurring at the final time  $t_f$ . Euler-Lagrange equations [Mer73, BH75] are used to solve for the tactical conflict resolution. In general, to minimize the cost function:

$$J = \varphi(x(t_f), t_f) \quad (71)$$

for a system with time domain  $t_0 \leq t \leq t_f$ , a set of coupled state and co-state equations must be solved:

$$\text{State:} \quad \dot{x} = f(x, u, t) \quad (72)$$

$$\text{Co-State:} \quad \dot{\lambda} = -\frac{\partial H}{\partial x} \quad (73)$$

with the controls  $u$  determined by:

Controls: 
$$\frac{\partial H}{\partial u} = 0 \quad (74)$$

subject to the initial conditions:  $x(t_0)$  and final conditions:  $\lambda(t_f) = \frac{\partial \varphi}{\partial x} \Big|_{t_f}$ . The

Hamiltonian function is defined as:

$$H = \lambda^T f = \lambda^T \dot{x}. \quad (75)$$

A two point boundary value problem results since the state is known at the initial time and the co-state is known at the final time.

Optimal maneuvers are obtained by solving the Euler-Lagrange equations for cooperative and non-cooperative cases. When the own aircraft A and intruder aircraft B have the same speed and the same maximum turn rate, analytic results for the Euler-Lagrange Equations may be found, as shown by [Mer73]. However, in general there is no closed form analytic solution to the described optimization problem. In any of these cases, though, numerical methods may be applied to construct maneuver charts giving the turn rates  $\omega_A$  and  $\omega_B$  as functions of the relative motion state  $(r, \phi, \theta)$ .

Example maneuver chart results are given in Figure 32. Maneuver charts are shown for the cooperative case when the own aircraft A and intruder aircraft B have the same speed and the same maximum turn rate. These results were computed using the analytic equations from [Mer73]. Further maneuver charts (not shown here) are computed using numerical methods for non-cooperative cases ( $\omega_B=0$ ), and for cases where the two aircraft have unequal speeds and turn rates. Given the relative motion state  $(r, \phi, \theta)$ , the location in the maneuver chart immediately identifies the cooperative maneuver, which is identified with the notation  $A_R$  for aircraft A turns Right,  $A_L$  for aircraft A turns Left,  $B_R$  for aircraft B turns Right, and  $B_L$  for aircraft B turns Left. The maneuver chart also indicates the maximum miss distance that can be achieved, and a zero range rate line, for which no maneuver is necessary once crossed.

An example trajectory of two aircraft performing an optimal tactical conflict resolution is shown in Figure 33. In this case, the start location of the intruder aircraft falls in the  $A_L B_L$  region of the maneuver chart, as shown in Figure 34, indicating that both aircraft should perform left turns for an optimal conflict resolution. Left turns should be applied until the relative position of the intruder aircraft B crosses the zero range rate line.

This is the point of closest approach, and after crossing it, the range rate becomes positive. In the maneuver chart, distances are normalized with respect to the turning radius of aircraft A. As shown in the maneuver chart, the maneuver follows a level curve near the value of 1.5, indicating that the point of closest approach will be slightly less than 1.5 times the turning radius of aircraft A. For this example, during the entire maneuver, the heading difference remains fixed at  $90^\circ$ , and one maneuver chart, the one shown in Figure 34, is applied throughout the maneuver. However, if the initial conditions were chosen such that the intruder aircraft fell in the  $A_R B_L$  region of the maneuver chart shown in Figure 34, then as these aircraft performed their right and left turns, the heading difference would have decreased to zero; several maneuver charts for fixed heading differences varying from  $90^\circ$  to  $0^\circ$  would have been consulted.

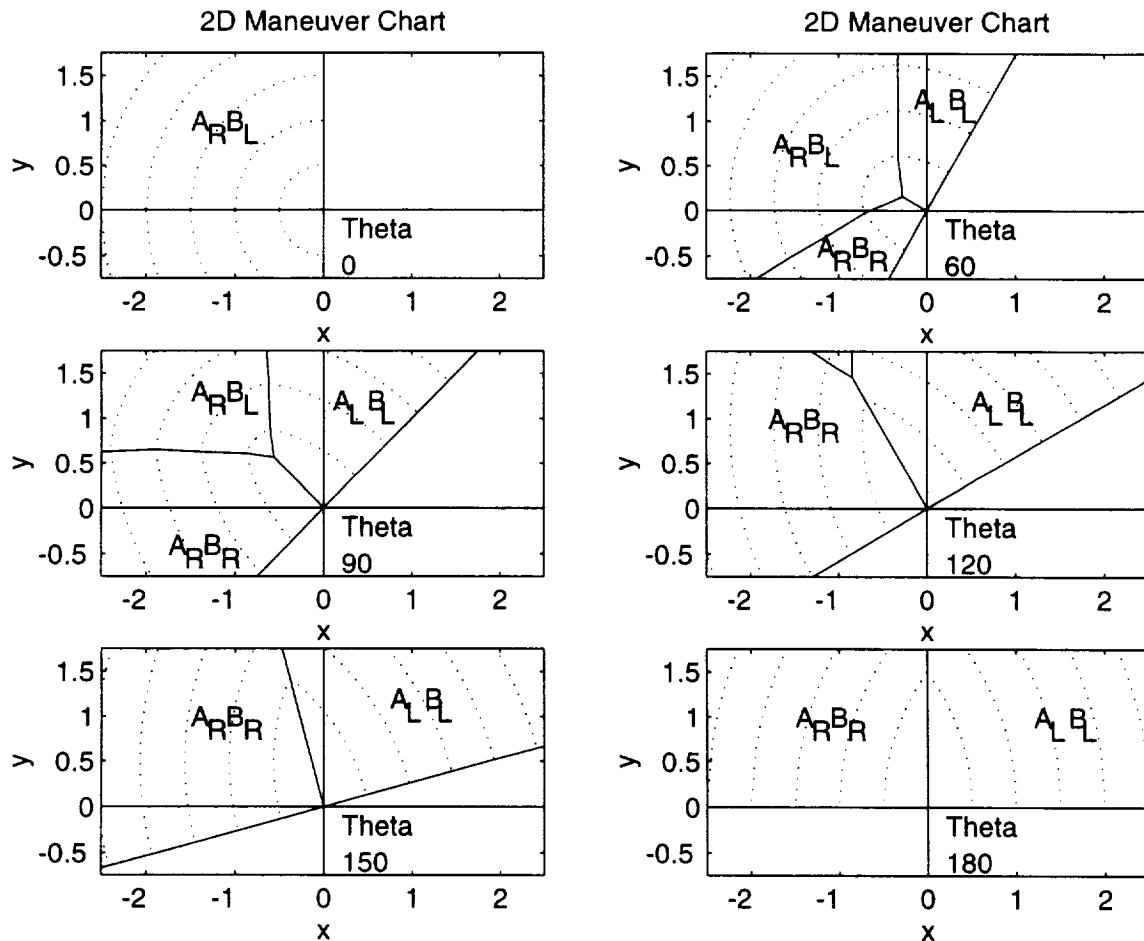


Figure 32. Maneuver Charts for maximum range (cooperative case; speed ratio  $\gamma = 1$ ; and equal turn radii).

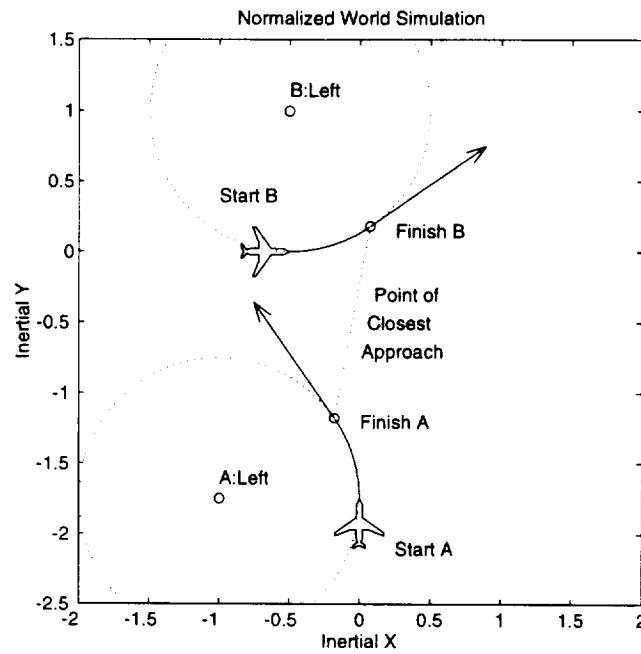


Figure 33. Optimal tactical conflict resolution example (cooperative case, speed ratio  $\gamma = 1$ , and equal turn radii).

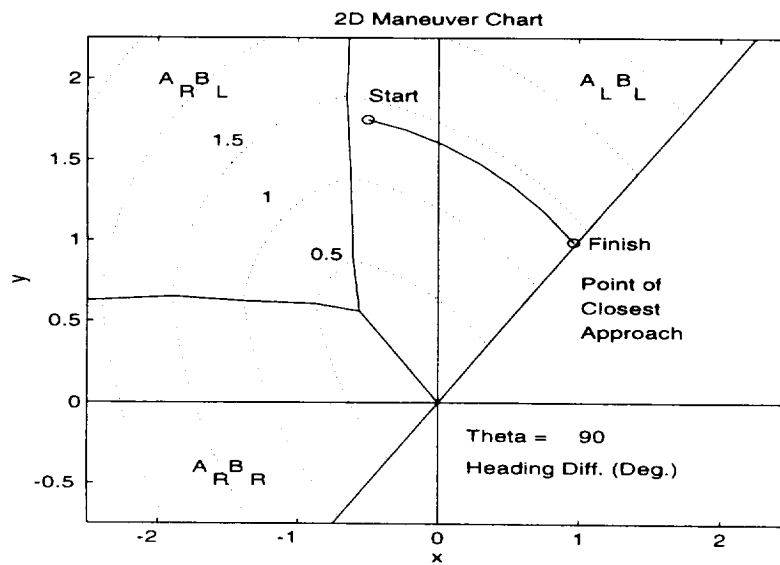


Figure 34. The maneuver chart consulted for the optimal tactical conflict resolution example of Figure 33 (cooperative case, speed ratio  $\gamma = 1$ , and equal turn radii).

Dynamic programming or numerical integration techniques may be implemented to solve non-equal velocity cases. For example, dynamic programming can be applied to the non-cooperative case for non-equal velocities as shown in Figure 35. In Figure 35, the envelope of feasible maneuvers is shown; candidate solutions include a turn followed by a straight line dash until the point of closest approach is reached. The optimal maneuver is identified from the set of candidate solutions. In some cases, more than one optimal solution may result, as shown in Figure 36, where three optimal solutions are shown. Repeated implementation of this algorithm establishes the maneuver charts for non-cooperative cases at a specified speed ratio. An example maneuver chart for a non-cooperative case is shown in Figure 37.

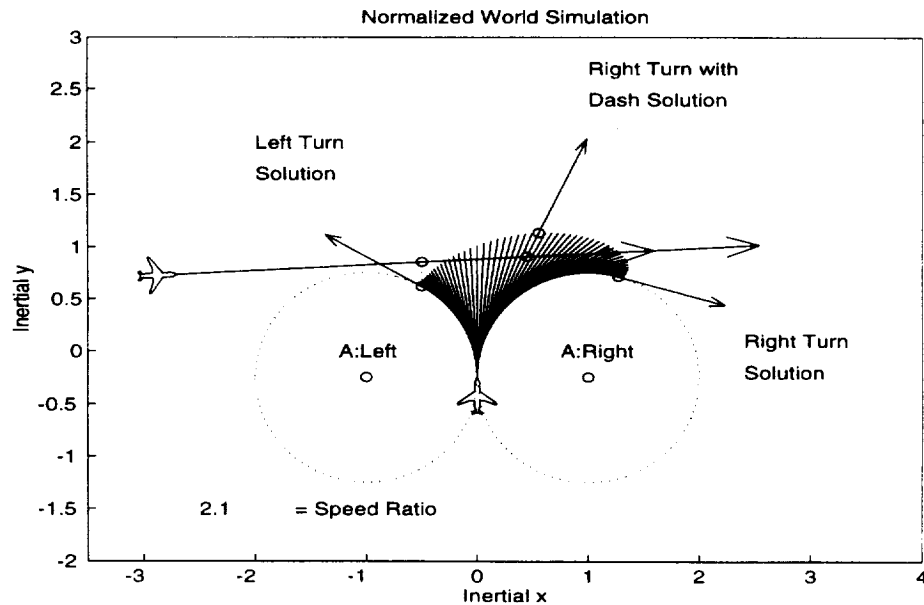


Figure 35. The dynamic programming search envelope for a non-cooperative case (speed ratio  $\gamma = 2.1$ ).

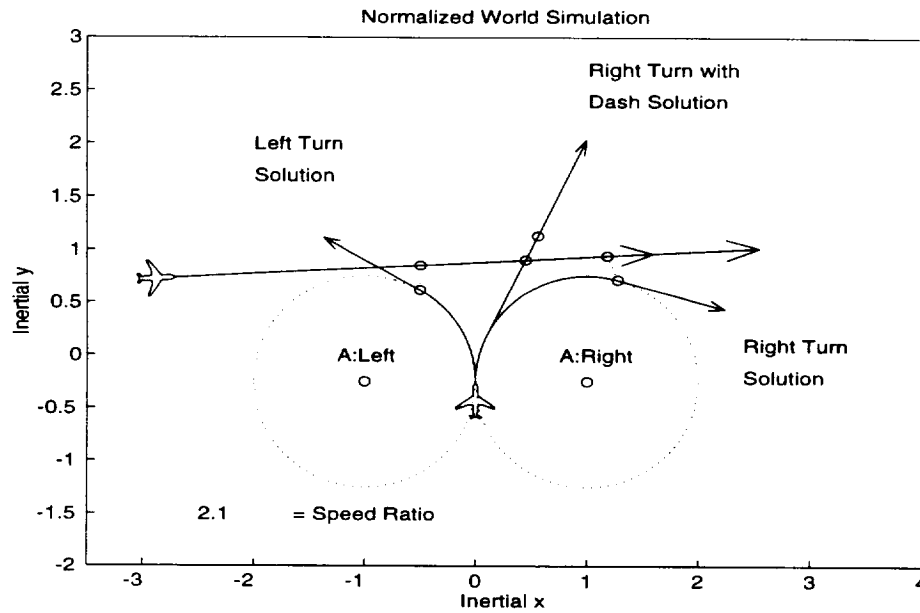


Figure 36. The three optimal maneuvers for the non-cooperative case of Figure 35 (speed ratio  $\gamma = 2.1$ ); circles highlight the points of closest approach for each of these three optimal maneuvers.

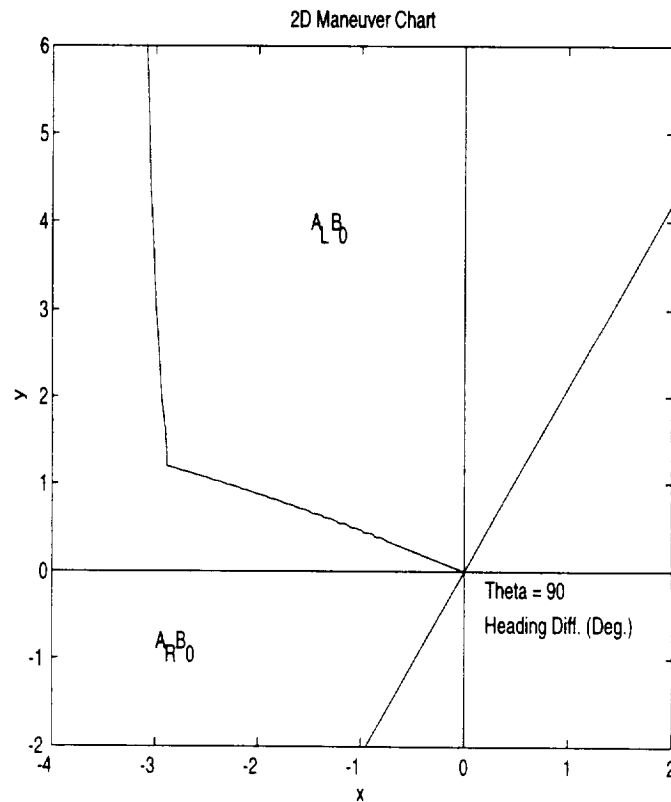


Figure 37. The maneuver chart for optimal tactical heading maneuvers for a non-cooperative case (heading difference  $\theta = 90^\circ$ , speed ratio  $\gamma = 2.1$ ).

Maneuver charts provide a generalization of optimal maneuvers given arbitrary initial conditions. One particular set of initial conditions establishes a Tactical Alert Zone. There exists a locus of points for which the initial conditions produce tactical maneuvers that have the same range of 5 nmi at closest approach, which under today's regulations, constitutes the Protected Airspace Zone. Under these conditions, for cooperative and non-cooperative cases, maneuver charts identify a Tactical Alert Zone on the surface of which the optimal tactical conflict resolution must be initiated in order not to penetrate the Protected Airspace Zone of the intruder aircraft, as shown in Figure 38. The result is not a circular or elliptic Alert Zone, as depicted in Figure 1, but is dependent on the speed ratio, range, angle-off, and heading difference. Outside this locus of points, the own aircraft may initiate a maneuver that maximizes the miss distance, at one extreme, or a maneuver that results in a trajectory that grazes the Protected Airspace Zone, at the other extreme. These extremes are referred to as the upper and lower bounds of tactical conflict resolution maneuvers.

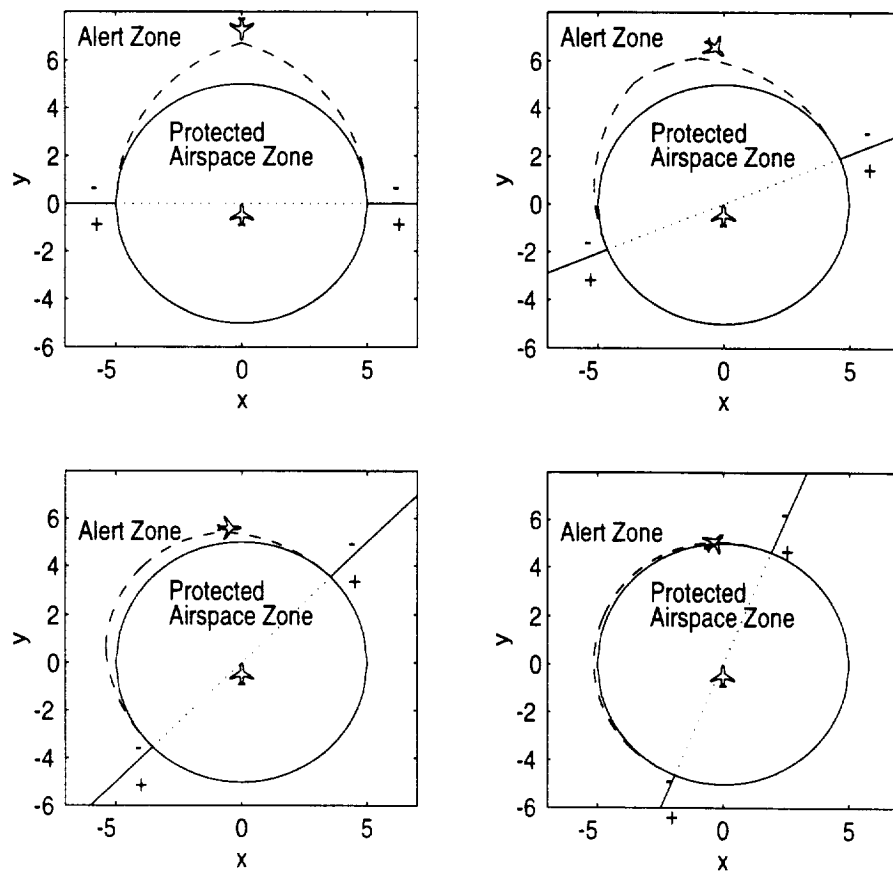


Figure 38. The Tactical Alert Zone: the locus of points for which a cooperative maneuver must be initiated in order to avoid penetrating the Protected Airspace Zone (note: +/- indicates the sign of the range rate near the zero range rate line).

Consider next the recovery trajectories required to bring both aircraft from the point of closest approach back to their original flight plans. Maximum bank angle maneuvers are not necessary for returning both aircraft on track after a tactical evasive maneuver. Instead, recovery maneuvers may be implemented using standard bank angles.

Recovery maneuvers must be coordinated so that stalemate conditions do not occur. As shown in Figure 39, when two aircraft initiate an optimal conflict resolution, they may end up in final conditions that may or may not allow for each aircraft to simply turn back to its original heading without an additional conflict occurring. The stalemate condition can last indefinitely if the two aircraft have equal speeds. If the speeds are not equal, then the slower aircraft can perform a backside maneuver to recover while the faster aircraft performs a frontside maneuver.

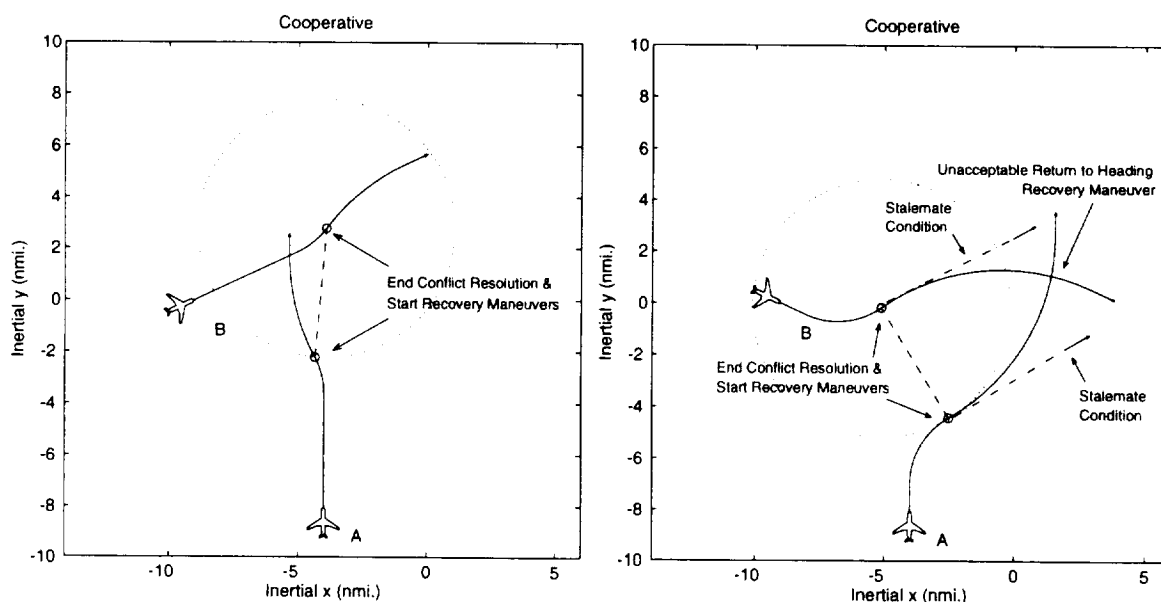


Figure 39. Two optimal conflict resolution maneuvers have final conditions that pose a simple recover trajectory (left) and a stalemate condition (right).

## 4.2 Tactical Speed Control Maneuvers

For horizontal speed control maneuvers, we consider the problem of maximizing the range at the point of closest approach, where one or both aircraft may execute optimal speed controls using maximum acceleration and an upper speed limit or maximum deceleration and a lower speed limit. Under speed control, the headings of both aircraft are

held constant, so the paths remain the same while the trajectories vary. Thus, speed control has the desirable feature that the aircraft need not deviate from their original flight paths. Since predicting which portions of the airspace will remain free of aircraft is easier when aircraft are not turning, workloads may be reduced for air traffic controllers and pilots. On the other hand, speed changes take a long time, so speed control maneuvers must be performed at fairly long ranges.

For most aircraft, the speed response has fairly slow dynamics in comparison to heading and altitude dynamics. For example, in Figure 40 an investigation of the dynamics of the Boeing 737 indicates that the time to accelerate to higher speeds is in the order of 2 to 3 minutes, and in the time to decelerate to slower speeds is in the order of a minute. For the purpose of developing maneuver charts, we consider a dynamics model with acceleration and deceleration limits as well as upper and lower speed limits. Figure 40 illustrates the model used for speed profiles, which is also fitted into Figure 40. Starting at an initial speed  $v_0$ , the aircraft may accelerate at  $a_{\max}$  to the upper speed limit  $v_{\max}$ , or decelerate at  $d_{\max}$  to the lower speed limit  $v_{\min}$ . At any time while accelerating (decelerating) or while at the upper (lower) speed limit, the aircraft may reach the Point of Closest Approach PCA.

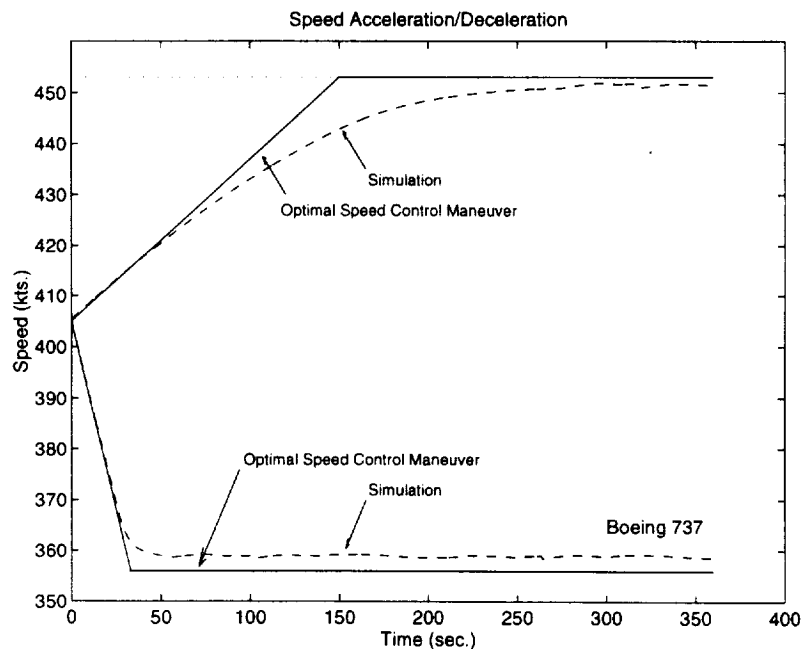


Figure 40. Maximum acceleration and deceleration responses for a Boeing 737 aircraft (34,000 ft operating condition).

A speed control conflict resolution strategy is the result of an optimization problem: Determine the speeds  $v_A$  and  $v_B$  as functions of the relative motion state  $(r, \phi, \theta)$  such that the minimum range is maximized. The payoff function is simply the range  $r$  at the point of closest approach. In general, the equations of motion are defined by equations (1) to (3), with zero turn rates, and with speed control variables  $v_A$  and  $v_B$  being chosen to follow one of the two speed profiles shown in Figure 41. Equations (1) to (3) apply for the derivation of speed control maneuvers with the turn rates  $\omega_A=0$  and  $\omega_B=0$ . Consequently, the heading difference  $\theta$  remains constant.

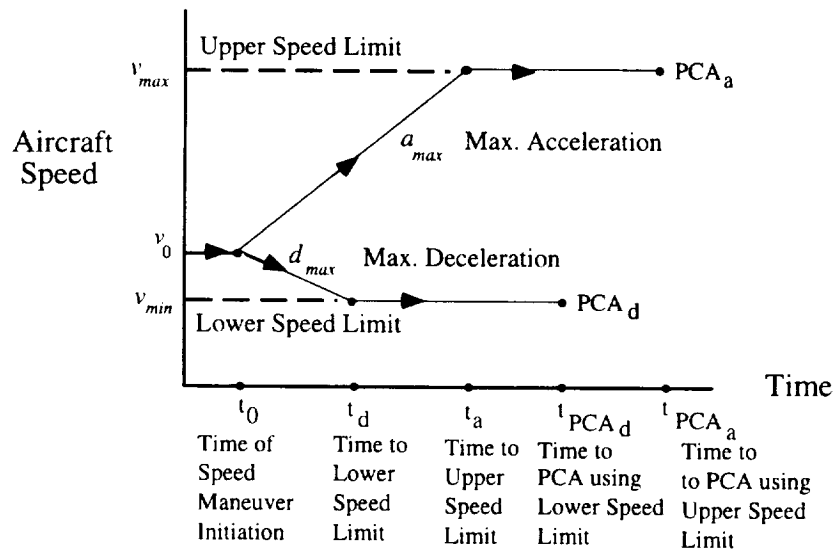


Figure 41. Each aircraft is limited by upper and lower speed limits and a maximum acceleration and deceleration.

Optimal speed control maneuvers may be obtained by solving Euler-Lagrange equations for cooperative and non-cooperative cases. We have implemented numerical methods to construct maneuver charts that indicate whether each aircraft should go faster or slower as a function of the relative motion state  $(r, \phi, \theta)$ . Speed control maneuver charts are generated for a fixed heading difference  $\theta$ , which remains constant throughout the maneuver. For non-cooperative maneuvers, the velocity of aircraft B does not change, so maneuver charts may be generated for fixed heading differences  $\theta$  and a fixed speed  $v_B$ .

Given the speed of aircraft B to be fixed at  $v_B$ , the maneuver chart identifies if aircraft A should speed up to a minimum speed ratio  $\gamma_{\min} = v_B/v_{A \max}$ , or if aircraft A should slow down to a maximum speed ratio  $\gamma_{\max} = v_B/v_{A \min}$ . For cooperative maneuvers, the optimal speeds of aircraft A and aircraft B will be either minimum and maximum, respectively, where the speed ratio becomes a minimum  $\gamma_{\min} = v_{B \min}/v_{A \max}$ , or the optimal speeds of aircraft A and aircraft B will be maximum and minimum, respectively, where the speed ratio becomes a maximum  $\gamma_{\max} = v_{B \max}/v_{A \min}$ .

The final conditions for a speed maneuver may or may not occur when one or both aircraft are at maximum or minimum speed limits. In the limiting case, both aircraft may be at their initial speeds and be oriented such that the aircraft B is located on the zero range rate line. Thus, the zero range rate line is determined by the initial velocities, rather than with the maximum and minimum velocities. For initial conditions with negative range rate close to the zero range rate line, the aircraft may reach the Point of Closest Approach with one or both of the aircraft still accelerating or decelerating to the upper or lower speed limit. In the maneuver chart, contour lines indicate the locus of points with equal maximum miss distance; initial conditions which represent points on these contour lines may have different final conditions and Points of Closest Approach. In terms of how the maneuver chart is used to guide conflict resolution, this means that during conflict resolution, the maneuver chart changes as the speeds are changing, and the maneuver chart only remains fixed when both aircraft have achieved upper or lower speed limits. Given the initial speeds of each aircraft, the maneuver chart indicates which aircraft should speed up or slow down and the final miss distance if the optimal maneuver is followed; however, the maneuver chart does not indicate the Point of Closest Approach unless the range rate is zero.

Example speed control maneuver chart results that incorporate a limited acceleration/deceleration dynamics model are given in Figures 42 through 45. Maneuver charts are shown for non-cooperative cases in Figures 42 and 43 and for cooperative cases in Figures 44 and 45. Given the relative motion state  $(r, \phi, \theta)$ , the location in the maneuver chart immediately identifies which aircraft should go faster or slower. The optimal speed is identified with the notation  $A_A$  for aircraft A to accelerate to the upper speed limit,  $A_D$  for aircraft A to decelerate to the lower speed limit,  $B_A$  for aircraft B to accelerate to the upper speed limit,  $B_D$  for aircraft B to decelerate to the lower speed limit, or  $B_0$  for aircraft B holds constant speed (the non-cooperative case). For non-cooperative maneuvers, the maneuver chart is indexed by the speed  $v_B$  of aircraft B, which is labeled on the chart. For

cooperative maneuvers, the maneuver chart is indexed by both aircraft speeds  $v_A$  and  $v_B$ . For all maneuver charts shown, the upper speed limit for both aircraft is  $v_{\max} = 550$  kts, and the lower speed limit for both aircraft is  $v_{\min} = 350$  kts. The maximum acceleration is  $a_{\max} = 1$  kt/sec and the maximum deceleration is  $d_{\max} = 1$  kt/sec. (These speeds and acceleration limits are parameters that can be changed for other scenarios.) The maneuver chart also indicates the optimal miss distance contours for odd distances (1,3,5, ... nmi) that can be achieved if the optimal maneuver is applied, and a zero range rate line (indicated by + for positive and - for negative range rate), for which no maneuver is necessary once crossed.

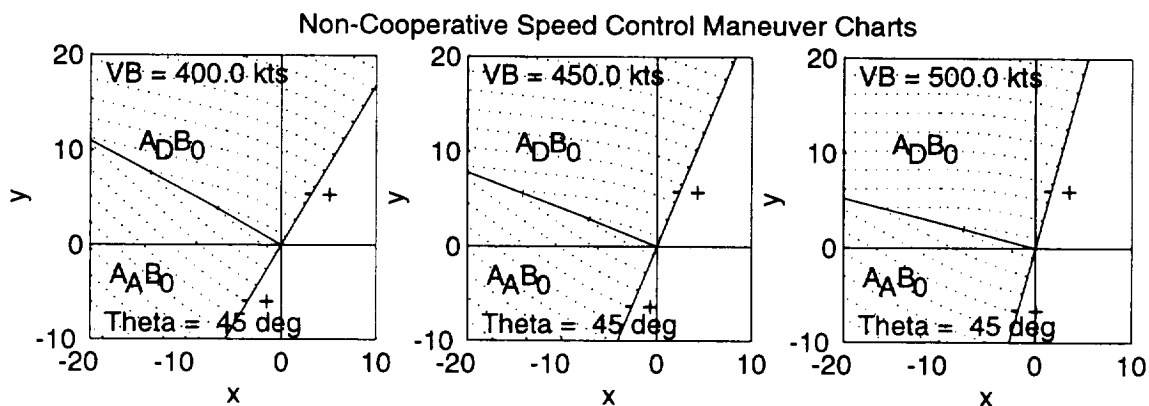


Figure 42. Speed control maneuver charts incorporating a limited acceleration/deceleration model; fixed maneuver heading difference and varying speeds for Aircraft B (non-cooperative case).

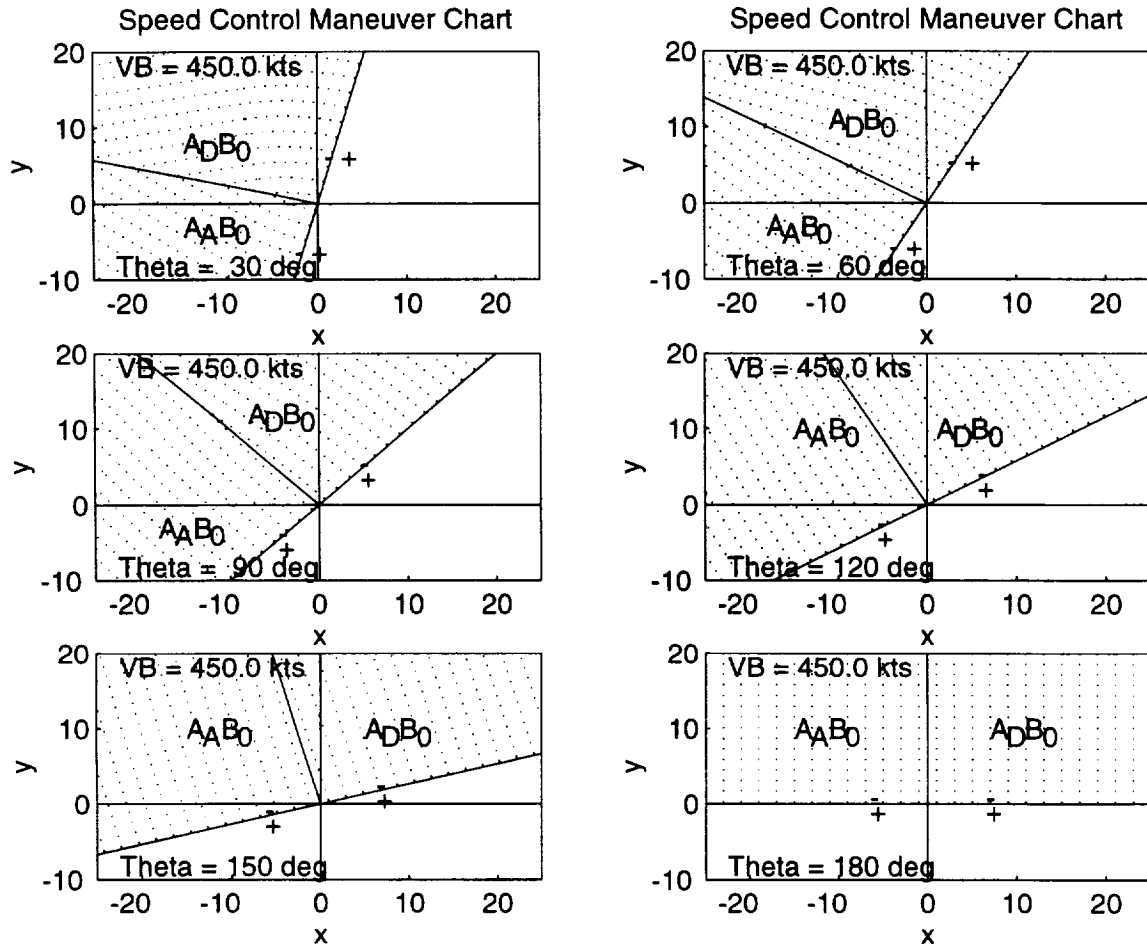


Figure 43. Speed control maneuver charts incorporating a limited acceleration/deceleration model considering different maneuver heading differences (non-cooperative case).

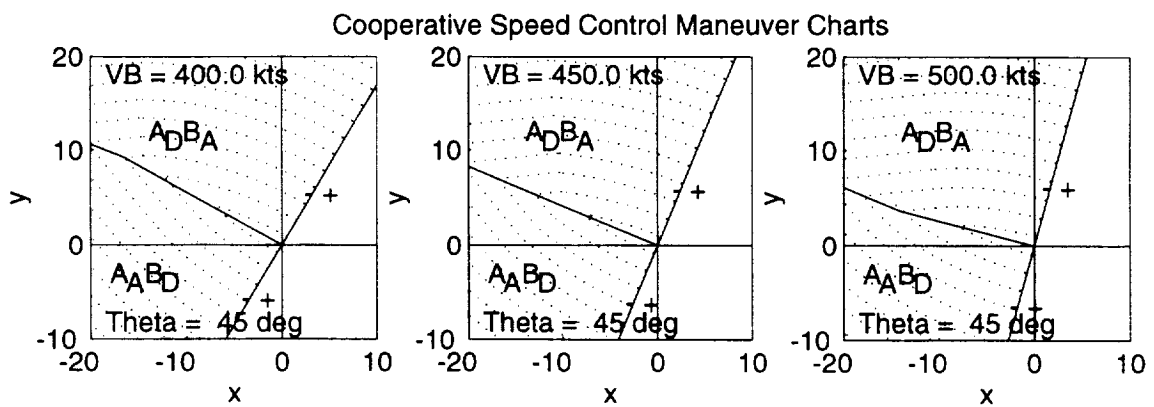


Figure 44. Speed control maneuver charts incorporating a limited acceleration/deceleration model; fixed maneuver heading difference and varying speeds for Aircraft B (cooperative case;  $v_{A0} = 450$  kts).

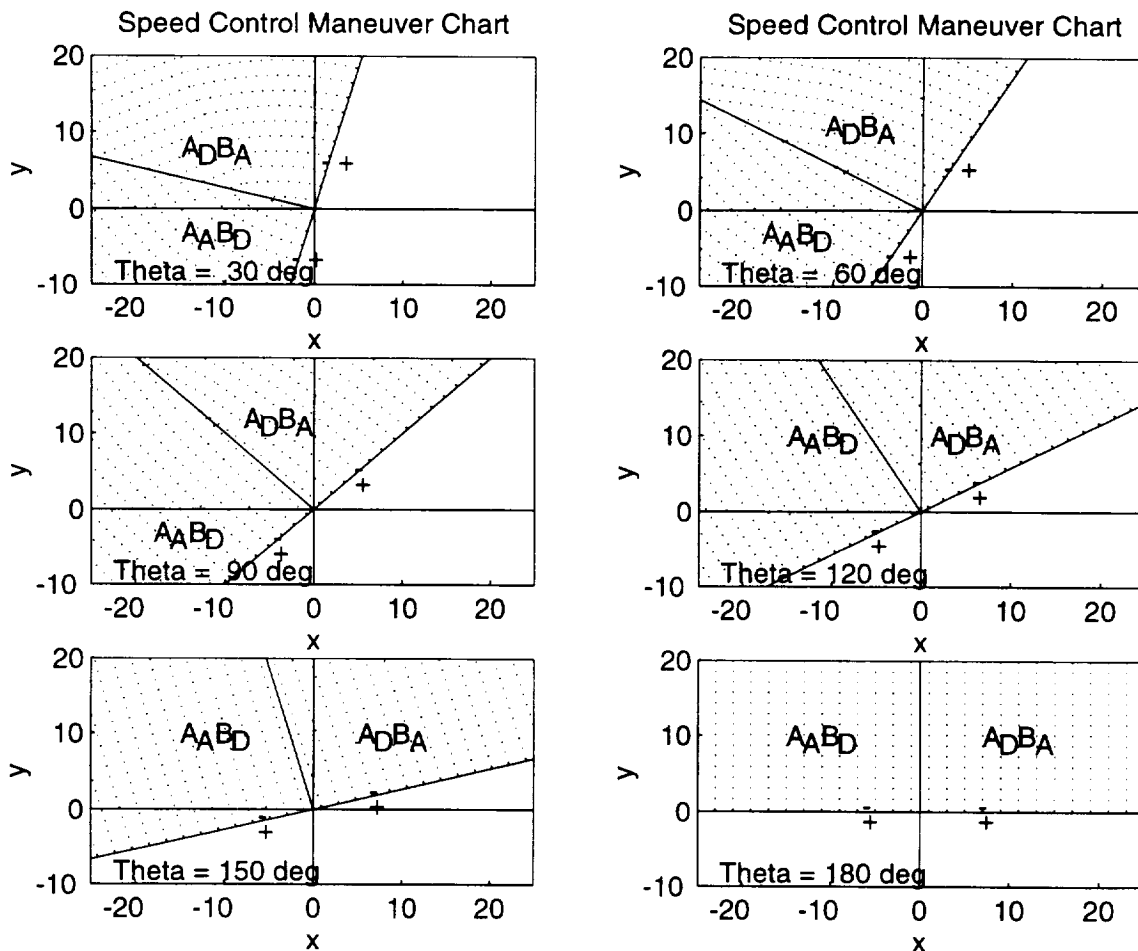


Figure 45. Speed control maneuver charts incorporating a limited acceleration/deceleration model considering different maneuver heading differences (cooperative case;  $v_{A0} = 450$  kts and  $v_{B0} = 450$  kts).

As was shown for heading maneuvers, one particular set of initial conditions establishes a Tactical Alert Zone (TAZ). There exists a locus of points for which the initial conditions produce tactical speed maneuvers that all have the same range of 5 nmi at closest approach, which under today's separation standards, constitutes the Protected Airspace Zone. Under these conditions, for cooperative and non-cooperative cases, maneuver charts identify a TAZ on the surface of which the optimal tactical conflict resolution must be initiated in order not to penetrate the Protected Airspace Zone of the intruder aircraft. Figure 41 shows the TAZ for both non-cooperative and cooperative cases. Notice also that the TAZ for heading maneuvers is considerably smaller than the TAZ for speed maneuvers (cf. Figure 38 and Figure 46). As was the case for heading maneuvers, the TAZ result is not a circular or elliptic Alert Zone, as depicted in Figure 1, but is dependent on the speed ratio, range, angle-off, and heading difference.

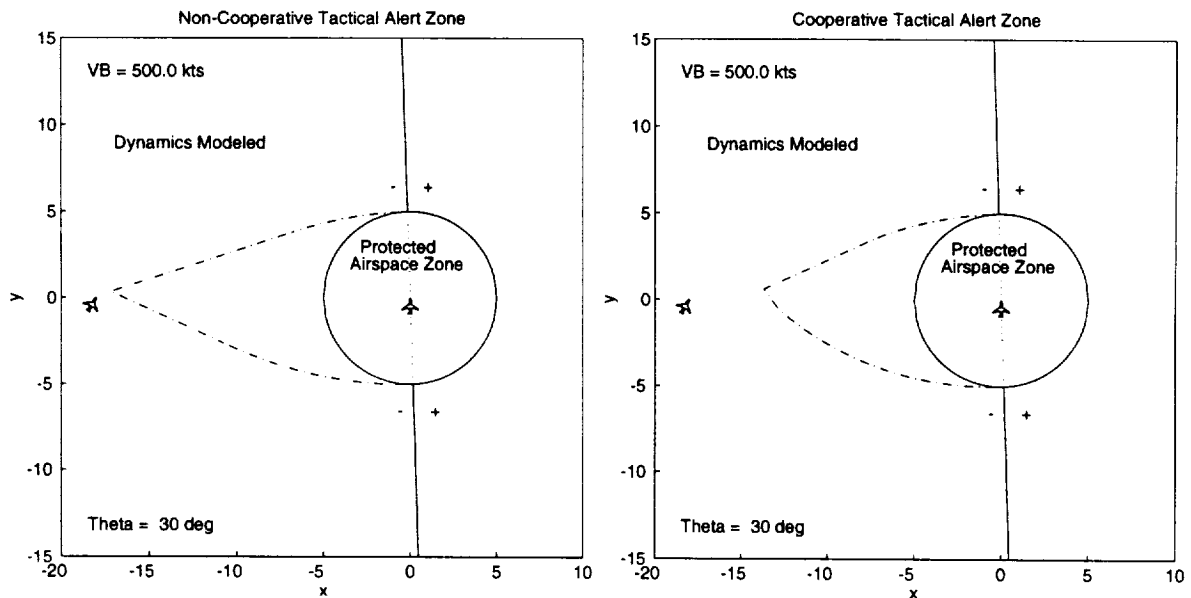


Figure 46. A non-cooperative (left) and cooperative (right) Tactical Alert Zone: the locus of points for which a maneuver must be initiated in order to avoid penetrating the Protected Airspace Zone (+/- indicates the sign of the range rate,  $v_{A0} = 425$  kts,  $v_{B0} = 500$  kts).

Recovery trajectories bringing both aircraft from the point of closest approach back to their original flight plans include simple accelerations or decelerations. Since both aircraft finish the speed control maneuver with positive range rate, and since both aircraft do not change their heading during the maneuver, the recovery maneuver is simply to accelerate or decelerate back to the original time schedule for each aircraft. No further conflicts or stalemate conditions may result. Alternatively, each aircraft can return to their original speeds at any rate of acceleration or deceleration or can accept the delay in time (if the aircraft decelerated during the conflict resolution maneuver) or advance in time (if the aircraft accelerated during the conflict resolution maneuver) from their original schedule.

### 4.3 Tactical Altitude Control Maneuvers

For altitude control maneuvers, we consider the problem of maximizing the vertical range with sufficient clearance of the Protected Airspace Zone. One or both aircraft may execute optimal climb or descent controls using maximal climb and descent rates. Under altitude control, the headings of both aircraft are held constant, so the paths of both aircraft remain in vertical geometric planes. Since the vertical separation requirements for the Protected Airspace Zone are much smaller than the horizontal requirements, and since climb and descent rates are fairly time responsive, altitude maneuvers have the beneficial quality that they may be used at the last minute. They also have the benefit of holding the heading of each aircraft constant, which allows for pilots and air traffic controllers to more easily predict the portions of the airspace that will remain free of aircraft.

In general, the geometry for altitude maneuvers is three-dimensional, although the relative motion of the two aircraft will reside in a two-dimensional plane. Assume that both aircraft have constant velocity vectors. For each aircraft, the velocity vector  $\bar{v}$  is oriented at the heading  $\Psi$  measured clockwise from North, at the flight path angle  $\gamma$  from the horizontal plane, and at the bank angle  $\Phi$  relative to the horizontal plane, as shown in Figure 47. It is assumed that the initial heading and flight path angles may be non-zero, and the bank angle is zero for this three-dimensional analysis. As was shown in Figure 23, the relative motion of two conflicting aircraft with constant velocity vectors defines a skewed relative motion plane; the relative motion plane is a horizontal plane if and only if both velocity vectors have zero flight path angle.

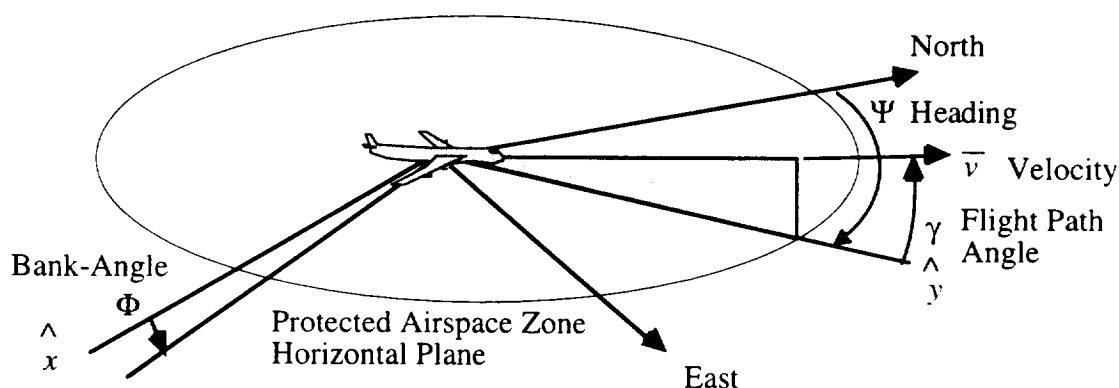


Figure 47. The orientation of the velocity vector for an aircraft.

The model for the vertical maneuver holds the horizontal speed constant as the vertical speed changes. Figure 48 illustrates the model. Vertical maneuvers will generally involve small changes in flight path angle in the order of  $5^\circ$  to  $10^\circ$ . Since the horizontal component of velocity remains fixed, when two aircraft climb or descend in a coordinated effort to maximize vertical separation, there is no change with respect to the horizontal component of relative velocity. The relative horizontal trajectory remains on the same horizontal path as before the vertical maneuver was initiated.

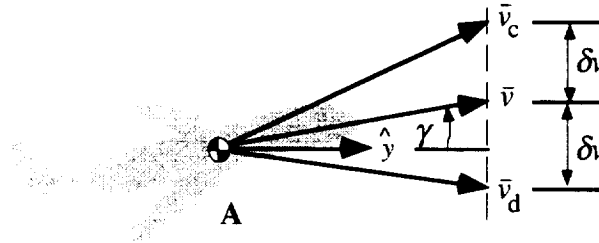


Figure 48. The vertical maneuver model where the horizontal component of the velocity remains constant while the vertical component changes.

The goal for the vertical maneuver is to have the intersection of the relative motion line occur on the upper or lower rim of the Protected Airspace Zone, as to just clear the separation requirements. Figure 49 illustrates two candidate goal locations for a given initial relative orientation of two aircraft. To determine a particular goal location requires a geometric analysis including the initial conditions and the optimal control strategy defined above. The projection of the line of relative motion onto the horizontal plane, defined as  $\vec{l}$  by equation (57) in the conflict detection section of this report, determines the cross sectional area. Assuming that a conflict exists, this projected line intercepts the Protected Airspace Zone at two points, as shown in the drawing in Figure 49. The point on the line  $\vec{l}$  that is closest to the origin is located at the position  $\vec{r}_*$ , which can be expressed in terms of the relative motion vector  $\vec{c}$  and the location  $\vec{r}$  of Aircraft B relative to Aircraft A as follows (by substituting eq. (59) into eq. (60)):

$$\underline{\bar{r}}_* = \underline{\bar{r}} - \underline{\bar{c}} \left( \frac{\underline{\bar{r}} \cdot \underline{\bar{c}}}{\underline{\bar{c}} \cdot \underline{\bar{c}}} \right). \quad (76)$$

The width  $w$  of the cross sectional area is defined from the right triangle with sides  $|\underline{\bar{r}}_*|$ ,  $w/2$ , and  $R$ , as illustrated in Figure 50, thus:

$$|\underline{\bar{r}}_*|^2 + \left( \frac{w}{2} \right)^2 = R^2. \quad (77)$$

The width  $w$  is:

$$w = 2\sqrt{R^2 - |\underline{\bar{r}}_*|^2}. \quad (78)$$

Finally, determining whether the location of the candidate goal location should be the closer or farther location on the rim depends on the case being cooperative or non-cooperative. If the altitude maneuver is a cooperative maneuver, both the candidate goal locations will be on the near side of the upper and lower rim of the Protected Airspace Zone. If the altitude maneuver is a non-cooperative maneuver, then the location of the candidate goal location will be on the farther side of the rim of the Protected Airspace Zone when the maneuvering aircraft has inferior performance relative to the steady state climb or descent rate of the non-cooperative aircraft; the cases are defined, and examples are given later in this section.

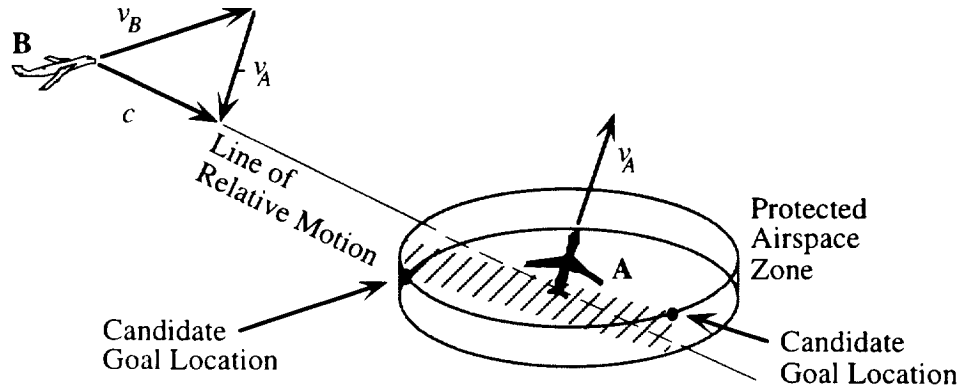


Figure 49. The line of relative motion determines a rectangular planar intersection with the Protected Airspace Zone and two candidate goal locations for a vertical maneuver.

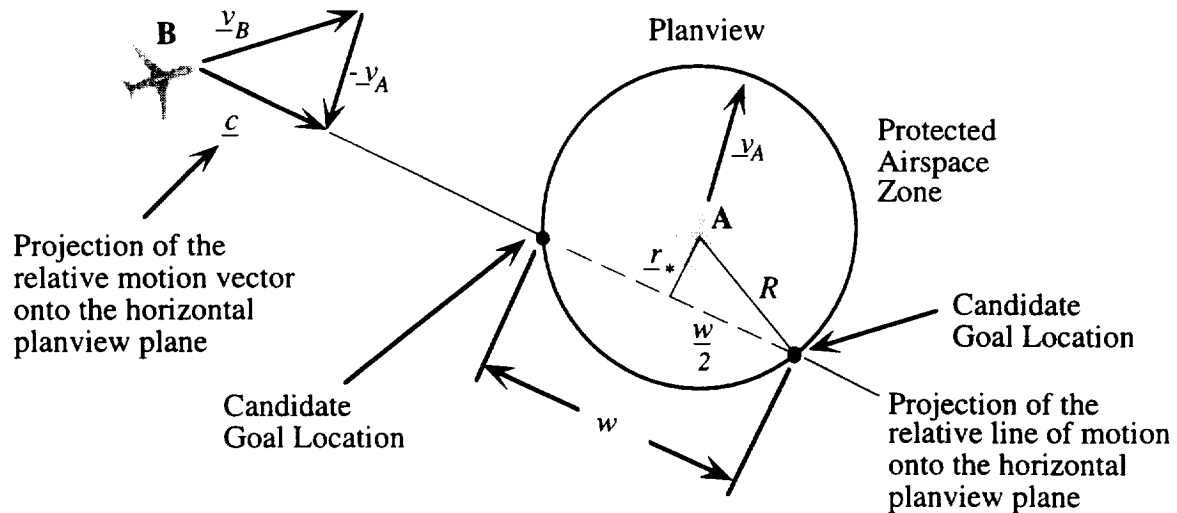


Figure 50. In the planview, the projection of the line of relative motion intercepts the Protected Airspace Zone and defines two candidate goal locations.

The response to commanded climb and descent rates has fairly quick dynamics for most aircraft. For most commercial aircraft, a 5 to 10 second rise time (time to reach 90% of maximum) can be realized for climb and descent maneuvers. For example, in Figure 51 an investigation of the dynamics of the Boeing 737 aircraft indicates that the rise time is roughly 9.9 seconds to climb from steady level flight to a maximum climb rate of 700 ft/minute and 9.4 seconds to descend to a maximum descent rate of 1500 ft/minute. With these rates, the Boeing 737 can achieve a 1000 ft separation from a non-cooperative aircraft in about 90 seconds for climb maneuvers and in about 40 seconds for a descent maneuver. In general, individual pilots will maneuver with different rates based on the conflict situation and level of experience. Climb rates are generally less than descent rates (which take advantage of gravity). Also, the loss of velocity in a climb maneuver will cause many pilots to reduce or level off a tactical climb maneuver after 10 to 20 seconds. In terms of modeling vertical maneuvers, quick changes in flight path angle are modeled by step changes in climb and descent rate.

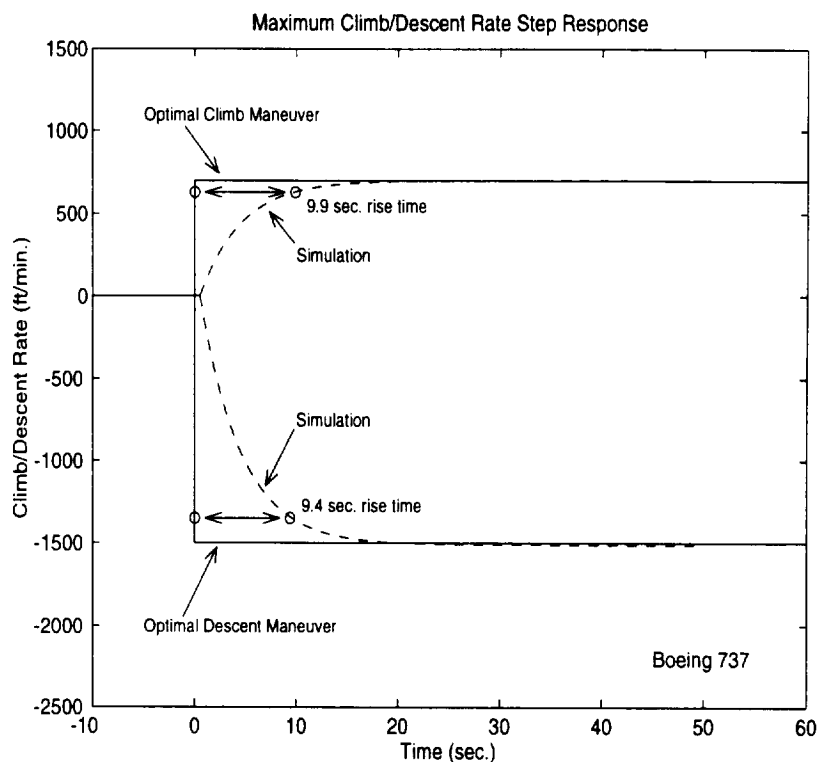


Figure 51. The dynamics of maximum climb and descent rates for a Boeing 737 aircraft.

Transients in altitude maneuvers may be accounted for by an appropriate lead time for initiating a maneuver. A lead time from 2 to 5 seconds is necessary for most aircraft. For the Boeing 737 example in Figure 51, the trajectory resulting from a step change in climb and descent rate is compared to a trajectory with simulated dynamics in Figure 52. When the maneuver is initiated with sufficient lead time, the resultant dynamics matches the desired optimal maneuver quite well, as shown in Figure 53 for a climb maneuver and in Figure 54 for a descent maneuver. Conflict advisories can be given with sufficient lead times to account for these transients.

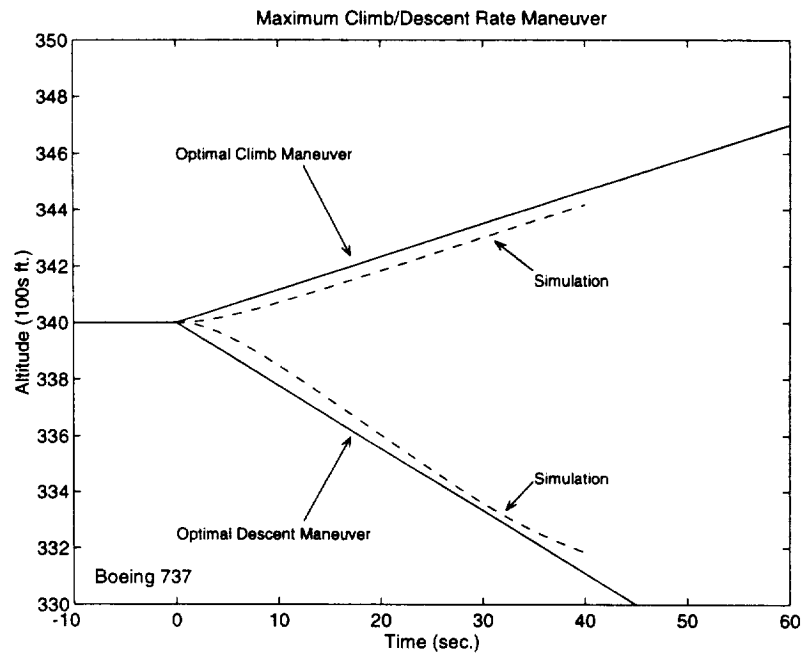


Figure 52. A comparison between the modeled optimal climb and descent maneuvers and a simulation for a Boeing 737.

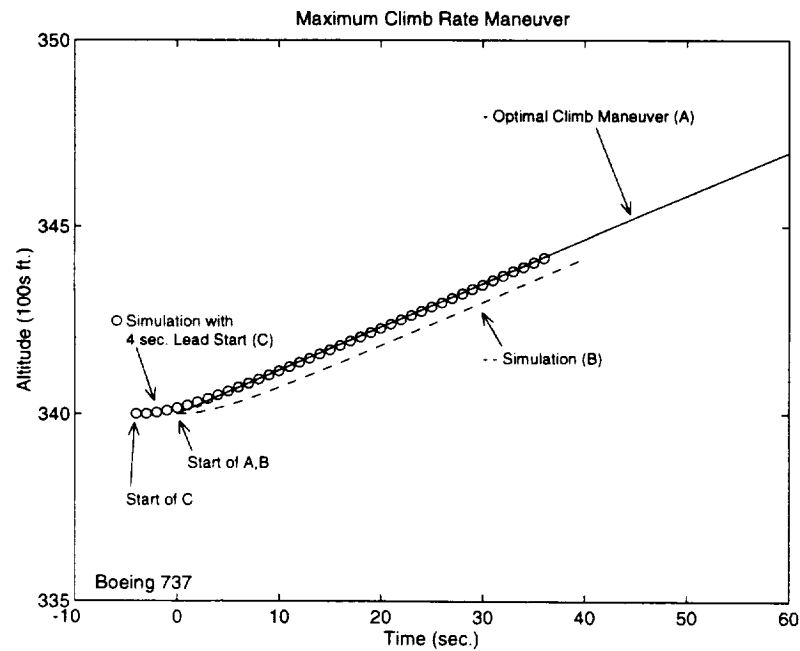


Figure 53. The effects of starting a climb maneuver with sufficient lead time to offset the dynamics transients.

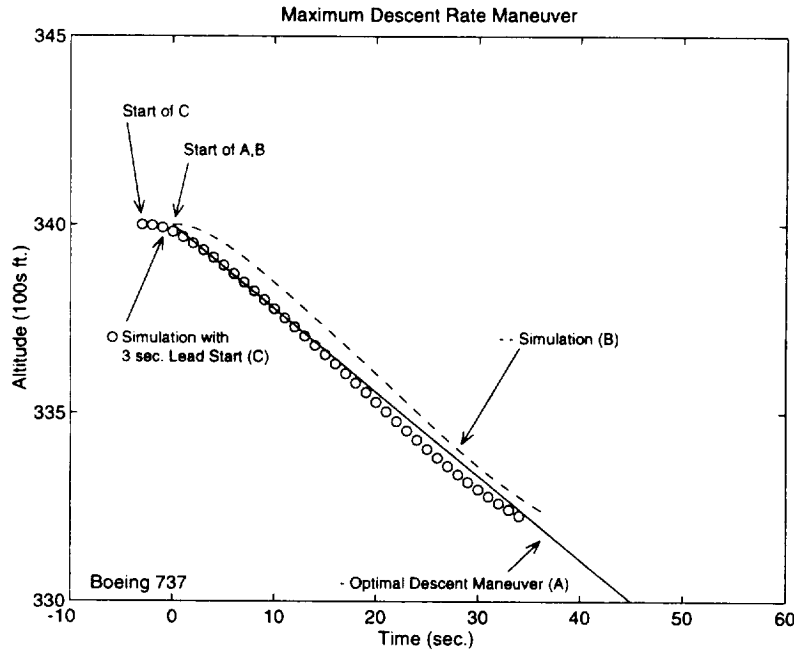


Figure 54. The effects of starting a descent maneuver with sufficient lead time to offset the dynamics transients.

An altitude control conflict resolution strategy is the result of an optimization problem: Determine the vertical speeds (climb or descent rates)  $\delta v_A$  and  $\delta v_B$  of aircraft A and B as functions of the relative motion state  $(r, \phi, \theta, z)$  such that the altitude separation is maximized. The payoff function is the relative vertical separation  $z$  at the Protected Airspace Zone goal location. In general, the equations of motion are defined by equations (1) to (4), with the turn rates  $\omega_A=0$  and  $\omega_B=0$ , constant horizontal speeds  $v_A$  and  $v_B$ , and vertical speeds  $\delta v_A$  and  $\delta v_B$  being chosen from maximum and minimum allowable climb and descent rates. Consequently, the heading difference  $\theta$  remains constant, and the relative horizontal velocities remain constant. Furthermore, the vertical velocity equation, or the altitude difference equation, is uncoupled with the horizontal equations. It is assumed that there are no vertical acceleration constraints, and either aircraft can increase or decrease flight path angle by a small amount enough to create the vertical velocity components  $\delta v_A$  and  $\delta v_B$ .

Optimal altitude control maneuvers may be obtained by solving Euler-Lagrange Equations for cooperative and non-cooperative cases. We have implemented numerical

methods to construct maneuver charts that indicate whether each aircraft should climb or descend as a function of the relative motion state  $(r, \phi, \theta, z)$ .

Example altitude control maneuver chart results are given in Figures 55 through 58. The optimal altitude maneuver is identified with the notation  $A_C$  for aircraft A to climb,  $A_D$  for aircraft A to descend,  $B_C$  for aircraft B to climb,  $B_D$  for aircraft B to descend, or  $B_0$  for aircraft B holds constant climb or descent rate (the non-cooperative case). The maneuver chart also indicates the optimal miss distance contours for 2000 ft distances (equivalent to the vertical separation standard) that can be achieved if the optimal maneuver is applied, and a clearance line, for which no maneuver is necessary once crossed.

Figure 55 illustrates a maneuver chart for a cooperative case. In this example, the maneuver chart is established for a cross velocity heading directly into the center of the Protected Airspace Zone; the cross section of the Protected Airspace Zone has a length of 10 nmi and height of 2000 ft. Once an aircraft climbs above or descends below the Protected Airspace Zone, it should hold a zero relative climb rate until clear of the far side of the Protected Airspace Zone.

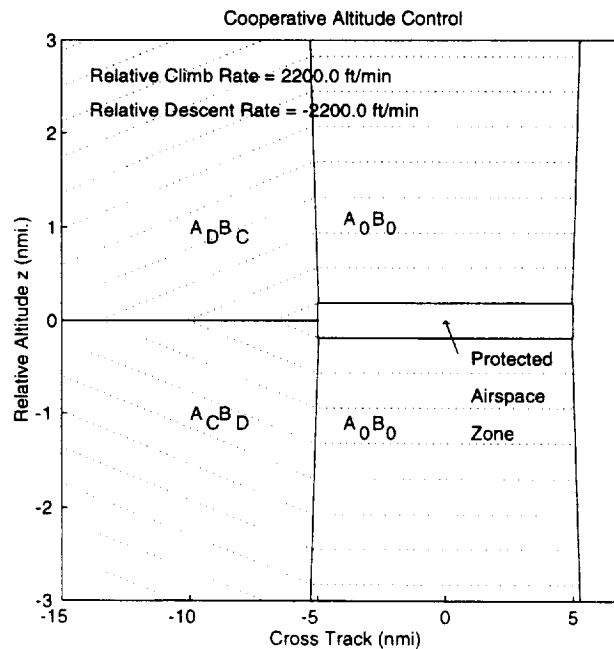


Figure 55. A cooperative altitude control maneuver chart.

Figure 56 through 58 illustrate maneuver charts for a non-cooperative cases. In these examples, maneuver charts are established for a cross velocity heading directly into the center of the Protected Airspace Zone; the cross section of the Protected Airspace Zone has a length of 10 nmi and height of 2000 ft. There are three cases for non-cooperative maneuver charts. First, the case when the non-cooperative aircraft A is climbing with a constant positive rate and aircraft B has a lower maximum climb rate:

Non-Cooperative Case I:  $\delta v_A \geq \delta v_B > 0.$  (79)

In this case, the goal locations are at the far upper rim of the Protected Airspace Zone cross section for climb maneuvers, and at the near lower rim of the Protected Airspace Zone cross section for descent maneuvers. Once an aircraft climbs above or descends below the Protected Airspace Zone, it is clear from a separation conflict.

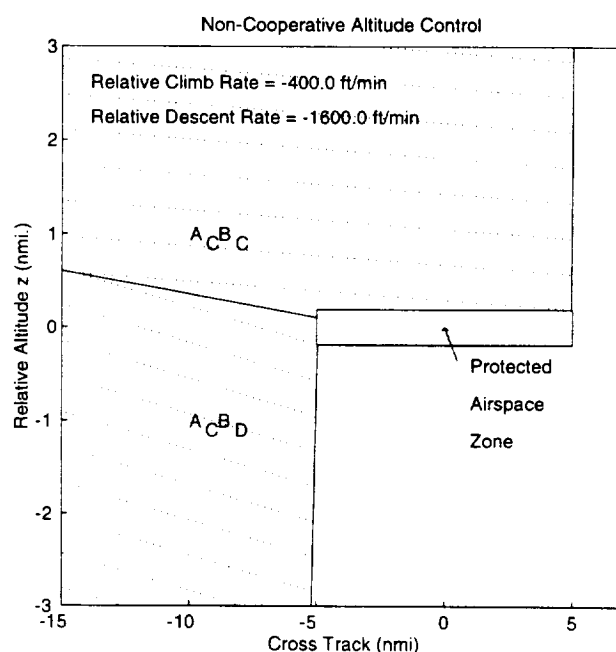


Figure 56. A non-cooperative altitude control maneuver chart for an aircraft with inferior climb performance relative to a non-cooperative climbing Aircraft A.

In the second case, the non-cooperative aircraft A is either climbing with a constant positive rate and aircraft B has a higher maximum climb rate, or aircraft A is descending with a constant negative rate and aircraft B has a lower negative descent rate:

Non-Cooperative Case II:  $\delta v_B > \delta v_A > 0$  or (80)

$$\delta v_B < \delta v_A < 0. \quad (81)$$

In this case, the goal locations are at the near upper and lower rim of the Protected Airspace Zone cross section for climb and descent maneuvers, respectively. Once an aircraft climbs above or descends below the Protected Airspace Zone, it is clear from a separation conflict. Once aircraft B climbs above or descends below the Protected Airspace Zone, it should hold a zero relative climb rate until clear of the far side of the Protected Airspace Zone. This non-cooperative case maneuver chart is very similar to the cooperative case maneuver chart, with the exception of the relative climb and descent rates have smaller magnitude due to the non-cooperative situation.

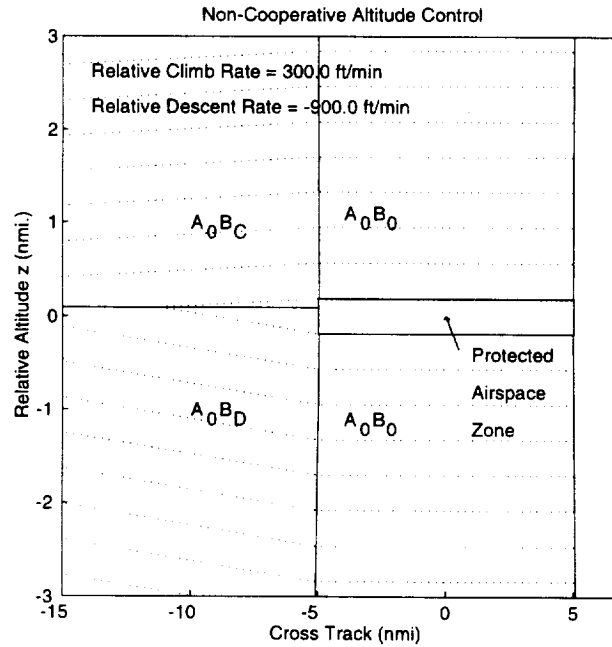


Figure 57. A non-cooperative altitude control maneuver chart for two aircraft with dissimilar climb and descent rate capabilities.

In the third case, the non-cooperative aircraft A is descending with a constant negative rate and aircraft B has a higher minimum descent rate:

Non-Cooperative Case III:  $0 > \delta v_B \geq \delta v_A.$  (82)

In this case, the goal locations are at the near upper rim of the Protected Airspace Zone cross section for climb maneuvers, and at the far lower rim of the Protected Airspace Zone cross section for descent maneuvers. Once an aircraft climbs above or descends below the Protected Airspace Zone, it is clear from a separation conflict.

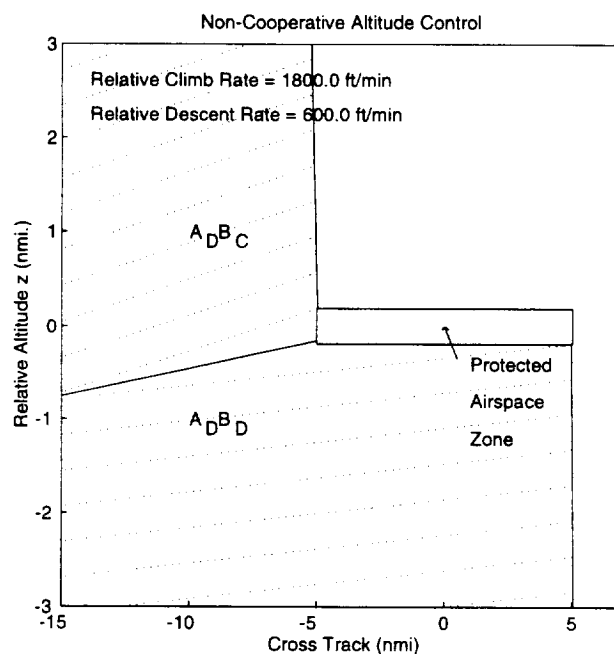


Figure 58. A non-cooperative altitude control maneuver chart for an aircraft with inferior descent performance relative to a non-cooperative descending Aircraft A.

As was shown for heading and speed maneuvers, one particular set of initial conditions establishes a Tactical Alert Zone. There exists a locus of points for which the initial conditions produce tactical altitude maneuvers that all have the same vertical separation clearance of 2000 ft at closest approach, which under today's regulations, constitutes the Protected Airspace Zone. Under these conditions, for cooperative and non-cooperative cases, maneuver charts identify a Tactical Alert Zone on the surface of which the optimal tactical conflict resolution must be initiated in order not to penetrate the Protected Airspace Zone of the intruder aircraft. Figure 59 (a) shows the Tactical Alert Zone for the cooperative case, and Figure 59 (b) shows the Tactical Alert Zone for the three non-cooperative cases.

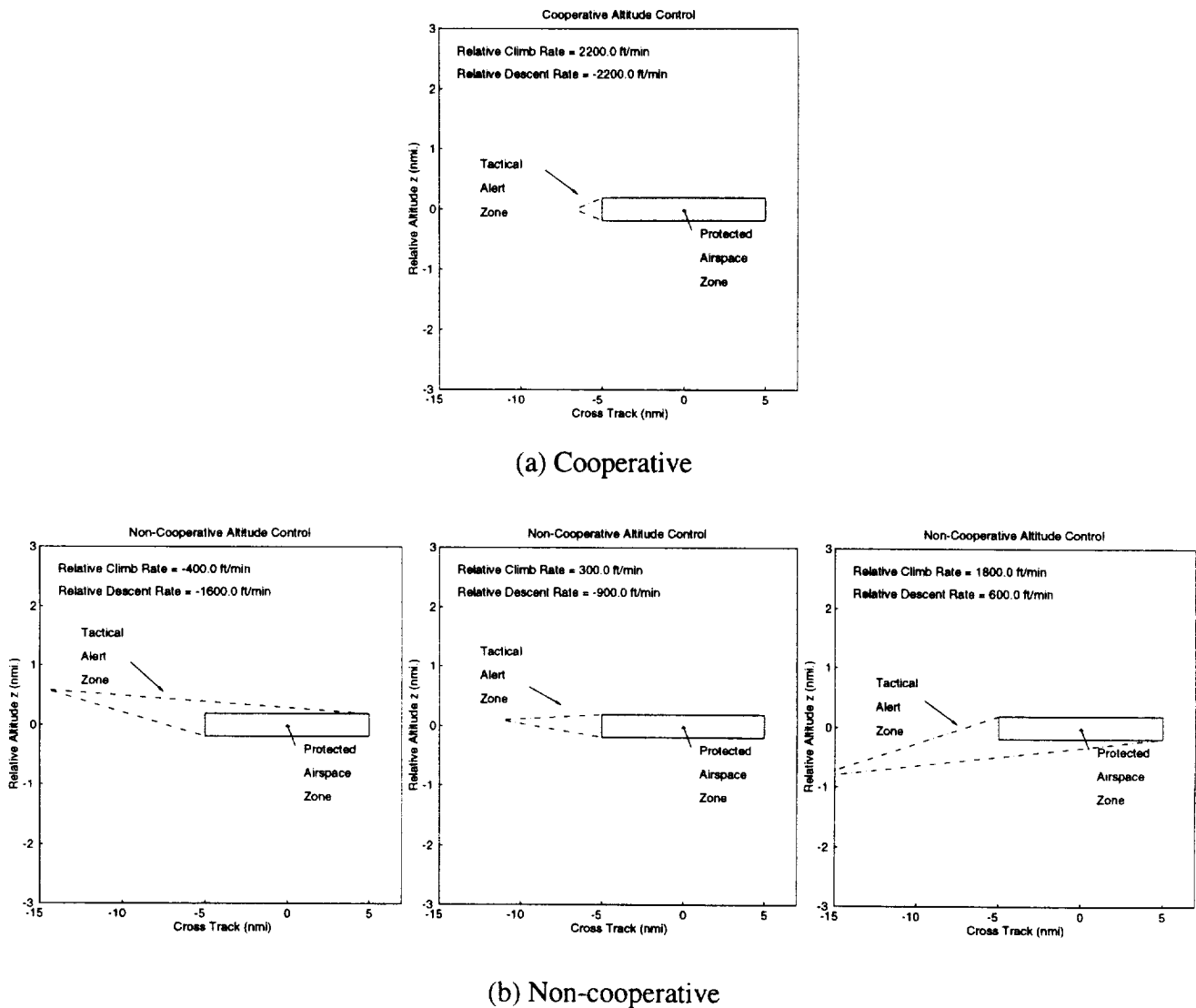


Figure 59. Cooperative (a) and non-cooperative (b) altitude control Tactical Alert Zone cases.

#### 4.4 Tactical Alert Zone Visualization

The Tactical Alert Zones for heading, speed, and altitude control may be viewed in a three-dimensional perspective view to aid a pilot or air traffic controller in understanding the control options at any given moment. This investigation is in part motivated by the work of Ford [F86] where the protected volume of airspace is identified for TCAS II. The assumptions for the derivation of heading control maneuvers was that both aircraft were in the same horizontal plane. However, the same results apply if both aircraft are flying trajectories in horizontal planes that are separated by less than the vertical separation requirement (currently 1000 ft). Thus, the Tactical Alert Zone region that is derived in a

horizontal plane can be extended above and below an intruder aircraft by the distance of the separation standard. This applies for both heading and speed control. Figures 60 and 61 illustrates the Tactical Alert Zone for two aircraft at nearly the same altitude.

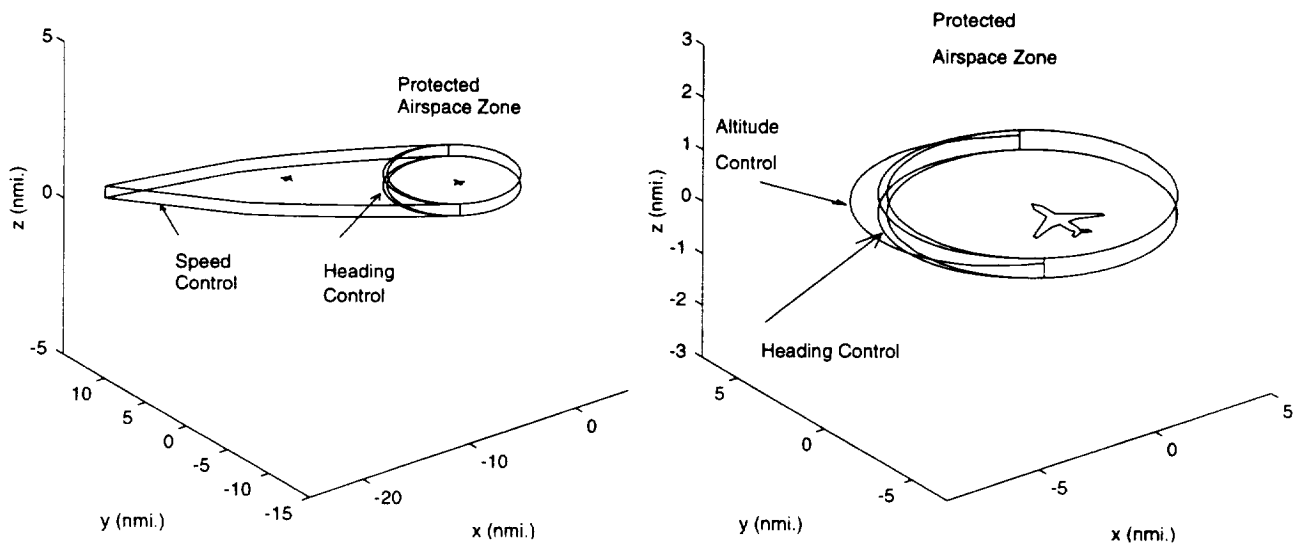


Figure 60. The 3D perspective view of Tactical Alert Zones; a comparison between speed control vs. heading control (left), and a comparison between altitude control vs. heading control (right).

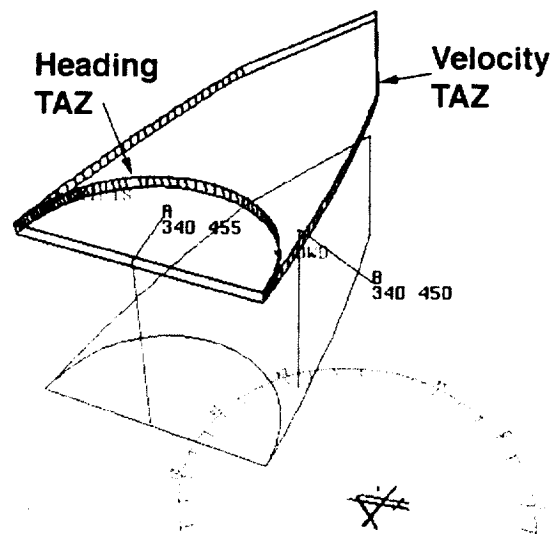


Figure 61. The 3D perspective view of Tactical Alert Zones for heading and speed control (taken from [ADK96] with permission from the authors).

Tactical Alert Zones (TAZs) around an aircraft advise what control logic should be applied for conflict resolution. In Figure 60, the left aircraft is located within the speed control TAZ, and thus cannot avoid penetrating the Protected Airspace Zone of the intruder aircraft without using another mode of control. Since the aircraft is located outside the heading control TAZ, a cooperative heading maneuver remains an option for conflict resolution.

Tactical Alert Zones and the Protected Airspace Zones are two important safety regions that, under a Free Flight policy, pilots and air traffic managers must clearly visualize to effectively perform conflict detection and resolution. Tactical Alert Zones cannot be easily generalized in terms of heuristics that a pilot or air traffic manager can apply in another non-visual mode. Displaying these regions around the aircraft could greatly aid both pilots and air traffic managers by presenting conflict resolution advisory information in a visually immersive presentation. The theoretical and algorithmic background behind these safety regions is retained within the computer.

#### **4.5 Multi-Aircraft Tactical Encounters**

A heuristic approach to multi-aircraft tactical conflict resolution may be applied using 2-aircraft conflict detection and resolution primitives. Consider the following heuristic algorithm which is stated for a 3-aircraft scenario:

- 1) Given 3 aircraft located in close proximity, determine the time-to-closest-approach for each pair of aircraft. Prioritize each pair of aircraft based on time-to-closest-approach. Identify the highest priority pair of aircraft as A and B, and the other aircraft as C.
- 2) For A and B, allow A and B to commit to resolve their conflict with a cooperative conflict resolution strategy. After A and B achieve a positive range rate, direct A and B to return to their original headings with appropriate recovery maneuvers.
- 3) If C comes in conflict with either A or B while A and B are committed to a cooperative maneuver, perform a non-cooperative conflict resolution strategy with C relative to the closer aircraft A or B (based on time-to-closest-approach to A or B) using the other aircraft from A or B as a constraint. A reachability conflict detection mechanism (see Chapter 3) is necessary here since both A and B is maneuvering.

- 4) If A and B resolve their conflict without becoming in conflict with C, then return to Step 1, or if all aircraft have positive range rates relative to each other, then the encounter is over.

This approach to 3-aircraft conflict resolution is a heuristic approach; it does not guarantee that all aircraft avoid each other successfully. Notice that in Step 3, aircraft C must perform a non-cooperative conflict resolution strategy with the closer of aircraft A and B. As noted, detecting this conflict should be performed with a reachability conflict detection mechanism, as described in Chapter 3 and illustrated in Figures 13 and 14. However, a complication may result even if the conflict is detected with a reachability type mechanism, because after conflict detection, aircraft C performs a non-cooperative conflict resolution. In this report, non-cooperative conflicts assume that the intruder aircraft is flying a straight path, which is not going to be the case for a 3-aircraft maneuver. Thus, there is no guarantee that the non-cooperative maneuver for aircraft C relative to A or B described in step 3 will be performed successfully. Aircraft C is in danger because either aircraft A or B may be performing turns that are counterproductive with respect to the safety objective of aircraft C. The worst case situation for aircraft C must consider that aircraft A and B are both turning in counterproductive directions (analogous to a suicidal aircraft) while aircraft C maximizes miss distance. In this report, we have not investigated such non-cooperative maneuvers; however, this 3-aircraft example illustrates the need for such an investigation.

Figures 62 through 66 illustrate a 3-aircraft encounter that uses the above heuristic approach for conflict resolution. The scenario considers only heading maneuvers for three aircraft flying at the same altitude. In Figure 62, the points of closest approach for each pair of aircraft are displayed assuming that no aircraft maneuvers from a straight constant speed flight. Dashed circles with 5 nmi radii help display the separation conflicts that occur. Figure 63 illustrates the conflict resolution strategy that results from the heuristic algorithm. Aircraft A and B have highest priority since the time-to-closest-approach between A and B will occur before the time-to-closest-approach between A and C or B and C. First, aircraft A and B perform left turns, as indicated by the tactical alert zone shown in Figure 64. After aircraft A clears the zero range rate line of aircraft B, a second conflict occurs just as aircraft B starts to perform a recovery maneuver from the conflict resolution with aircraft A. As shown in Figure 65, a second application of the conflict resolution tactical alert zone advisories allows for the safe passage of aircraft C to the backside of aircraft B; however, the motion of aircraft C then becomes counter productive with respect to the safety of aircraft A. Aircraft A performs a non-cooperative maneuver towards the side of aircraft A that is free of congestion, as shown in Figure 65. Finally, as

shown in Figure 66, all aircraft perform recovery maneuvers back to their original courses. This example exhibits a particularly difficult tactical multi-aircraft conflict situation where three aircraft are converging to a single location, which could occur in Free Flight. However, this type of 3-aircraft maneuver should be considered very unlikely, since strategic maneuvers should be performed prior to this tactical encounter.

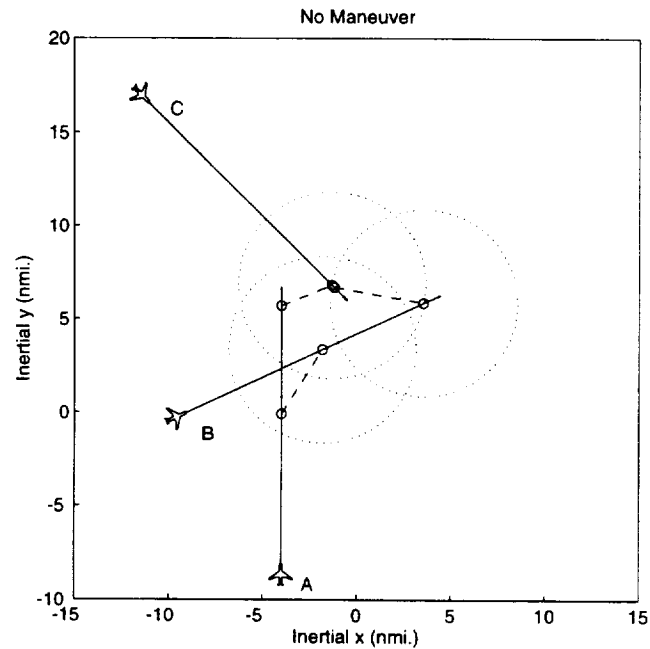


Figure 62. A 3-aircraft conflict detection example where no conflict resolution maneuvers are executed (○ denotes points of closest approach).

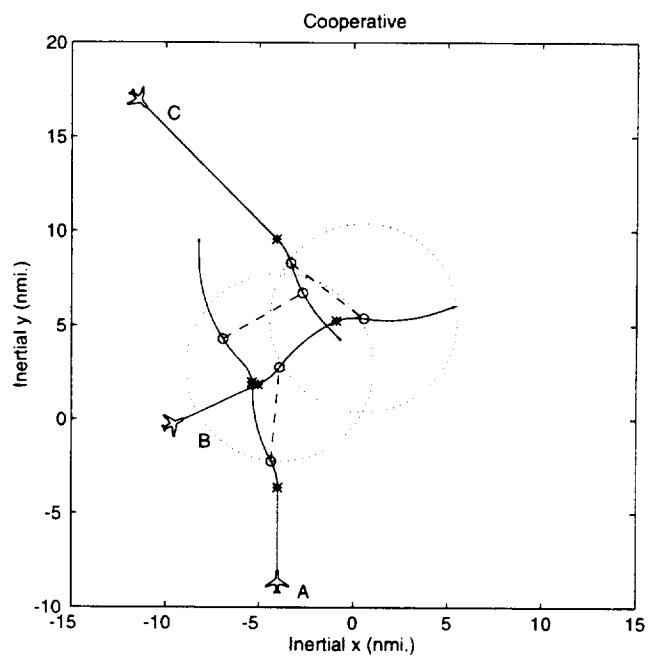


Figure 63. A 3-aircraft conflict detection and resolution example (\* denotes the location when a conflict resolution maneuver is initiated; o denotes points of closest approach).

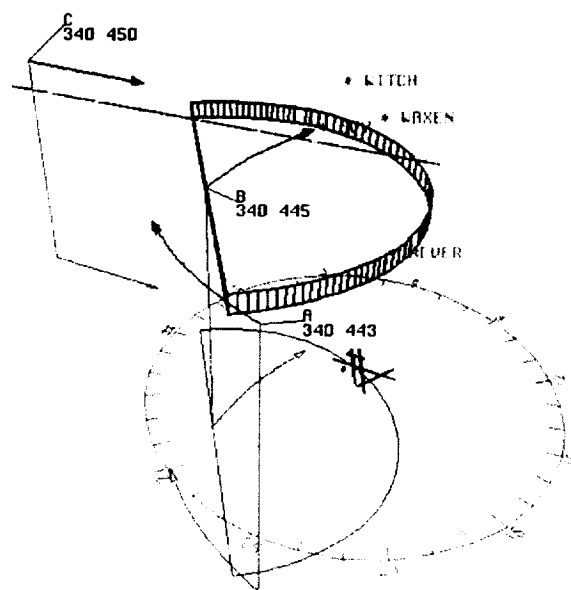


Figure 64. The 3-aircraft conflict resolution maneuver between aircraft A, B, and C; the Tactical Alert Zone of aircraft B is shown with aircraft A just clearing the zero range rate line (taken from [ADK96] with permission from the authors).

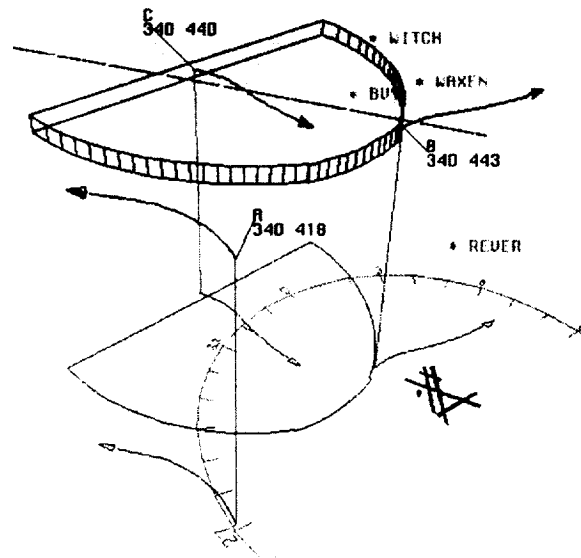


Figure 65. The 3-aircraft conflict resolution maneuver between aircraft A, B, and C; the Tactical Alert Zone of aircraft C is shown with aircraft B maneuvering away from aircraft C (taken from [ADK96] with permission from the authors).

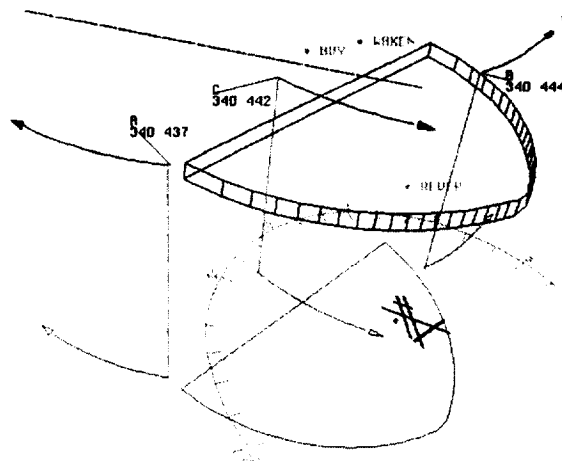


Figure 66. The 3-aircraft conflict resolution maneuver between aircraft A, B, and C; the Tactical Alert Zone of aircraft C is shown with aircraft B finishing the maneuvering away from aircraft C and aircraft A initiating a recovery maneuver (taken from [ADK96] with permission from the authors).

The subject of multi-aircraft conflict detection and resolution is a complex challenge for Free Flight, and should be investigated as a subject in itself. The cooperative and non-cooperative conflict resolution strategies of this report may serve as a good basis for such an investigation. As noted from the investigation of a 3-aircraft example, an additional analysis of proximity management must be carried along for multi-aircraft scenarios. Figure 67 illustrates the three components needed for multi-aircraft scenarios: 1) multi-aircraft proximity management, 2) multi-aircraft conflict detection, and 3) multi-aircraft conflict resolution.

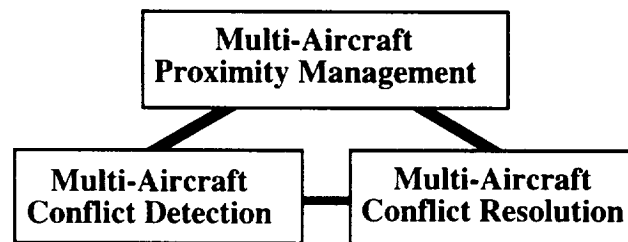


Figure 67. Tasks for multi-aircraft conflict detection and resolution.

The proximity management system maintains spatial-temporal proximity information for all aircraft. The proximity management system would manage surveillance data including radar and GPS to establish the current location of aircraft as well as intent data including flight plans. The size and shape of the sector analyzed should be determined through the results of dynamic density measurements. In Chapter 3, a proximity management system based on Delaunay Triangulations was presented; such a proximity management system would be adequate for multi-aircraft scenarios.

Conflict detection works with proximity management to identify conflicts based on present and future Tactical and Strategic Alert Zone and Protected Airspace Zone overlaps, and runs cluster analysis and free space analysis in order to support conflict resolution. Cluster analysis may be performed on the aircraft position data to identify aircraft in close temporal and spatial proximity, based on time-to-closest-approach and range at the point-of-closest-approach. Further analysis of clusters of neighboring aircraft also indicates where there is a potential for the domino effect in conflict resolution, where the conflict resolution between a subset of aircraft propagates further conflicts that may or may not have been directly connected with the original subset of conflicting aircraft. Cluster analysis also identifies the free space for conflict resolution. It is important to note that the conflict resolution free space changes as a function of time, and this free space must be

analyzed from the current time through the end time of conflict resolution. The time required for a conflict resolution is identified by a time until achieving a zero range rate for any pair of two aircraft, as discussed in this report.

The 3-aircraft conflict detection and resolution example given above provides insight into the complexity of multi-aircraft conflict resolution. Free space analysis is needed to compare the available free space determined by conflict detection to maneuver envelope needs for pairs of conflicting aircraft with constraints imposed by third, fourth, or more aircraft located nearby. Heuristic algorithms, like the one given above or the genetic algorithm based solution given in [DAC96], must be investigated for feasibility to identify their weak points. A fully cooperative maneuver with 3 or more aircraft coordinating their motion may be necessary to guarantee safety.

## 5. STRATEGIC CONFLICT RESOLUTION

In this chapter, strategic conflict resolution strategies are investigated. Whereas the tactical encounter is concerned primarily with safety (maintaining separation), the strategic encounter is concerned with economics as well as safety. Economics is treated by considering direct operating costs, composed of fuel and flight time costs, involved in maneuvering to avoid a conflict. In this way, one of the primary objectives of Free Flight, namely, enhancement of flight efficiency, is being addressed. The objectives of our strategic encounter research are: to evaluate different strategic maneuvers for arbitrary initial conditions, to evaluate the direct operating cost of a maneuver, to define a logical set of “rules-of-the-road” for conflict resolution, and to evaluate the economical savings of reduced separation requirements.

Under the strategic evasion scenario, the intent is to sufficiently achieve the required separation while minimizing economic factors. Economic factors may include: reducing time delay, fuel cost, and direct operating cost, in addition to minimizing conflicts with other (third aircraft) traffic, and minimizing passenger discomfort. This might lead to the selection of any of a set of standard maneuvers: heading, speed, or altitude control, or a combination of these. In all these cases, the emphasis will be on minimum deviations of the original flight track while achieving the required minimum separation distance at closest approach. An opposing criteria, which leads to initiating these maneuvers closer to the intruding aircraft, is the uncertainty in accurately predicting the time and location of the point of closest approach. Hence, while the desire to minimize the economic penalty leads to a gradual maneuver at a longer initial range, a tradeoff exists due to the uncertainty at the longer range in predicting the actual separation at closest approach as well as accurately performing the conflict resolution guidance maneuver.

In the sections that follow, first strategic heading control maneuvers are investigated, followed by speed control and altitude control maneuvers. After investigations of the theory of these maneuvers are presented, the economics of these maneuvers is investigated. Finally, these strategic results are combined with tactical conflict resolution results in one set of “rules-of-the-road”.

### 5.1 Strategic Heading Control Maneuvers

Strategic heading control maneuvers are investigated with the following assumptions. It is assumed that the heading maneuver performed will consist of a series of standard vectoring maneuvers (heading changes) such that straight line motion occurs in between heading changes. The time and distance to implement the change in heading for one or both aircraft is small in comparison to the time and distance of the overall maneuver. Heading maneuvers are performed in the horizontal plane with standard turn rates. No uncertainty analysis will be performed in the design of heading maneuvers, although the effects of uncertainties was investigated in Chapter 3 to determine if a maneuver should or should not be initiated for a given set of initial conditions. Finally, non-cooperative and cooperative cases will be considered for strategic heading maneuvers.

The design of strategic heading maneuvers considers an arbitrary initial condition, a separation constraint, and several possible final conditions. As done in previous analysis, the motion of aircraft B may be described relative to aircraft A in the moving reference frame of aircraft A. Aircraft B will follow a trajectory in the direction of the line of relative motion if no heading maneuver is performed. If the line of relative motion does not pierce the Protected Airspace Zone, then there is no need for a conflict resolution maneuver. Thus, there is a limited region of initial conditions for which heading maneuvers are necessary, as shown in Figure 68. The horizontal separation constraint, currently established at 5 nmi, thus requires the relative motion to pass around the Protected Airspace Zone. Optimal paths [Mi86] around circular obstacles, namely the Protected Airspace Zone, consist of straight line segments tangent to the circular obstacle and arcs of the circular obstacle – the portion of the optimal path that passes along the arc is sometimes referred to as in the saturated constraint period [DAC95]. The final condition establishes the point of departure from the circular arc around the separation constraint. Three final conditions may be appropriate: return both aircraft back to track using a symmetric heading maneuver, return both aircraft back to course (original heading), or return both aircraft towards their next waypoints (a heading angle typically in between the angles required for the return to course and return to track). With these final conditions, the point of departure from the circular arc constraint is determined by the point of tangency between the circular constraint and the symmetric point for return to track, the point of tangency that matches the original course direction for the return to course, and a point of tangency determined by the next waypoints for the return to the next waypoints.



backside maneuver is described by the velocity vector  $\bar{v}_B^-$ , the relative motion vector  $\bar{c}^-$ , and the point of tangency located with the unit direction vector  $\hat{\beta}^-$ .

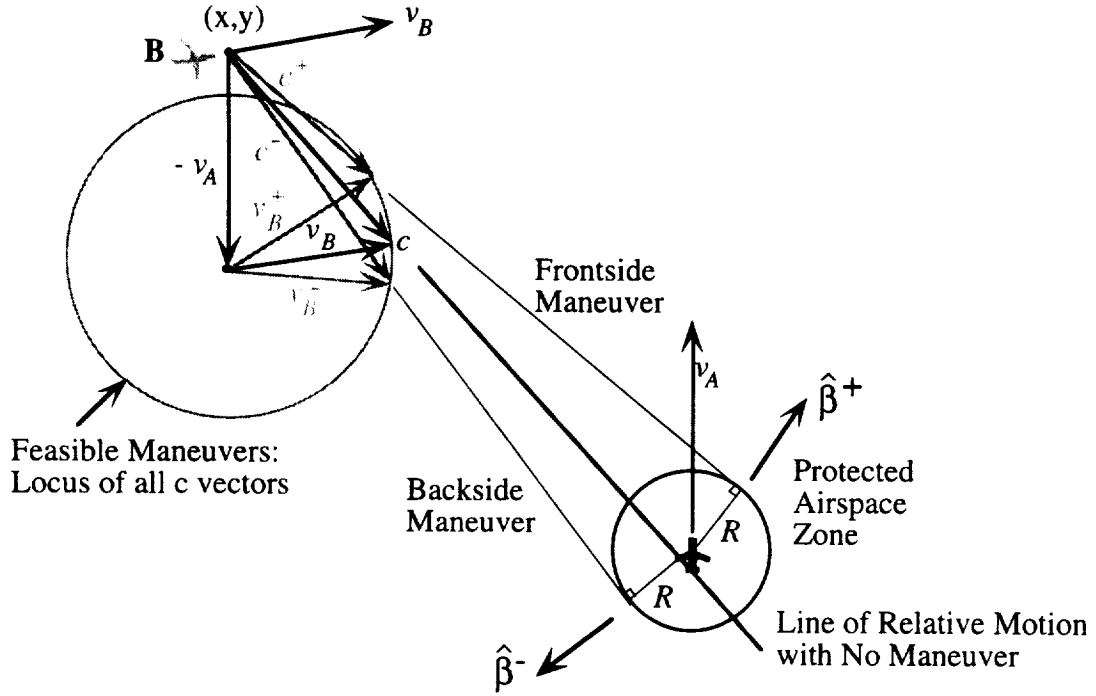


Figure 69. The relative geometry for strategic frontside and backside heading maneuvers.

The point of tangency location is determined by geometry. The projection of the range vector  $\bar{r}$  and the unit direction vector  $\hat{\beta}$  pointing to the point of tangency gives:

$$\bar{r} \cdot \hat{\beta} = R \quad (83)$$

where  $\hat{\beta}$  could be either the frontside or backside unit direction vector, and  $R$  is the desired miss distance. This equation (83) can be expressed in the scalar form:

$$x\beta_x + y\beta_y = R \quad (84)$$

where the unit direction vector is  $\hat{\beta} = \beta_x \hat{x} + \beta_y \hat{y}$  and the location of aircraft B relative to aircraft A is at  $(x,y)$ , as shown in Figure 70. Furthermore, since the vector  $\hat{\beta}$  is a unit vector, it has unit magnitude:

$$\beta_x^2 + \beta_y^2 = 1. \quad (85)$$

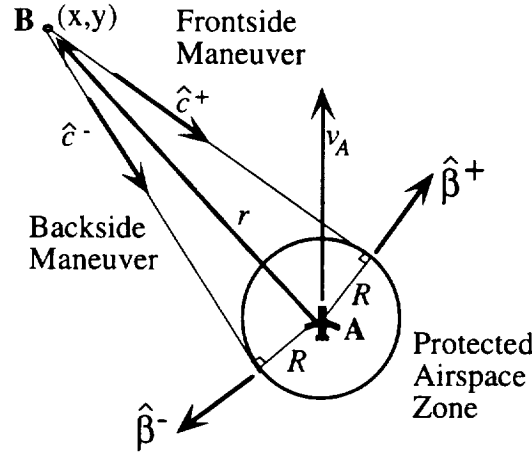


Figure 70. The vector analysis for frontside and backside heading maneuvers.

Combining equations (84) and (85) gives a quadratic equation:

$$r^2 \beta_y^2 - 2Ry\beta_y + (R^2 - x^2) = 0 \quad (86)$$

which has the two real solutions:  $\beta_{y1}$  and  $\beta_{y2}$ . (It is easy to show that as long as aircraft B is outside the Protected Airspace Zone of aircraft A, then these solutions are real numbers.) Next, given either  $\beta_y = \beta_{y1}$  or  $\beta_y = \beta_{y2}$ , the value for  $\beta_x$  can be determined from:

$$\beta_x = \frac{R - y\beta_y}{x}. \quad (87)$$

Finally, the two solutions  $\hat{\beta}_1 = \beta_{x1}\hat{x} + \beta_{y1}\hat{y}$  and  $\hat{\beta}_2 = \beta_{x2}\hat{x} + \beta_{y2}\hat{y}$  can be distinguished as frontside and backside maneuvers by checking the sign of  $\bar{r} \times \hat{\beta}$ .

The directions of the frontside and backside maneuvers are determined next. As illustrated in Figure 70, the point of tangency location establishes:

$$\hat{c} \cdot \hat{\beta} = 0 \text{ and } \hat{c} \times \hat{\beta} = \pm \hat{z}. \quad (88)$$

Solving these equations (88) gives the directions of frontside and backside maneuvers.

Next, the magnitudes of the relative motion vectors are determined. For the non-cooperative case, the magnitude and direction of the velocity vector of aircraft A is described by  $\bar{v}_A = v_A \hat{y}$ . As shown in Figure 69 and 70, the model for the heading maneuver of aircraft B allows the velocity vector  $\bar{v}_B$  to be located on a circle described by:

$$c_x^2 + (c_y + v_A)^2 = v_B^2 \quad (89)$$

where the relative motion is  $\bar{c} = c_x \hat{x} + c_y \hat{y}$ , the speed of aircraft A is  $v_A$ , and the speed of aircraft B is  $v_B$ . Given the direction of a maneuver to be  $\bar{c} = c\hat{c} = c\hat{c}_x \hat{x} + c\hat{c}_y \hat{y}$ , equation (89) becomes:

$$(c\hat{c}_x)^2 + (c\hat{c}_y + v_A)^2 = v_B^2. \quad (90)$$

Equation (90) establishes the following relationship for the unknown  $c$ :

$$c^2 + (2\hat{c}_y v_A)c + (v_A^2 - v_B^2) = 0 \quad (91)$$

which can be solved using the quadratic equation:

$$c = -\hat{c}_y v_A \pm \sqrt{v_B^2 - \hat{c}_x^2 v_A^2}. \quad (92)$$

Two solutions  $c_1$  and  $c_2$  result. However, equation (92) applies to both frontside and backside maneuvers, so a total of four candidate solutions exist, as illustrated in Figure 71.

For frontside maneuvers, the two solutions  $\bar{c}_1^+ = c_1 \hat{c}^+$  and  $\bar{c}_2^+ = c_2 \hat{c}^+$  are determined by equation (92) using  $\hat{c}^+ = \hat{c}_x^+ \hat{x} + \hat{c}_y^+ \hat{y}$ , and for backside maneuvers, there are the two solutions  $\bar{c}_1^- = c_1 \hat{c}^-$  and  $\bar{c}_2^- = c_2 \hat{c}^-$  determined by equation (92) using  $\hat{c}^- = \hat{c}_x^- \hat{x} + \hat{c}_y^- \hat{y}$ .

Given the four candidate solutions  $\bar{c}_1^+$ ,  $\bar{c}_2^+$ ,  $\bar{c}_1^-$ , or  $\bar{c}_2^-$ , the candidate solution that is closest to the current relative motion  $\bar{c}$  is the best maneuver since it requires the smallest heading change. The required heading change is computed using the candidate maneuver velocity:

$$\text{Frontside: } \bar{v}_B^+ = \bar{c}^+ - \bar{v}_A \quad \text{or} \quad \text{Backside: } \bar{v}_B^- = \bar{c}^- - \bar{v}_A \quad (93)$$

for the angle between the velocity vector  $\bar{v}_B$  (before the maneuver) and the new velocity vector (after the maneuver):

$$\text{Frontside: } \Delta\Psi_B = \cos^{-1}(\bar{v}_B^+ \cdot \bar{v}_B) \quad \text{or} \quad \text{Backside: } \Delta\Psi_B = \cos^{-1}(\bar{v}_B^- \cdot \bar{v}_B). \quad (94)$$

However, limitations for candidate maneuvers occur when the quadratic equation (91) has complex roots; these limitations will be investigated later.

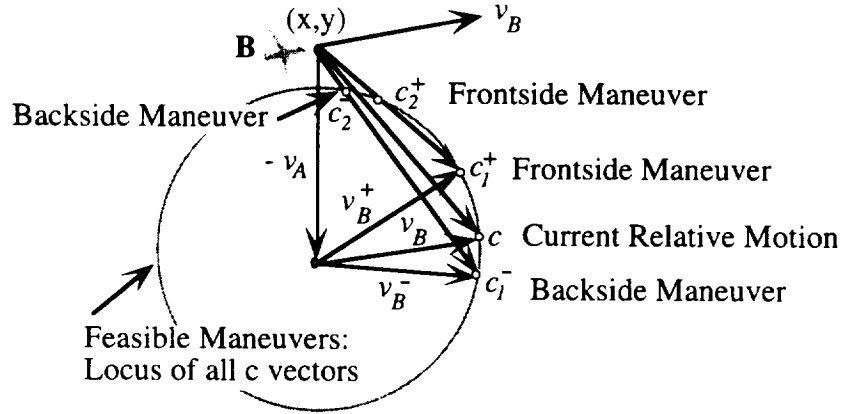


Figure 71. The four frontside and backside non-cooperative maneuvers.

For cooperative cases, the magnitudes of the relative motion vectors are similarly derived. In the cooperative case, the velocity vector for aircraft A can be changed to have components  $\bar{v}_A = v_{A_x}\hat{x} + v_{A_y}\hat{y}$ , in contrast to the non-cooperative case where  $\bar{v}_A = v_A\hat{y}$ . The model for the heading maneuver of aircraft B relative to aircraft A allows the velocity vector  $\bar{v}_B$  to be located on a circle described by the equation:

$$(c_x + v_{A_x})^2 + (c_y + v_{A_y})^2 = v_B^2 \quad (95)$$

where the relative motion is  $\bar{c} = c_x\hat{x} + c_y\hat{y}$ , and the speed of aircraft B is  $v_B$ . Given the direction of a maneuver to be  $\bar{c} = c\hat{c} = c\hat{c}_x\hat{x} + c\hat{c}_y\hat{y}$ , equation (95) becomes:

$$(c\hat{c}_x + v_{A_x})^2 + (c\hat{c}_y + v_{A_y})^2 = v_B^2. \quad (96)$$

This equation (96) establishes the following equation for the unknown  $c$ :

$$c^2 + (2\hat{c}_x v_{A_x} + 2\hat{c}_y v_{A_y})c + (v_A^2 - v_B^2) = 0 \quad (97)$$

which can be solved using the quadratic equation, provided that the components of the velocity vector  $\vec{v}_A = v_{A_x}\hat{x} + v_{A_y}\hat{y}$  are known. Since these components for the velocity vector of aircraft A are unspecified at this time (to be determined by further economics analysis), there are an infinite number of candidate solutions for the magnitude  $c$ . In comparison, the non-cooperative case results in four candidate solutions.

In both non-cooperative and cooperative cases, there are limitations on heading maneuvers in both the magnitude and direction of the maneuver. The basic geometry of a heading maneuver is determined by the relative motion  $\vec{c} = \vec{v}_B - \vec{v}_A$ , as shown in Figures 68 and 69. In general, this relative motion vector has the following magnitude lower and upper bounds:

$$\|\vec{v}_B\| - \|\vec{v}_A\| \leq |\vec{c}| = \|\vec{v}_B - \vec{v}_A\| \leq \|\vec{v}_B\| + \|\vec{v}_A\|. \quad (98)$$

Consider three cases based on speed ratio  $\gamma = v_B/v_A$ . When  $\gamma > 1$  or  $\gamma < 1$ , there is a finite lower bounds for the magnitude of  $\vec{c}$ , but when  $\gamma = 1$ , it is possible to have a zero relative motion vector,  $\vec{c} = 0$ , and at or near this condition the conflict resolution maneuver may take an impractical amount of time. As for the direction of  $\vec{c}$ , illustrated in Figure 72 and 73, cooperative scenarios have no direction limitations for  $\vec{c}$ , but for non-cooperative scenarios, there are limitations on the magnitude and direction of  $\vec{c}$  when  $\gamma \leq 1$ . This is bounded by two concentric circles, as shown in Figure 73. The magnitude of the  $\vec{c}$  vector is represented by the distance from the base point (o) to the points on the outer limit circle. When  $\gamma = 1$ , the inner circle vanishes, otherwise, for  $\gamma > 1$  or  $\gamma < 1$ , the lower bounds on the magnitude of  $\vec{c}$  creates the inner limit circle. The angle the  $\vec{c}$  vector makes with the y-axis of the aircraft A moving axis system defines a relative maneuver angle  $\beta_c$  for  $\vec{c}$ . For  $\gamma > 1$ , there are no limitations on the direction of  $\vec{c}$ . For  $\gamma \leq 1$  in the non-cooperative case, the  $\vec{c}$  vector becomes more and more constrained in direction as the speed ratio  $\gamma$  decreases;  $\vec{c}$  is limited in direction by the angles  $\beta_c < -\pi + \sin^{-1} \gamma$  and  $\beta_c > \pi - \sin^{-1} \gamma$ . When  $\gamma < 1$  and aircraft A is non-cooperative, aircraft B is flying slow in compared to the faster but non-cooperative aircraft A. If  $\vec{c}$  is directed at the Protected Airspace Zone, this situation represents an extremely dangerous non-cooperative situation; aircraft B may not be able to avoid a conflict no matter how much maneuvering is performed. This analysis of

the limitations of the magnitude and direction of the maneuver vector  $\bar{c}$  indicates that there may be some cases where one or both of the front and backside maneuvers are unachievable.

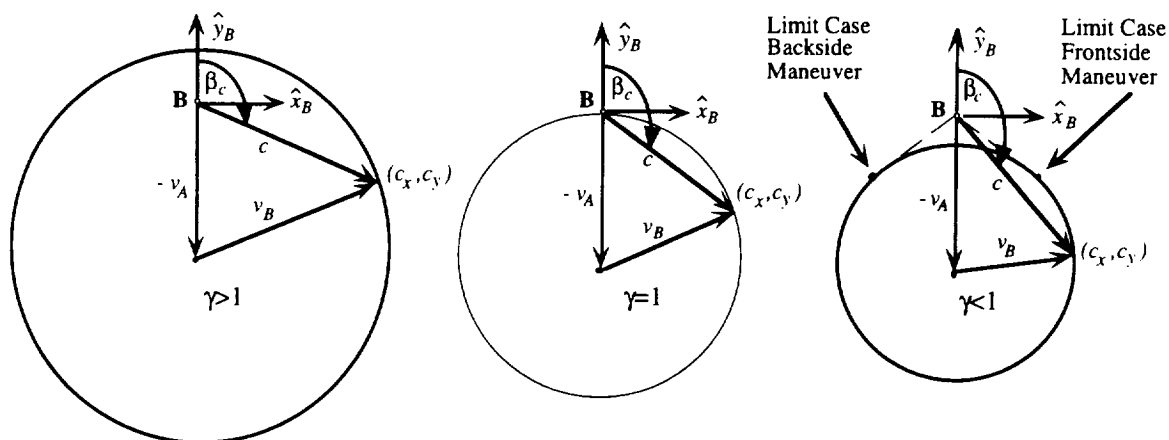


Figure 72. Three cases for non-cooperative strategic heading maneuvers; the geometry limits the magnitude and direction of the relative motion  $\bar{c}$  maneuver vectors depending on the speed ratio  $\gamma$ .

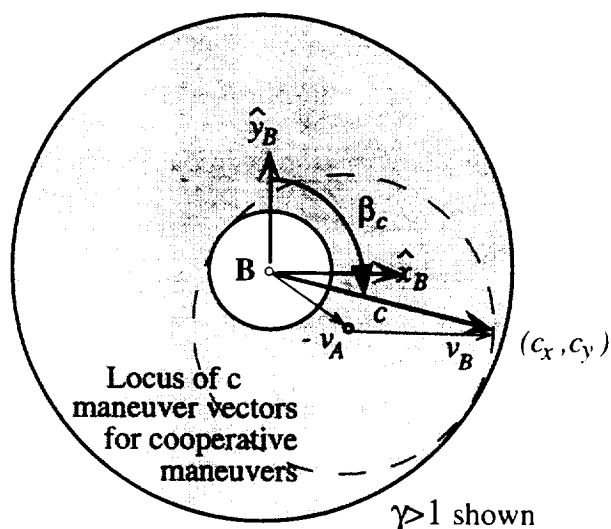


Figure 73. The geometry of the relative motion  $\bar{c}$  for cooperative strategic heading maneuvers defines a locus of all maneuver vectors in the form of two concentric circles.

Maneuver charts for optimal strategic heading control maneuvers may be formed by computing the optimal heading maneuver trajectories for arbitrary initial conditions. Example maneuver chart results are shown in Figure 74 through 76. As previously discussed, the frontside or backside maneuvers are applicable in a limited region, a band

around the pure collision relative motion line; outside this band, there is no maneuver necessary. However, a pure collision line is not always the separator (dispersal surface) between frontside and backside maneuvers. When constructing the maneuver chart, considerations must be made for the direction limitations of the relative motion vector for frontside and backside maneuvers, as previously discussed. If the speed ratio condition is Case I,  $\gamma > 1$ , then there are no limitations on the direction for a heading maneuver, and the dispersal surface is the pure collision line, as shown in Figure 74. If the speed ratio condition is Case II,  $\gamma = 1$ , then the relative motion heading is limited by the relative maneuver angle  $\beta_c < -\frac{\pi}{2}$  or  $\beta_c > \frac{\pi}{2}$ . Consequently, there are regions where only a backside maneuver can be performed, as shown in Figure 75. If the speed ratio condition is Case III,  $\gamma < 1$ , then the relative motion heading is even more limited by the relative maneuver angles  $\beta_c < -\pi + \sin^{-1} \gamma$  and on the other side by  $\beta_c > \pi - \sin^{-1} \gamma$ . Consequently, there are regions where only backside maneuvers can be performed, and a region where neither a frontside nor a backside maneuver may successfully accomplish a strategic maneuver (note that the assumptions for a strategic maneuver greatly deteriorate here as well). Figure 76 shows a maneuver chart result for Case III.

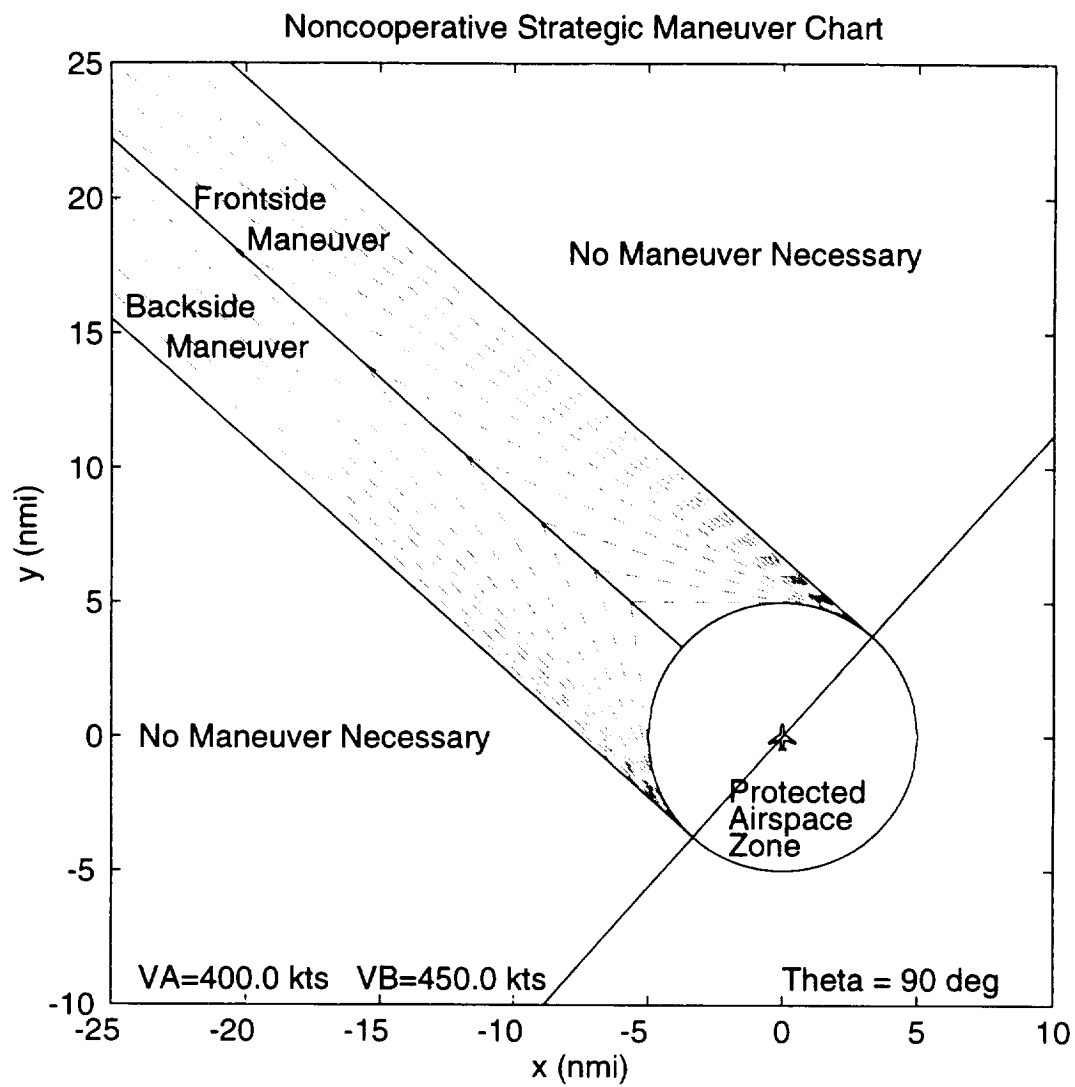


Figure 74. A non-cooperative strategic heading maneuver chart for a speed ratio  $\gamma > 1$ .

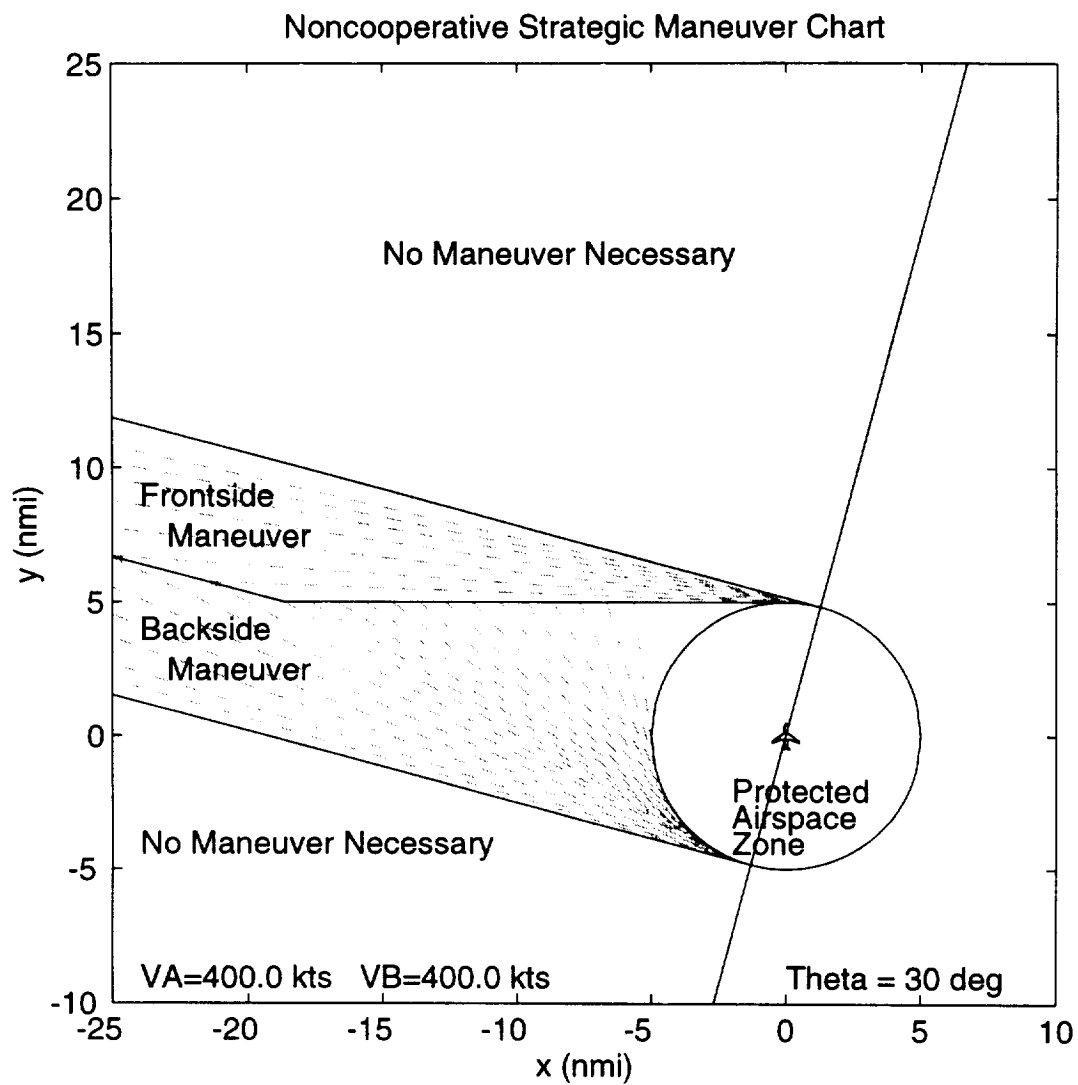


Figure 75. A non-cooperative strategic heading maneuver chart for a speed ratio  $\gamma=1$ .

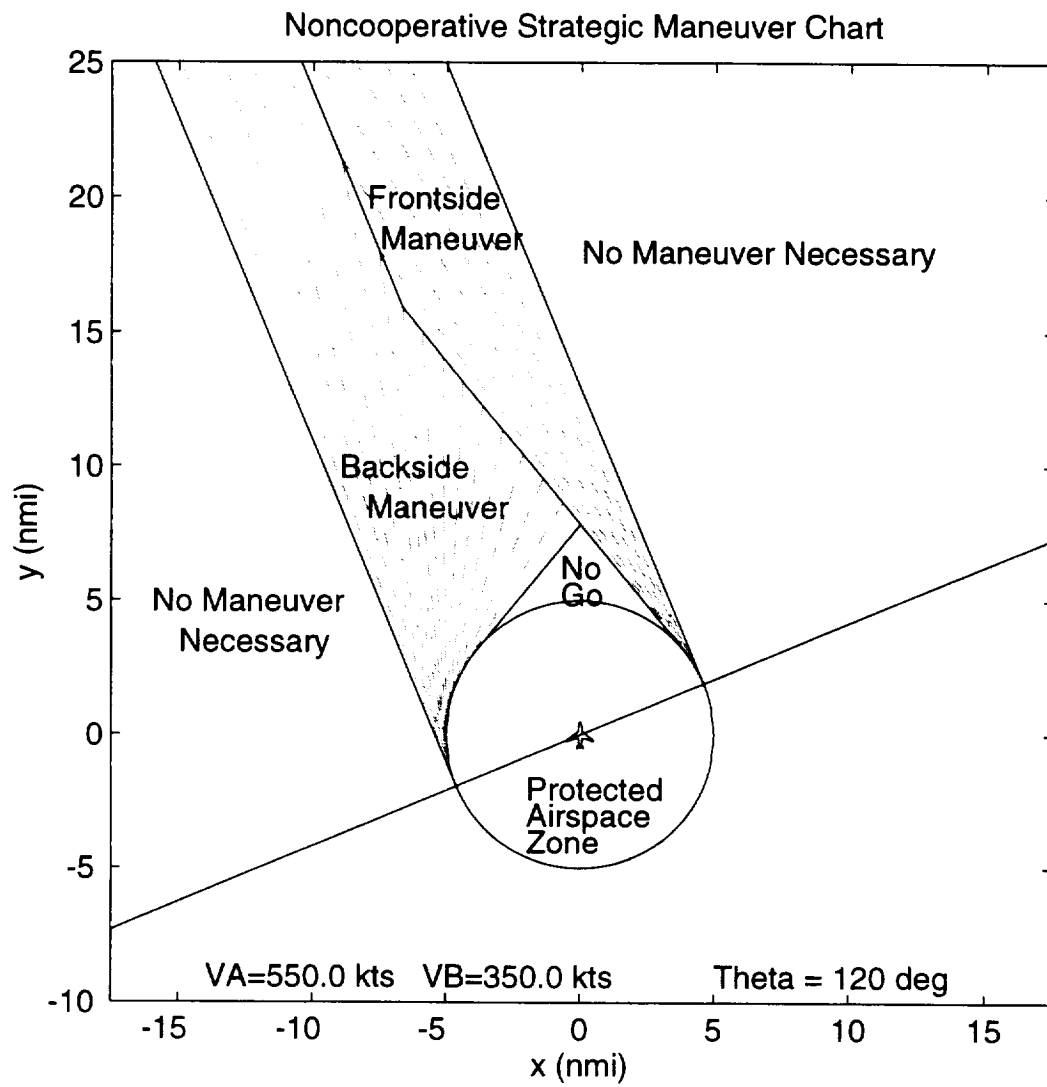


Figure 76. A non-cooperative strategic heading maneuver chart for a speed ratio  $\gamma < 1$ .

Since the optimal paths contain a saturated constraint portion, they may be difficult for a pilot to accurately follow. For easier implementation, a turning point approximation or offset approximation [DAC95] for the optimal trajectory simplifies the heading maneuver to be a series of vector heading changes, as shown in Figure 77. In this way, standard ATC vectoring commands can be given at each turning point. For our analysis, the turning point is defined by the intersection between the tangency line connecting the initial location of aircraft B to the Protected Airspace Zone constraint circle and the zero range rate line corresponding to the original course, as shown in Figure 77(a); and the offset maneuver is tangent to the Protected Airspace Zone constraint circle and parallel to the original track, as shown in Figure 77(b). While the turning point approximation has one fewer turn command, the offset approximation limits the lateral deviation for conflict resolution. To minimize the communications needed for conflict resolution, the turning point approximation can be applied with an initial turn and a return to the next way point occurring at the zero range rate point. In this way, only two commands are given, reducing the amount of communications to two transactions.

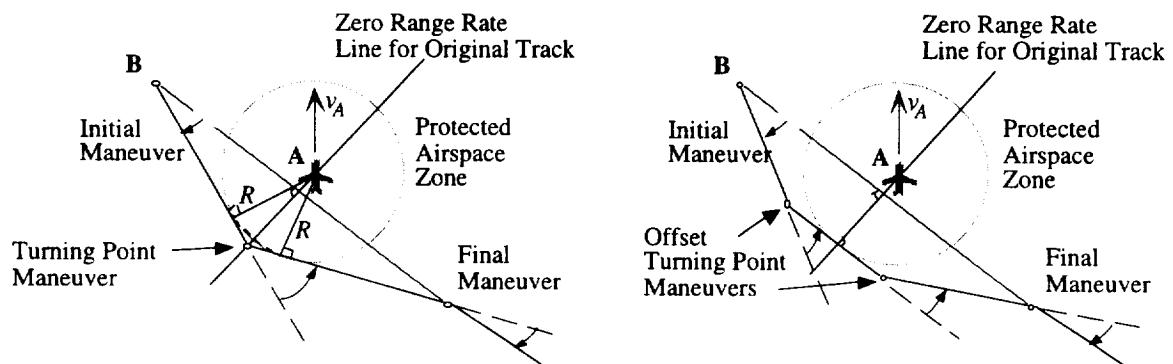


Figure 77. Two strategic heading maneuver approximations: (a) a turning point approximation, and (b) an offset approximation.

The final consideration in designing maneuver charts that are acceptable for air traffic controllers and pilots is to consider navigation methods and aids. Today, an air traffic controller typically advises an aircraft to vector in angles that are multiples of  $10^\circ$ . Perhaps in the future multiples of  $2^\circ$  or  $5^\circ$  may be more typical as more accurate navigation equipment is onboard aircraft and more precise surveillance is available for air traffic controllers. The optimal maneuver charts presented so far would advise arbitrary heading

changes, for instance  $3.7^\circ$ ,  $5.2^\circ$ , or  $8.7^\circ$ . However, these types of heading advisories may be difficult to follow by pilots without advanced navigation equipment. Instead, maneuver charts can be created to allow for heading changes that are only multiples of a standard heading change of  $2^\circ$ ,  $5^\circ$ , or  $10^\circ$ . These more practical maneuver charts can be based on the optimal precise maneuver charts with the optimal heading maneuver angle rounded up to the nearest  $2^\circ$ ,  $5^\circ$ , or  $10^\circ$ .

## 5.2 Strategic Speed Control Maneuvers

Strategic speed control maneuvers are investigated with the following assumptions. The aircraft speed profile for a strategic maneuver is illustrated in Figure 78. The aircraft accelerates or decelerates to an upper or lower speed limit. The speed limit is established such that the aircraft will arrive at the Point of Closest Approach PCA exactly at the minimum separation standard. Furthermore, a symmetric maneuver is executed such that the aircraft remains at the minimum or maximum speed until accelerating or decelerating back to the original speed. The original speed is reached at a symmetric point opposite from the initial speed maneuver point, as shown in Figure 78. Both frontside and backside maneuvers are considered for the strategic analysis.

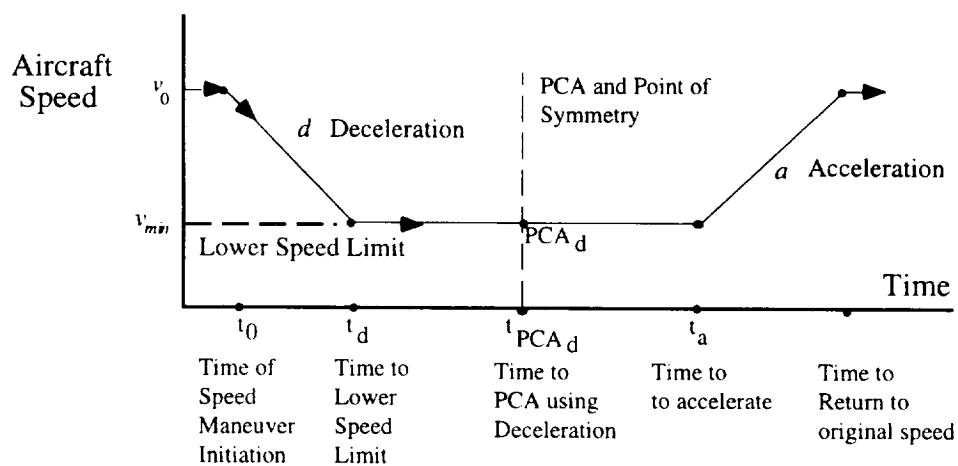


Figure 78. The symmetric speed profile used for the strategic analysis.

### 5.3 Strategic Altitude Control Maneuvers

Strategic altitude maneuvers are investigated with the following assumptions. The aircraft vertical profile for a strategic maneuver is illustrated in Figure 79. It is assumed that both aircraft are initially flying at the same altitude, both aircraft are flying steady level flight paths, and both aircraft have a relative geometry such that a pure collision would occur if no conflict resolution maneuver were performed. The geometry analysis of tactical altitude maneuvers from Chapter 4 is also used for this strategic analysis; the only difference is that maximum and minimum climb and descent rates are not used for strategic maneuvers, rather, the climb and descent rates are determined such that the aircraft B sufficiently climbs or descends from the initial condition point to clear the Protected Airspace Zone, as shown in Figure 79. Furthermore, a symmetric maneuver is executed such that the aircraft B returns to the original altitude at a distance  $d$  from aircraft A, which corresponds to the distance that aircraft B was from aircraft A when the maneuver was initiated. Since we consider only aircraft that are initially at the same altitude, there is no initial benefit to being closer to the topside or the bottomside of the other aircraft.

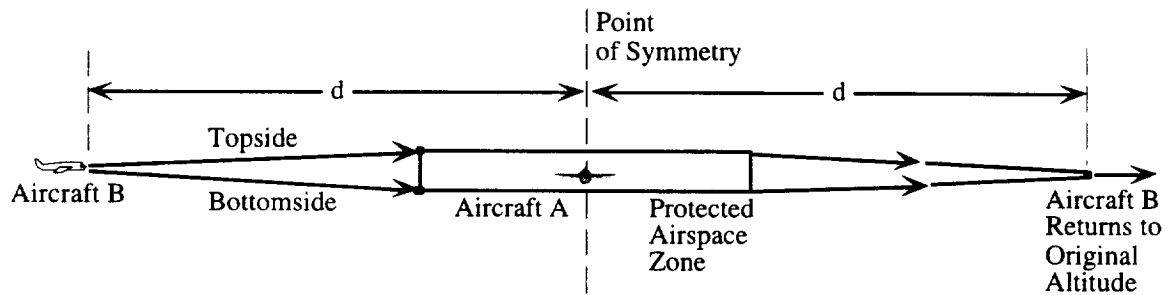


Figure 79. The symmetric speed profile used for the strategic analysis.

### 5.4 Economics Analysis

Next, we examine the economics of strategic maneuvers. The non-cooperative maneuver puts all of the additional cost on the own aircraft, and the economics analysis is used to determine when (or at what cost) to start the strategic maneuver. The cooperative maneuver lets both aircraft share the responsibility for conflict avoidance, so in this case the economics analysis determines when to start the strategic maneuver as well as how to evenly split the maneuver effort. One could argue that *even* is when each aircraft executes the same heading (speed or altitude) change or when each aircraft incurs the same fuel cost to resolve the conflict. From the standpoint of the global economics of fleets of aircraft, the

maneuver can be divided such that the total cost to both aircraft is minimized; however, this might force the more efficient aircraft to take on most of the effort. A fair way of maneuvering the aircraft can not be determined without considering the cost that each aircraft incurs for each maneuver. Also, alternative maneuvers using heading, speed, and altitude control must be compared based on economical considerations to determine the best strategic solution. Next, a model for estimating the cost of the maneuver is established.

One of the primary cost factors for aircraft is the Direct Operating Cost (DOC) penalty incurred by executing conflict resolution maneuvers. The DOC penalty function used in this research effort incorporates both fuel and time elements. Included in the DOC are 1) the additional fuel required due to the increased drag and flight path distance traveled during a maneuver and 2) the additional (non-fuel) operating costs due to the additional time required to execute the maneuver and return back to course:

$$DOC = C_{fuel}\Delta W_{fuel} + C_{time}\Delta T \quad (99)$$

where  $C_{fuel}$  is the cost of fuel,  $\Delta W_{fuel}$  is the additional fuel used in the maneuver,  $C_{time}$  is the time dependent aircraft operating cost, and  $\Delta T$  is the additional time used in the maneuver. The DOC terms  $C_{fuel}$  and  $C_{time}$  are investigated by [CD95], for example  $C_{fuel} = \$0.10/\text{lb}$  and  $C_{time} = \$15.22/\text{min}$ . A maneuver is modeled by flight segment components such as turn segments, climb segments, steady level flight segments, and acceleration segments. The time and fuel burn for each segment is summed to give a total time and fuel burn. Finally, the DOC of the maneuver is compared to the DOC for performing no maneuver at all to determine the additional fuel and time costs. Calculating the fuel burn for the aircraft is the most difficult part of the analysis and the method used is outlined below. Another factor which needs to be considered is the additional DOC incurred by neighboring traffic if it is impacted by conflict resolution maneuvers; however, we do not model this cost in our current analysis.

A fuel burn estimate is required to properly estimate the cost of maneuvering an aircraft for conflict resolution. Such an analysis is performed with the Breugot range/endurance equation [An89]. To start, consider the fuel burn equation:

$$\frac{dW}{dt} = T_R c_j \quad (100)$$

where  $W$  is the weight,  $c_j$  is the specific fuel consumption, and  $T_R$  is the required thrust. For horizontal or climbing maneuvers the required thrust will be:

$$T_R = D + W \sin \gamma_{ss} \quad (101)$$

where  $D$  is the drag and  $\gamma_{ss}$  is the steady state flight path angle. Aircraft are modeled with parabolic drag polars and fuel consumptions which vary linearly with airspeed. The lift coefficient  $C_L$  is described in terms of the aircraft weight and speed as follows:

$$C_L = \frac{2W \cos \gamma_{ss}}{\rho V^2 S_w} \quad (102)$$

where  $V$  is speed,  $\rho$  is air density, and  $S_w$  is the reference wing area. The drag is modeled:

$$D = \frac{1}{2} C_D \rho V^2 S_w \quad (103)$$

where  $C_D$  is the drag coefficient, approximated by:

$$C_D = C_{D_0} + K C_L^2. \quad (104)$$

Here,  $C_{D_0}$  is the zero lift drag coefficient,  $K = \frac{1}{\pi e AR}$  is the induced drag factor,  $e$  is Oswald's efficiency factor, and  $AR$  is the wing aspect ratio. Furthermore, the thrust specific fuel consumption of a turbojet or turbofan engine increases nearly linearly with mach number [Ra92]. For this reason, the fuel consumption can be modeled as:

$$c_j = \sigma V \quad (105)$$

where  $\sigma$  is the linear coefficient. Next, these endurance equations can be combined to obtain the fuel burn equation:

$$\frac{dW}{dt} = - \left( \frac{1}{2} \rho V^2 S_w \left( C_{D_0} + K \left( \frac{2W \cos \gamma_{ss}}{\rho V^2 S_w} \right)^2 \right) + W \sin \gamma_{ss} \right) \sigma V. \quad (106)$$

Equation (106) is integrated to calculate the fuel burn, given the geometry of the previously defined turning point heading maneuvers, symmetric altitude maneuvers, or symmetric speed control maneuvers. For cases of constant altitude and constant climb rate, the airspeed is constant, allowing equation (106) to be evaluated analytically. For acceleration cases where the velocity is not constant, the equation must be integrated numerically.

Heading maneuvers, altitude maneuvers, and speed control maneuvers are compared based on economics. Consider the following example. Two identical generic turbojet aircraft flying at the same speed are positioned such that a pure collision will result if no evasive action is taken. The specifications for the aircraft are shown in Table 1. The

speed of the aircraft is chosen so that the direct operating cost DOC is minimized. For example, Figure 80 shows this speed is 400 kts for a hypothetical aircraft. At some specified range from the point of conflict, one of the aircraft maneuvers to avoid the conflict using a non-cooperative maneuver. Figure 81 through 86 illustrate heading, speed, and altitude cost analysis results when the scenario geometry is varied. This analysis can identify the cost to maneuver, which in turn, can be used to determine which maneuver to use and when to initiate the non-cooperative maneuver.

Table 1. Specifications for a conflict resolution investigation.

Altitude	34000 <i>ft</i>
Zero lift drag coefficient , $C_{D0}$	0.019
Induced drag factor, $K_2$	0.054
Fuel efficiency factor, $\sigma$	$2.08 \times 10^{-3} \text{ lb}/(\text{lb hr kt})$
Gross Weight	110000 <i>lbs</i>
Wing Area	1889 <i>ft</i> <sup>2</sup>
Cost of fuel	\$0.12/ <i>lb</i>
Cost of flight time	\$ 913.20/ <i>hr</i>

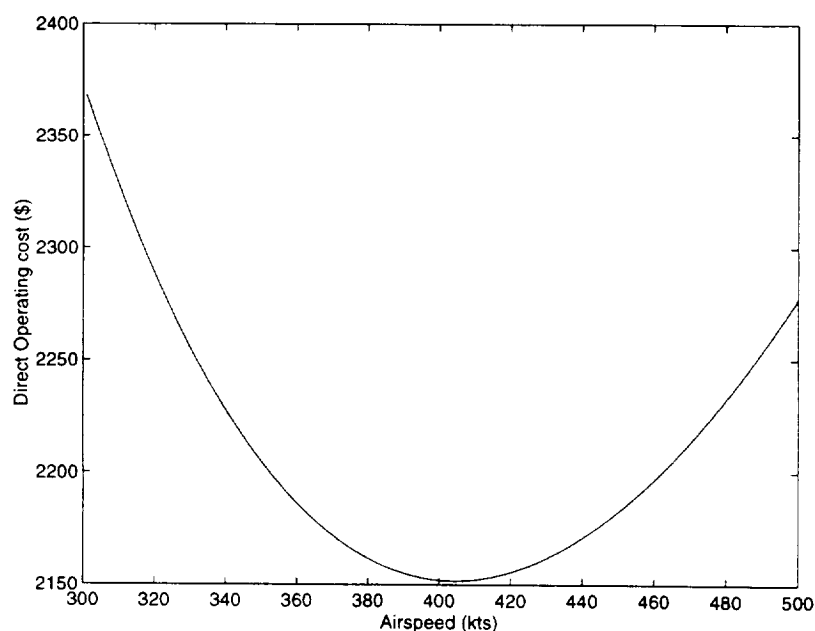


Figure 80. Example aircraft DOC versus airspeed for a 500 nmi cruise.

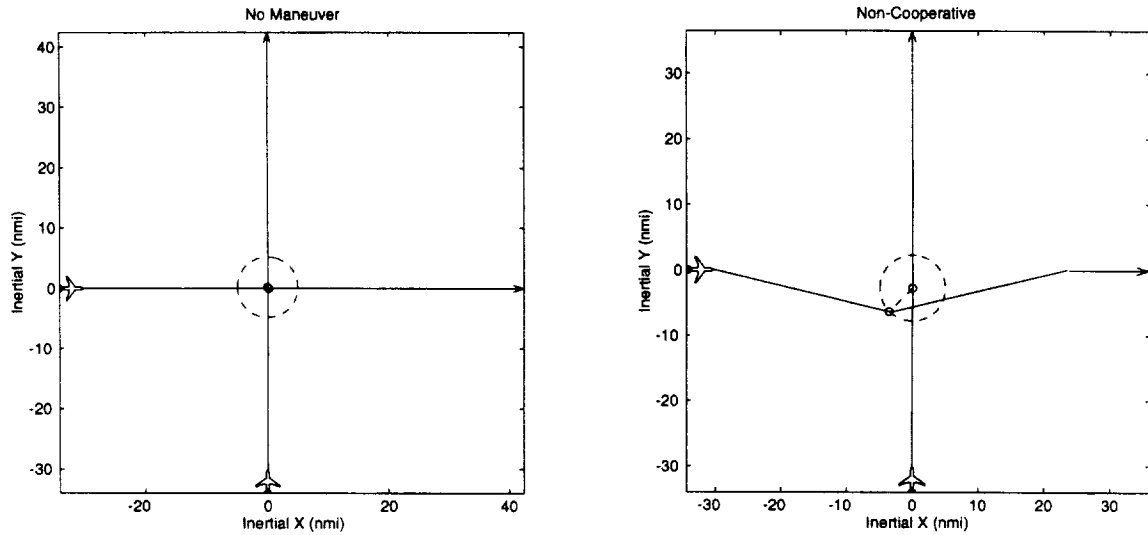


Figure 81. Example solution for no maneuver (left) and a non-cooperative heading maneuver (right) for an initial heading difference  $\theta = 90^\circ$  and 30 nmi distance from a pure collision.

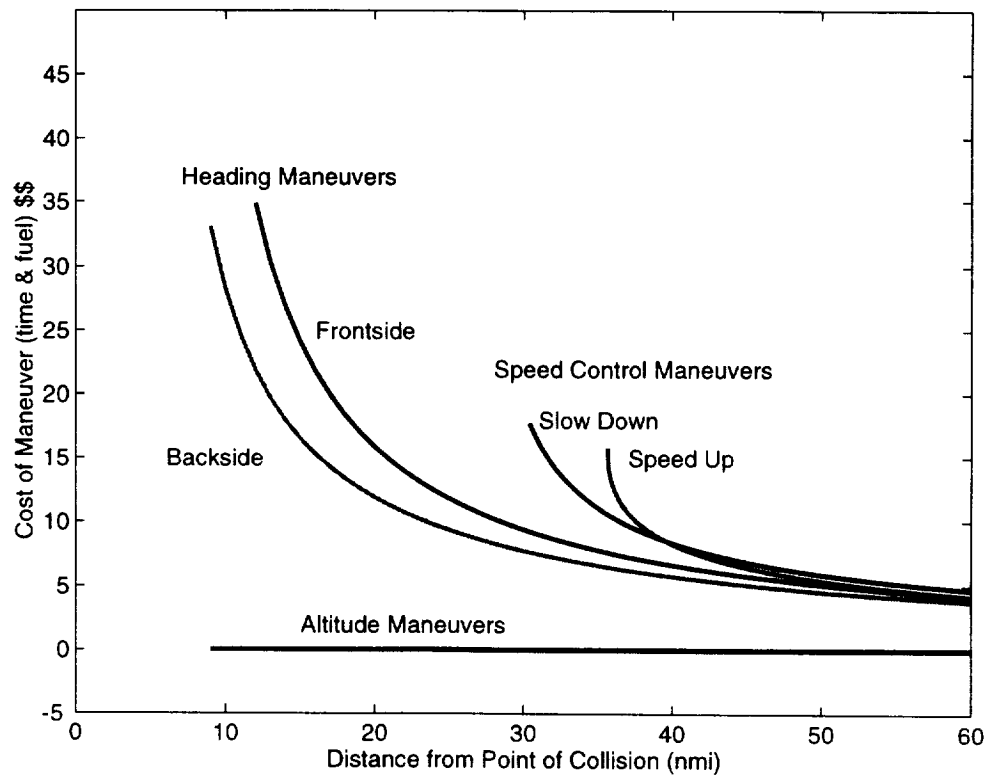


Figure 82. Maneuver costs for non-cooperative maneuvers with an initial heading difference of  $\theta = 90^\circ$ .

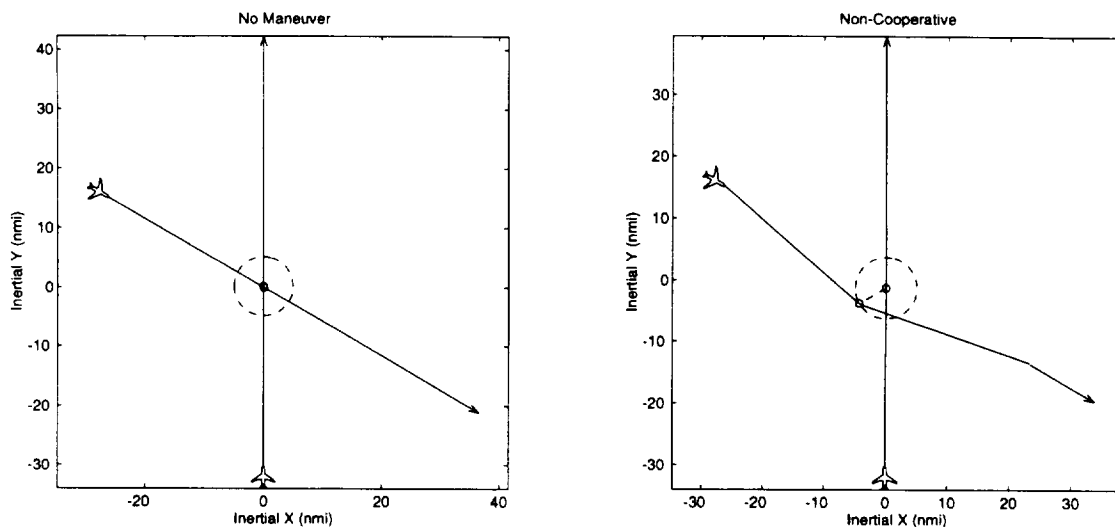


Figure 83. Example solution for no maneuver (left) and a non-cooperative heading maneuver (right) for an initial heading difference  $\theta = 120^\circ$  and 30 nmi distance from a pure collision.

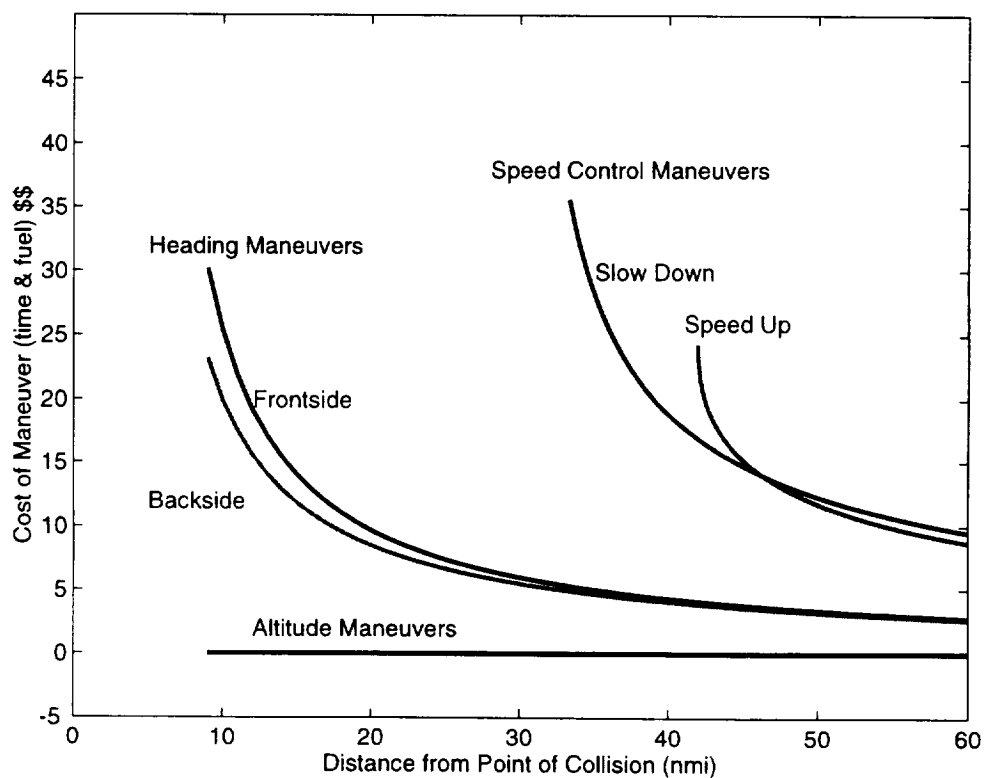


Figure 84. Maneuver costs for non-cooperative maneuvers with an initial heading difference of  $\theta = 120^\circ$ .

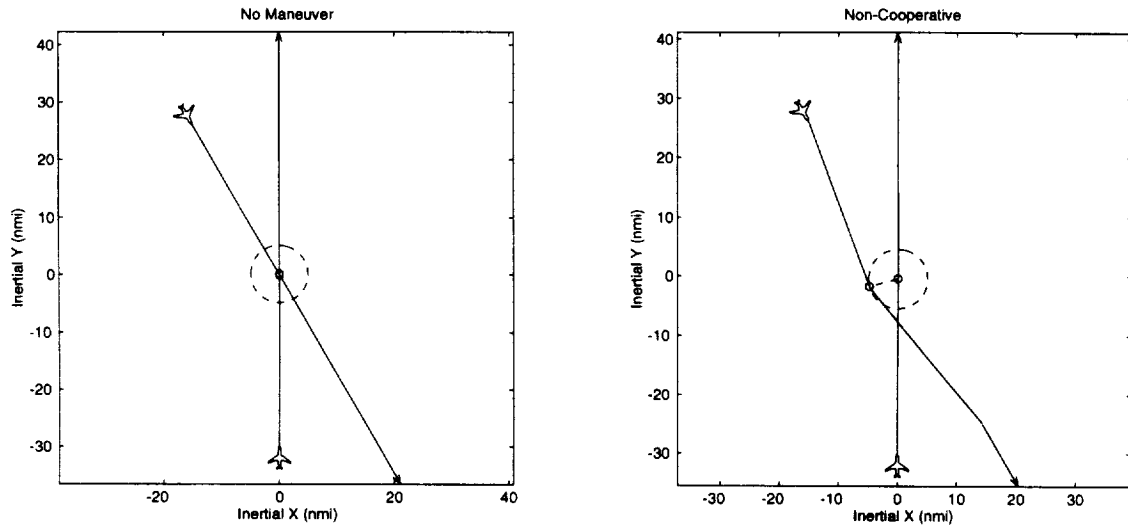


Figure 85. Example solution for no maneuver (left) and a non-cooperative heading maneuver (right) for an initial heading difference  $\theta = 150^\circ$  and 30 nmi distance from a pure collision.

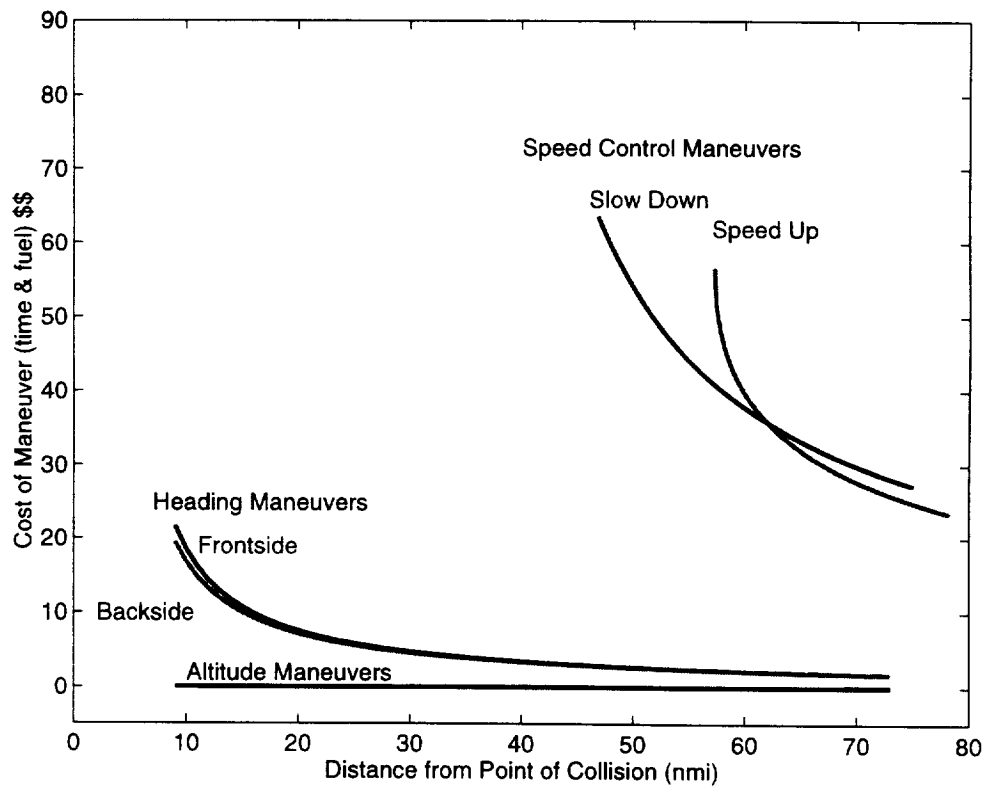


Figure 86. Maneuver costs for non-cooperative maneuvers with an initial heading difference of  $\theta = 150^\circ$ .

These results imply several important conclusions. The most obvious conclusion is that altitude maneuvers are far less costly to perform than either speed or heading maneuvers. Furthermore, altitude maneuvers appear to be independent of initial aircraft orientation and the range at which the aircraft start the maneuver. Notice that speed maneuvers become prohibitively expensive when closer than a range of 30-40 nmi. Also, as the heading difference  $\theta$  increases for the two aircraft, the heading maneuvers become less expensive and the speed maneuvers become more expensive.

Altitude maneuvers prove to be favorable for a couple of reasons. First, the vertical separation requirements are less stringent than the horizontal separation requirements, thus making altitude maneuvers easier to achieve. An aircraft only needs 1000 ft vertical separation compared to 5 nmi (30380 ft) horizontal separation. If one only considers clearance distance required by each maneuver, the altitude maneuver is 30 times less demanding. (As the horizontal separation constraint is reduced with better surveillance, for instance, from 5 to 3 to 1 nmi, this argument will change.) The second advantage for altitude maneuvers is that they are largely conservative. The aircraft gains potential energy while climbing which it, in turn, uses during the descent. Since the climb rate required to gain 1000 ft over a range of 10 to 50 nmi is very low, the airspeed of the aircraft hardly changes. The resulting increase in drag is small, making the maneuver almost conservative. In comparison, the turning aircraft increases its load factor which increases drag considerably, and consumes energy nonconservatively. Furthermore, the detour that the turning aircraft makes has no subsequent benefit.

The speed maneuvers are the most costly of all of the maneuvers. Slowing the aircraft not only wastes time but also operates the aircraft at a speed which is inefficient. Speeding the aircraft up, while not wasting time, again operates the aircraft at an inefficient speed. To explain the inefficiency, recall that drag increases with the square of velocity and the power required for flight increases with the cube of velocity.

Next, the direct operating cost DOC model is used to investigate cooperative strategic maneuvers. The purpose of the analysis is to determine the best way for two aircraft to *evenly* split the strategic maneuver. The key word *even* is dependent on a criterion yet to be established; indeed, it is not necessarily the intent of this research to define *even*, but rather to discuss the options and illustrate the results. Consider the case where simple heading vectors are used as is shown in Figure 87. One could argue that *even* is when each aircraft executes the same heading change. However, when the same heading change is executed by two aircraft traveling at different speeds, the faster aircraft

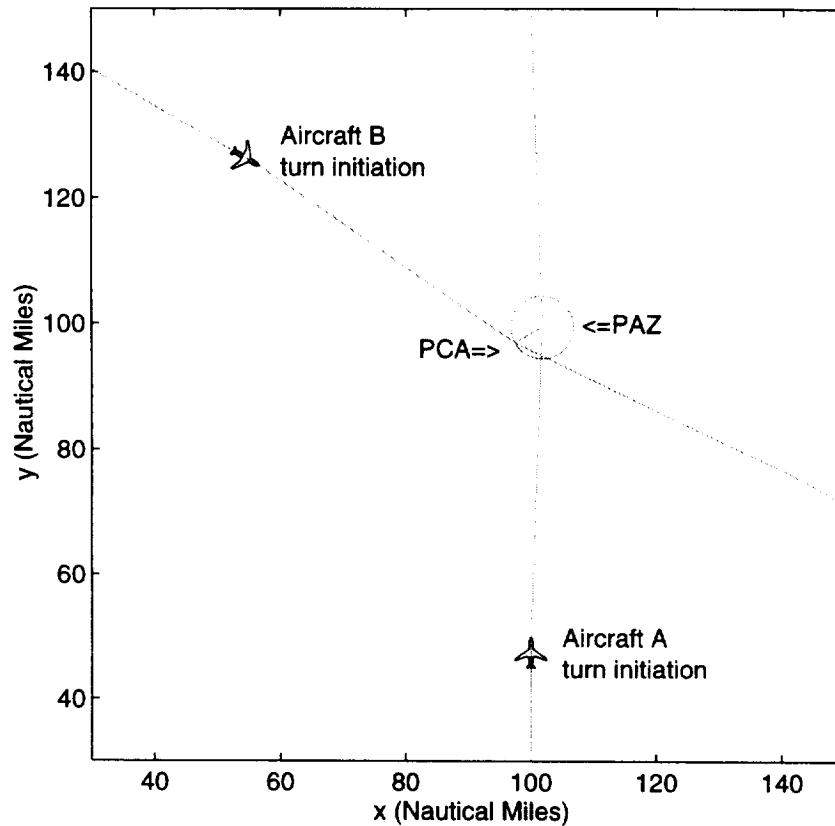


Figure 87. The flight paths for Aircraft A and B during a cooperative strategic maneuver; a line connects the trajectories at the Point of Closest Approach PCA.

will contribute more to the miss distance. Next, *even* could also be defined when each aircraft contributes equal amounts of fuel cost in resolving the conflict. Yet another way to define *even* would be to choose a maneuver which minimizes each aircraft's conflict resolution direct operating cost. Note also that the information available to a decision support algorithm is likely to only include the positions, speeds and headings of both aircraft. With such limited information, it is difficult to determine the most economic maneuver when the economics is so dependent on individual aircraft performance. Thus, any algorithm based on economics will necessarily have to be fairly general. Also, the method developed should be a suitable economical analysis for virtually any two aircraft.

The purpose of the analysis is to economically compare maneuvers; the purpose is *not* to evaluate nor to rank the most economical aircraft. Comparisons of specific aircraft pairs do not lend themselves to general conclusions. Consider the comparison of a business jet encountering a large commercial transport. The business jet, generally being one tenth the weight of the transport, will always burn less fuel regardless of the maneuver. The subsequent economic analysis suggests that total cost is minimized by always placing

the total burden of the maneuver on the business jet regardless of the speed of the two aircraft. Such results do not suit our purpose. To make generalized conclusions, we must specifically avoid results which are biased by aircraft performance.

The problem with comparing the operating costs for cooperative maneuvers is that the more efficient aircraft typically bears more of the burden of maneuvering. To avoid an unfair bias towards issuing larger heading changes to the more efficient aircraft, a special effort must be taken to artificially set both aircraft to be equally efficient. Under these conditions, we then split the effort equally. If they are not equally efficient in reality, which is most likely the case, then the less efficient aircraft ends up incurring a greater cost.

To develop a general result, some economic equivalence must be imposed. Therefore, the following rule is applied to both aircraft models in the analysis: the DOC in terms of \$/nmi will be assumed identical for all aircraft regardless of speed. The operating cost could also have been determined in terms of \$/hr, since maintenance schedules are often determined by hours of operation. This definition stems from the standard metric of cost/seat /mile, commonly used by the airlines.

To achieve the economic equivalency, five constraints are imposed on the two aircraft models which are used in the analysis: 1) establish the same drag polar with  $K_A = K_B$ , 2) establish the same initial lift coefficient  $C_{L_A} = C_{L_B}$  to insure equal aerodynamic efficiency, 3) use the same specific fuel consumptions  $\sigma_A = \sigma_B$ , 4) establish the same weight  $W_A = W_B$ , and 5) establish crew times proportional to aircraft speeds:

$$\frac{C_{time\ B}}{C_{time\ A}} = \frac{v_B}{v_A}. \quad (107)$$

Both aircraft must be fixed to have identical drag polars so that they have the same drag coefficient at a given lift coefficient. To insure equal lift to drag  $L/D$  ratios, both aircraft must also be fixed to have the same lift coefficient. This requires  $C_{D_{0A}} = C_{D_{0B}}$ , and for aircraft at different speeds, the reference area,  $S_w$ , for each aircraft must be adjusted so that the lift coefficients are the same:

$$C_{L_A} = \frac{2W_A}{\rho V_A^2 S_{w_A}} = C_{L_B} = \frac{2W_B}{\rho V_B^2 S_{w_B}} \text{ so that } S_{w_B} = S_{w_A} \frac{V_A^2}{V_B^2}. \quad (108)$$

To insure that the fuel consumption yields equivalent fuel burns for both aircraft, the fuel consumptions are scaled as follows:  $c_{j_A} = \sigma V_A$  and  $c_{j_B} = \sigma V_B$ , where  $\sigma$  is the fuel efficiency factor of the generic aircraft as indicated in Table 1.

Using this analysis, two economically equivalent aircraft are investigated to establish the cooperative maneuver. Consider the case where aircraft B is flying at 300 kts and aircraft A is flying at 400 kts, where these are the ideal operating speeds for each aircraft, as shown in Figure 88. Notice both aircraft are fixed to have the same unit cost per nmi even though they have different operating speeds. Figure 89 shows the required heading changes and DOC for both aircraft plotted as a function of the percentage of the final miss distance that aircraft A contributes (B contributes the difference). The cost of the maneuver is shared equally where the DOC lines for each aircraft cross. Note that this is not necessarily where both aircraft execute the same heading change. Furthermore, the point where the overall DOC is minimized is where aircraft A bears 68% of the burden for the turn (marked \*). This plot indicates that it is more economical to let the faster aircraft bear more of the maneuvering burden. For two aircraft with equal speeds, plots indicate that backside maneuvers are generally less costly than frontside maneuvers. The backside maneuver is generally more efficient because the relative velocity,  $\bar{c}$ , is faster with backside maneuvers; the point of closest approach is then reached sooner than when the frontside maneuver is used.

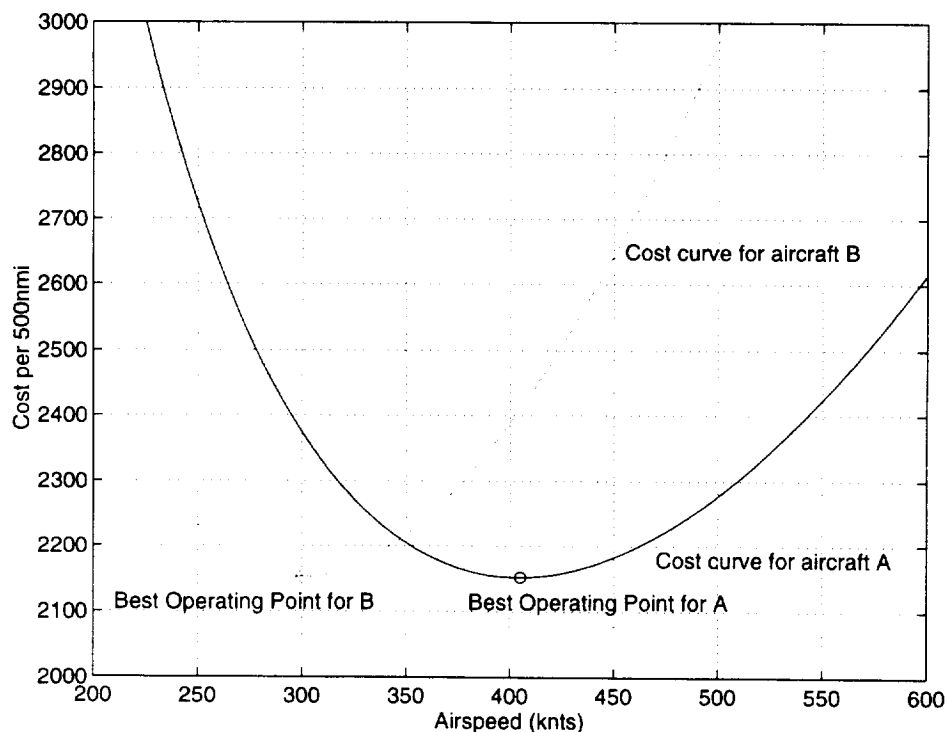


Figure 88. A cost curve comparison between two different aircraft, Aircraft A and Aircraft B, over a 500 nmi distance.

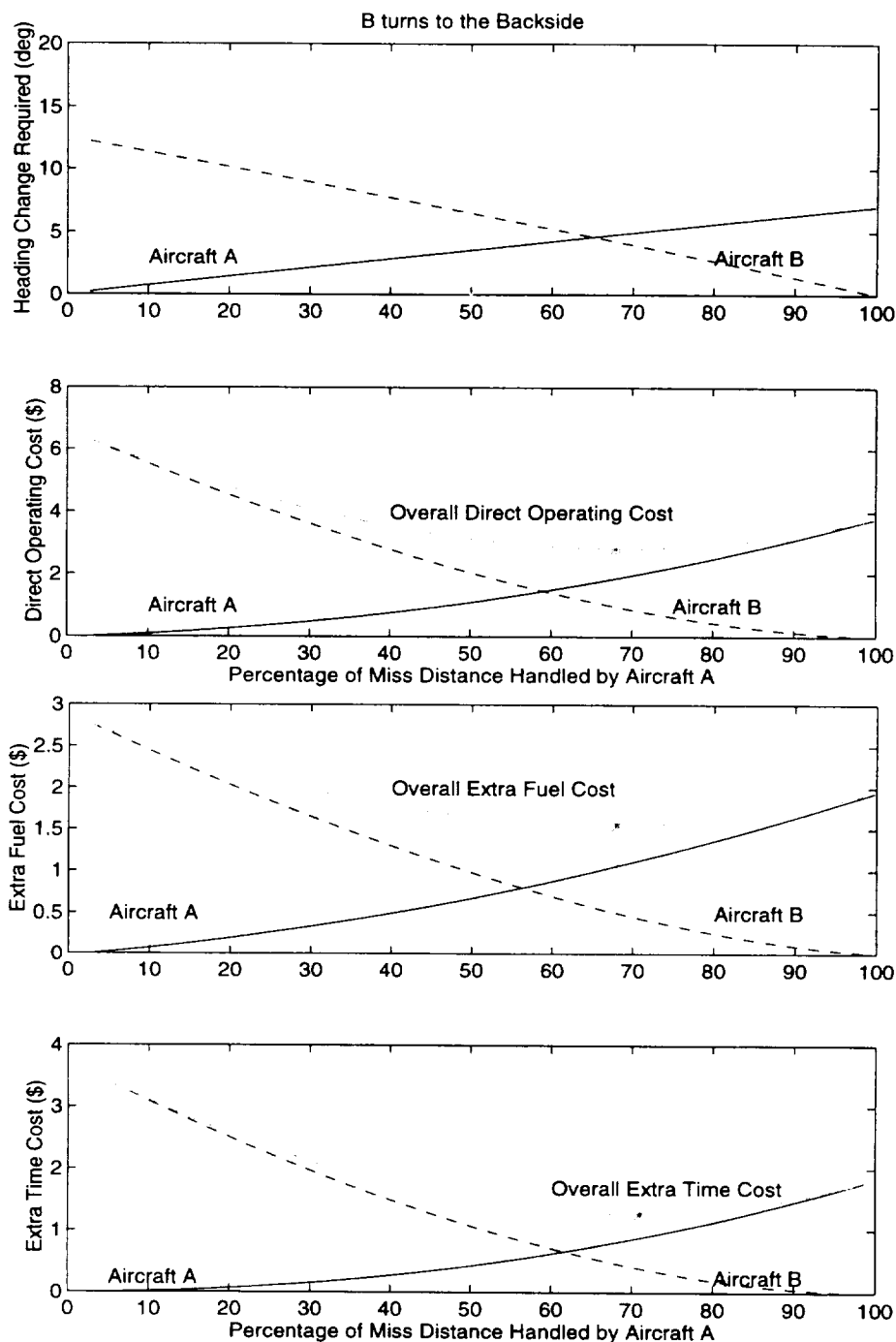


Figure 89. Required heading change and DOC for aircraft at different speeds; Aircraft A at 400 kts and Aircraft B at 300 kts in a 90 degree conflict; the top plot identifies the heading changes required for aircraft A and B for feasible conflict resolutions, the second plot identifies the minimum DOC solution, the third plot identifies the total minimum fuel solution, and the bottom plot identifies the minimum total time delay solution. Also indicated in each plot is the equal heading, DOC, fuel, and time solutions where the individual solutions for aircraft A and B cross.

## 5.5 Benefits of Reduced Separations Standards

Next, the benefits of reduced separation standards can be investigated by performing this analysis for cases where the Protected Airspace Zone PAZ radius is reduced from 5 to 3 or 1 nmi – feasible due to more accurate navigation information, such as provided by GPS. Figures 90 through 92 illustrate the economics of reducing the separation requirements. The results indicate that a reduction in the horizontal separation standard from 5 to 3 nmi can reduce the cost of a maneuver by roughly 3 times. Reducing the horizontal separation standard from 5 to 1 nmi can reduce the cost of a maneuver by roughly 10 times. No significant change occurs in the cost of altitude maneuvers, which are relatively inexpensive for all cases.

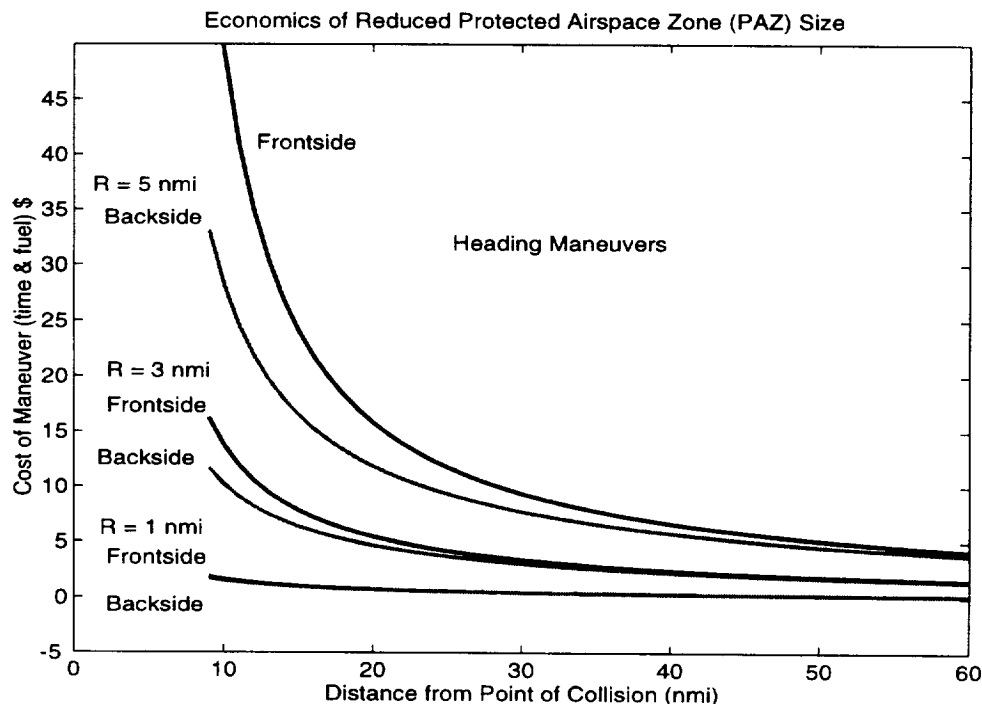


Figure 90. The cost of non-cooperative heading maneuvers where aircraft B flies to the frontside or backside of aircraft A; trends show the economic advantage of reducing the horizontal separation requirement from 5 to 3 or 1 nmi (heading difference of  $\theta = 90^\circ$ ).

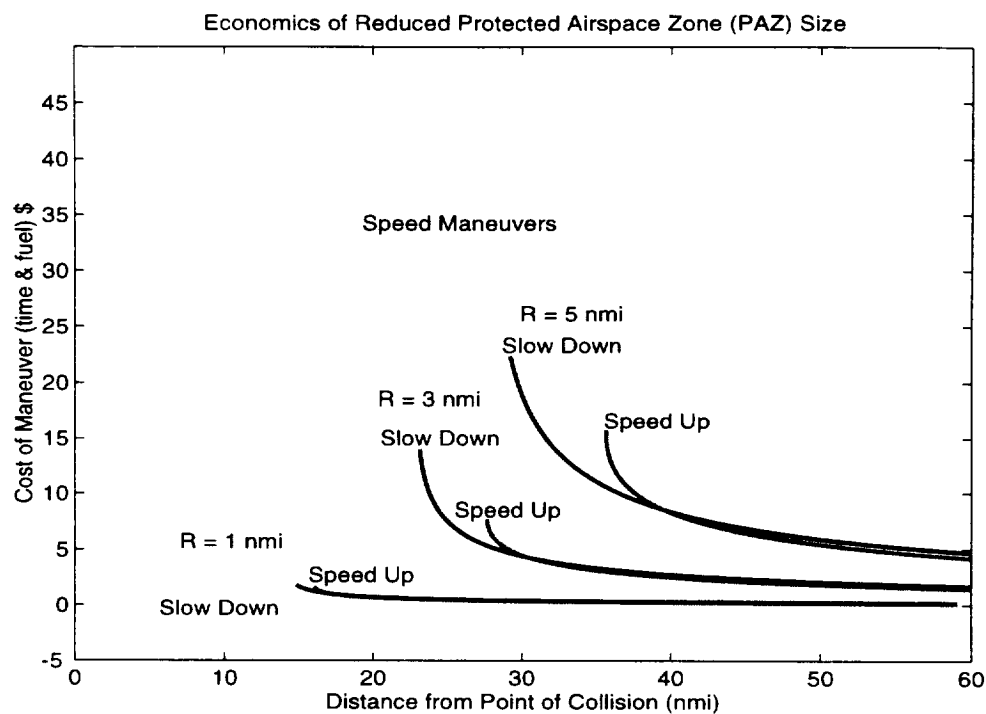


Figure 91. The cost of non-cooperative speed control maneuvers where aircraft B slows down or speeds up with respect to aircraft A; trends show the economical advantage of reducing the horizontal separation requirement from 5 to 3 or 1 nmi (heading difference of  $\theta = 90^\circ$ ).

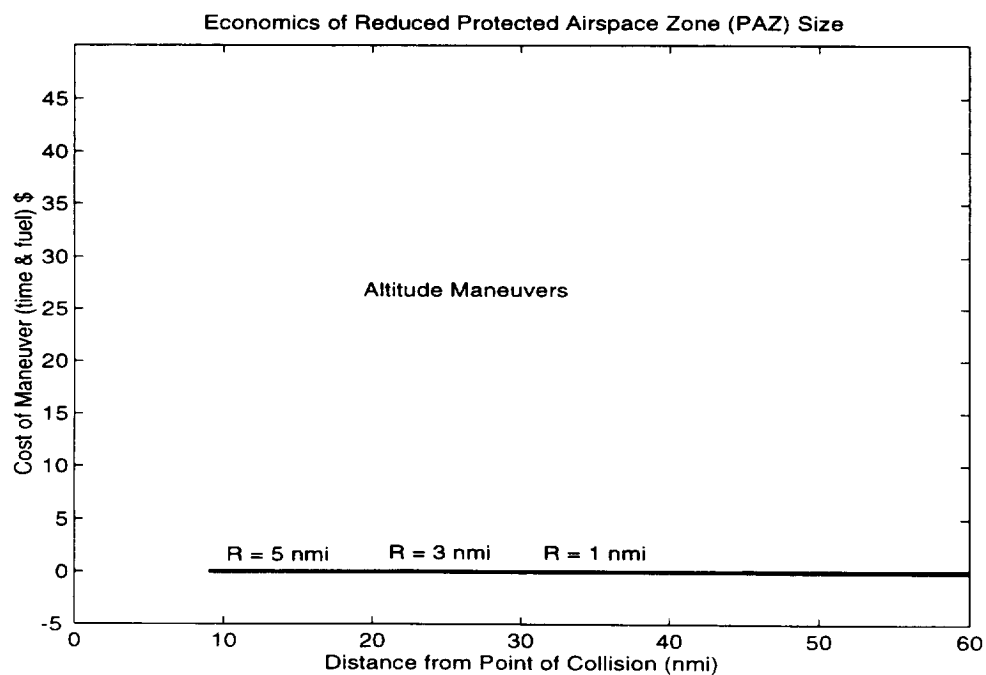


Figure 92. The cost of non-cooperative altitude control maneuvers where aircraft B slows climbs up 1000 ft with respect to aircraft A; trends show little difference in reducing the horizontal separation requirement from 5 to 3 or 1 nmi (heading difference of  $\theta = 90^\circ$ ).

## 5.6 Combined Tactical and Strategic Maneuver Charts

Finally, transitioning from no maneuver to strategic cases and between strategic and tactical cases needs further analysis. While the desire to minimize the economic penalty leads to a more gradual maneuver at a longer initial range, a tradeoff exists due to the greater uncertainty in predicting the separation at closest approach. When vary far away, no maneuver should be performed until the probability of false alarm is sufficiently reduced, as shown in Figure 93. Deciding when the strategic situation becomes a tactical situation will require human factors research, which is not discussed here. This transition may be triggered by some warning time-to-go to the Tactical Alert Zone, essentially the last chance to maneuver. Examples of such time-to-go warnings were covered in Chapter 3.

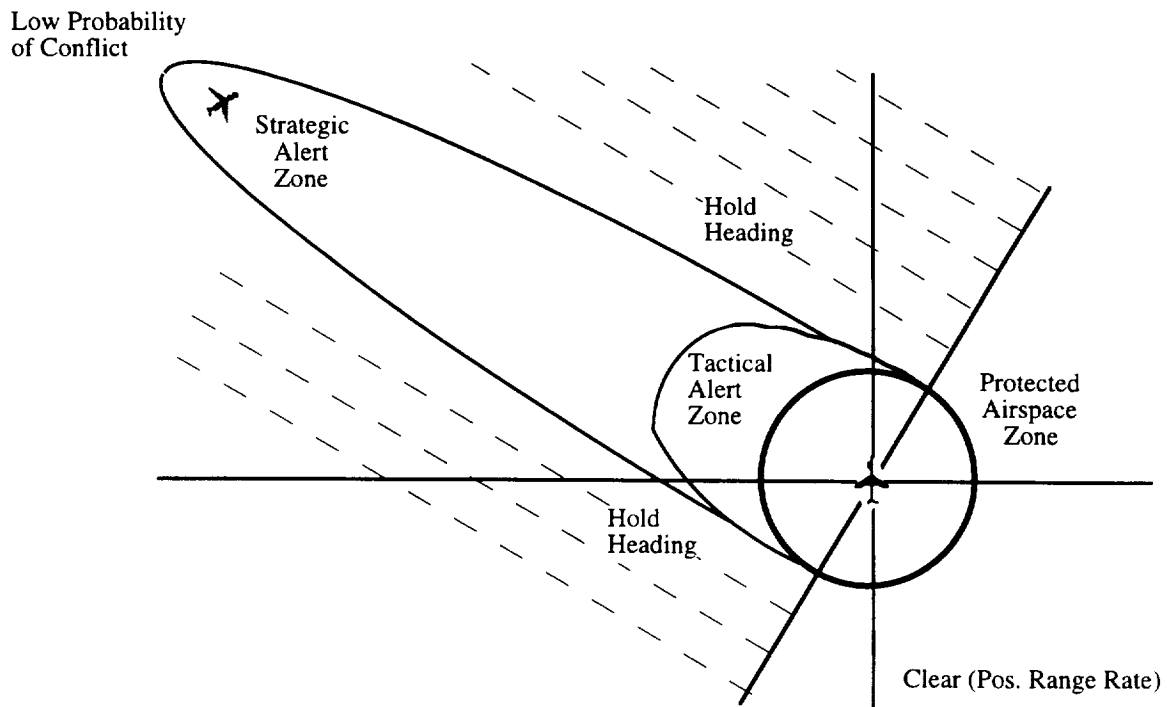


Figure 93. Regions around the Protected Airspace Zone help to define when no maneuver is performed due to a low probability of conflict, when the strategic maneuver is used, and when the tactical maneuver is used.

## 6. SYSTEM MECHANIZATION ISSUES

In this chapter, mechanization issues associated with fielding an effective conflict detection and resolution system are discussed. First, the various system elements, or components, are identified. Then, we discuss the mechanization of the conflict detection logic including the effects of measurement error on probabilities of false alarm, missed alarm, and incorrect maneuver selection. Next, the coordination of maneuvers via data exchange between two cooperative aircraft is discussed, including communication requirements. Displays and human factors issues are described next, and finally, the uses of simulations and flight tests to evaluate a prototype system are summarized.

### 6.1 Mechanization Elements

Figure 94 is a block diagram that depicts the elements, or components, that make up or affect a conflict detection and resolution system within the context of an aircraft system.

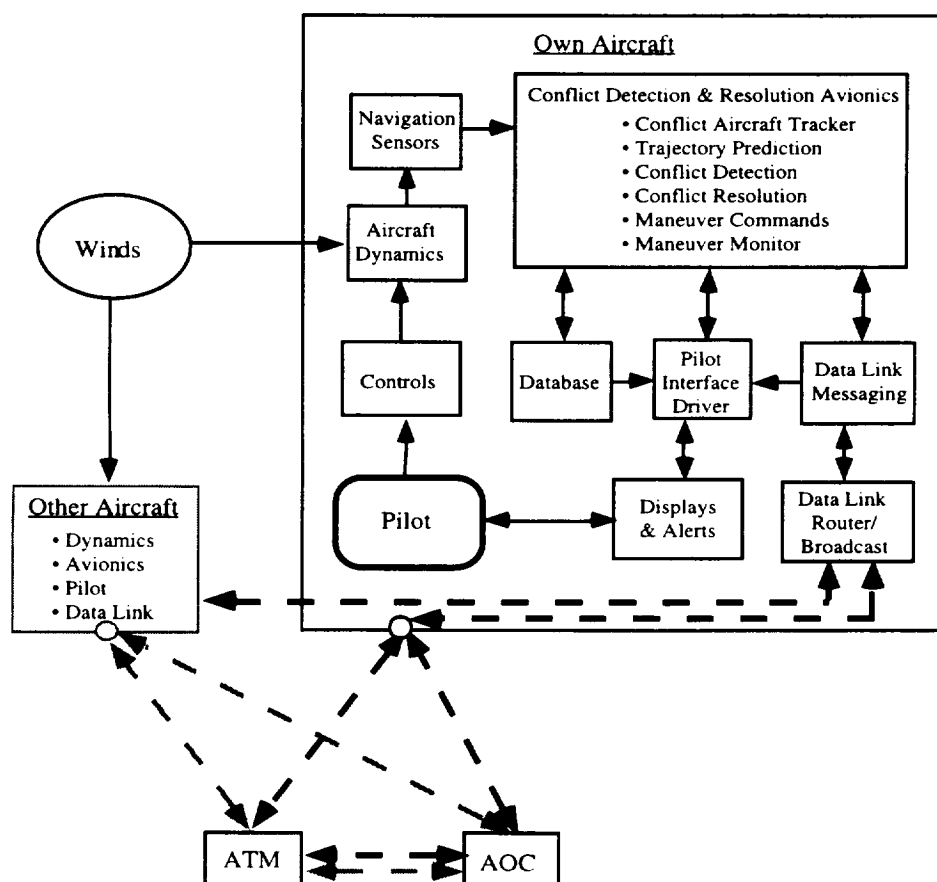


Figure 94. Mechanization elements of a traffic conflict detection and resolution system.

Included in this system block diagram are the following:

- 1) *Own Aircraft Dynamics*. This is the controllable “plant” that is being maneuvered to avoid the conflict. The plant is modeled with point mass dynamics, as presented earlier in this report.
- 2) *Navigation Sensors*. This includes GPS complemented possibly by baro-altimeter, INS, WAAS, or LAAS signals. An air data computer may also be used to derive true airspeed. These sensors are used to compute the current position and velocity (state) of the own aircraft.
- 3) *Conflict Detection and Resolution Avionics*. This is the collection of avionics that implement the conflict detection and resolution algorithms. Included are the following components:
  - a. *Conflict Aircraft Tracker* based on received state and intent messages, either directly from the other aircraft or from ground ATM sources;
  - b. *Trajectory Prediction* of aircraft based on state and intent data for the own and other aircraft;
  - c. *Conflict Detection* based on relative range, range rate, speed, altitude, point of closest approach PCA, time-to-PCA, and conflict probability;
  - d. *Conflict Resolution* consisting of the maneuver and timing selection logic to resolve conflicts;
  - e. *Maneuver Commands* consisting of the collaboration logic needed to execute the maneuver and coordinate motion with associated maneuvers of other aircraft; and
  - f. *Maneuver Monitor* consisting of the logic that insures that conflicts are being resolved as planned. Vernier control commands may be required to remove trajectory errors.
- 4) *Pilot Interface Driver*. This function computes the visual information that can be projected onto a 2D plan view, 2D profile view, or 3D perspective view display and aural alarms to alert the pilot of conflict situations. It includes the logic for icon shape, orientation, placement, color, color changes, projection vectors, etc. as determined by human factors studies to create an effective situational awareness display. Textual messages may also be displayed. Information communicated to the pilot also includes the command information that suggests how to respond to a detected conflict – which maneuver to make, when to begin and end segments of the maneuver, how other aircraft in the conflict are responding, and how to return to the flight plan after the conflict has been resolved.

- 5) *Displays and Alerts.* This includes a 2D plan view or 3D perspective view display and aural alarms to alert the pilot of conflict situations. Also included is pilot interface mechanisms for selecting maneuver options, setting map range scale, and adjusting the flight plans for conflict resolution follow-up. In a sense, the displays work as a flight director.
- 6) *Database.* The database contains the various data needed for an effective conflict detection and resolution system. These data include:
  - a. *Flight Plan Data* used to determine the own aircraft intent;
  - b. *Tracked Trajectory Data* and known intent data maintained for other aircraft which may pose conflict threats;
  - c. *Wind Field Data* assisting in trajectory prediction for own and other aircraft; this is used for conflict detection assessment and strategic resolution maneuvers;
  - d. *Airspace Constraint Data* identifying Special Use Airspace (SUA), convective weather, or other airspace which the own aircraft should avoid;
  - e. *Terrain Data* used for aircraft-terrain conflicts and for modeling the terrain if this is included as part of a display; and
  - f. *Data Link Message Data* from other aircraft, ATM, and AOC, coordinated and prioritized for conflict detection, forming the basis of communication and coordination data for conflict resolution.
- 7) *Data Link Messaging.* This component forms or processes data messages to be sent to and received from other aircraft, the AOC dispatcher, and ATM. Outgoing messages include own aircraft state (position, velocity, aircraft identification, aircraft type) and intent, conflict detection status, conflict resolution maneuver intent and status, flight plan changes, and other information such as weather measurements useful to the AOC dispatcher and ATM for forming wind field data. Incoming messages include other aircraft state and intent data, conflict detection and resolution messages (which could come from ATM or other aircraft), and updated wind field data.
- 8) *Data Link Router/Broadcast.* This device transmits and receives data link messages to suitable onboard and/or external information consumers. External information consumers include other aircraft, ATM, and AOC dispatchers.

- 9) *Pilot*. With respect to conflict detection and resolution, the pilot typically flies the aircraft in response to maneuvers suggested by the conflict detection and resolution system. However, the pilot retains override command of the aircraft.
- 10) *Controls*. This includes the usual throttle, elevator, aileron, and rudder controls for affecting heading, speed, or altitude maneuvers.
- 11) *Other Aircraft*. Other aircraft have their own dynamics, data link, and avionics logic, perhaps with different equipment from the own aircraft. These must be appropriately modeled to the same fidelity as the own aircraft system model (Items 1-10) when evaluating the effectiveness of the conflict detection and resolution logic and designing pilot interfaces.
- 12) *Winds*. The wind field has an effect on the aircraft trajectory, particularly on the relative velocity vector and how it directs an aircraft to travel to the point of closest approach PCA. The further apart the two aircraft are at the initial point of the detected conflict, the greater is the uncertainty in the wind field between them, affecting the time-to-PCA.

Models are required of each of these components when analyzing or simulating a conflict detection and resolution system. Analyses and fast-time simulations are required for establishing various system parameters (*e.g.*, nominal “acceptable miss distance” taking into account trajectory uncertainties, time-to-PCA to begin strategic maneuvers, etc.), for determining the sensitivity of the system performance to errors so that standards can be established, for validating the reliability of the software logic for every point in the potential operating envelope, and as a prelude to real-time simulations for establishing pilot interface requirements.

## 6.2 System Sources of Errors and Uncertainties

With respect to the exchange of data, communications, computation of conflict detection and resolution algorithms, etc., the effects of modeling errors and uncertainties in the real world play an important role in mechanization. The navigation sensor, pilot, controls, aircraft dynamics, and wind components shown in Figure 94 are sources of errors or variations from nominal performance that affect the aircraft trajectories. For example, variations in wind field model, longitudinal speed, climb rate, turn rate, navigation accuracy, and pilot delay from the ideal model used to compute trajectories, point of closest approach PCA, conflict probability, and resolution maneuvers are all important. The actual

maneuvers and miss distance at PCA will be perturbed from the trajectory prediction logic solution because of these errors.

A significant part of the conflict detection logic development must deal with measurement and trajectory prediction uncertainty. For the case of air-to-air conflict detection and resolution for Free Flight, it may be assumed that both aircraft are equipped with GPS receivers that are corrected with WAAS or LAAS differential corrections, and ADS-B to exchange position, velocity, aircraft identification, aircraft type, and intent information directly between aircraft. Thus, the relative position errors are expected to be less than 10 meters. The velocities may be in error on the order of 2 kts in magnitude and  $1^\circ$  in direction. Miss distances and PCA locations/times predicted from such a navigation sensor will have uncertainty, the magnitude of which is dependent upon the initial range between the conflicting aircraft and the measurement uncertainty properties, as discussed in Chapter 3. Furthermore, while it is important to have confidence in the predicted positions, there are at least two reasons why the prediction time should be limited, even if perfect navigation fixes were available. First, an aircraft may not hold a constant velocity vector. Second, a long *prediction* time implies a long *resolution* time, and this increases the probability of multiple strategic encounters, overlapping in time — a so-called “domino effect”, which is to be avoided. To mitigate these long term prediction problems, the Free Flight domain may need a stable planning horizon enforced by the broadcast of aircraft intent data. How strategic conflict resolution affects planning stability is an area in need of further investigation.

Another type of error is in the execution of the trajectories relative to those directed by the conflict resolution logic. This refers to the action of the pilot (or autopilot) to steer the aircraft along the presented normal flight plan or a conflict avoidance maneuver path indicated on the display. Actuation error is the difference between the aircraft state, as measured by the navigation sensor and presented to the pilot, and the desired state as dictated by the flight plan or conflict resolution maneuver plan. For example, pilots initiating conflict resolution maneuvers will have timing errors. Pilots and even autopilots will not keep the aircraft on perfect lines in space; there will be position and velocity errors. These will all affect the actual miss distance and time-to-PCA.

A third type of error is due to the wind uncertainty along both aircraft paths leading to the PCA between the two aircraft. This has a negligible effect on tactical maneuvers because of the relative short ranges involved; both aircraft essentially experience the same wind conditions. However, as the distance between the aircraft increases, as is the case in

strategic maneuvers, the winds that both aircraft are experiencing may be vastly different. A simple constant velocity wind model may not be appropriate.

The effects of these various measurement and trajectory prediction errors can be analyzed using both statistical covariance analysis and Monte Carlo simulation techniques (see Chapter 3). Both techniques are based upon using the model of the perfect, error free maneuver as the baseline. The outcomes of statistical analyses can include: (a) a set of statistical performance metrics of goodness of the conflict detection and resolution system; and (b) a set of sensitivity factors that determine the quantitative relationship of the metrics to the magnitudes of the various error and system parameters.

Performance metrics are used to determine if a conflict detection and resolution scheme meets established standards for safety, reliability, and efficiency. The sensitivities can be used to specify performance requirements of system components and the standard settings for system parameters – how good the state measurements have to be, where the maneuvers should be started, and what constitutes an adequate safe miss distance. To address these metrics, three different measures of miss distance in the horizontal and vertical dimensions need to be defined. First, as previously defined in Chapter 3, the horizontal miss distance is  $r_f$  and the Protected Airspace Zone radius is  $R$ . Define a collision distance parameter  $r_C < R$  as:

$$r_C = 0.5(b_A + b_B) \quad (109)$$

where  $b_A$  and  $b_B$  are defined to be the wing spans for aircraft A and aircraft B. By definition, a collision occurs if  $r_f \leq r_C$ . Next, define a near miss distance parameter  $r_{NM}$  ( $r_C < r_{NM}$ ) as a threshold value close to the separation requirement  $R$ :

$$r_{NM} = kR. \quad (110)$$

By definition, a near miss occurs if  $r_C < r_f \leq r_{NM}$ . The constant  $k$  is defined less than or equal to 1. If the constant  $k$  is less than 1, for example  $k=0.75$ , then this may allow the average conflict resolution miss distance to be at or near the separation standard  $R$ , as shown in Figure 95. If the constant  $k$  were to be defined greater than 1, then the mean miss distance is likely to be far outside the separation standard, which might be overly conservative and add an economic penalty to the average conflict resolution maneuver. Finally, define an acceptable miss distance parameter  $r_{AM}$  ( $r_{NM} < r_{AM}$ ) to be, for example, 50% over the separation standard:

$$r_{AM} = 1.5R. \quad (111)$$

By definition, an acceptable miss occurs if  $r_{NM} < r_f \leq r_{AM}$ , and an excessive miss occurs if the conflict detection and resolution logic commands a maneuver such that  $r_f > r_{AM}$ . Miss distance outcome probabilities include the probability of a collision, near miss, acceptable miss, or excessive miss, as shown in Figure 95. Three similar vertical distance parameters,  $h_C$ ,  $h_{NM}$ , and  $h_{AM}$ , can be defined for separation requirements in the vertical dimension.

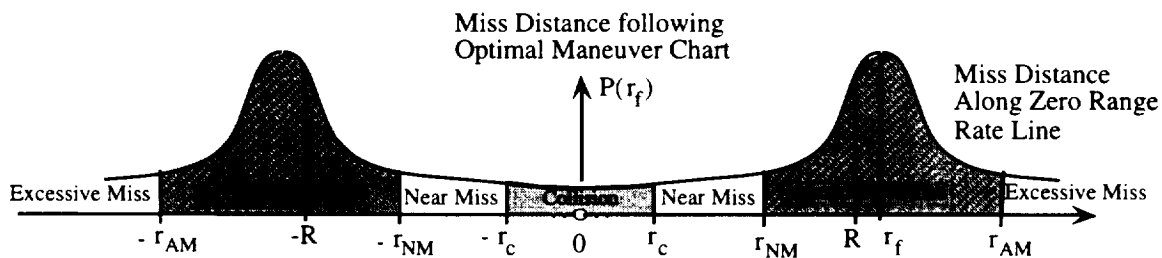


Figure 95. The statistical distribution of horizontal miss distance which defines collision, near miss, acceptable miss, and excessive miss (drawing not to scale).

The values of these six miss distance parameters need to be established for practical future conflict detection and resolution scenarios. A statistical analysis must be performed by using a model including the elements in Figure 94 and separation standards of safety that are acceptable to the aviation community. Unlike the analysis performed in Chapter 3 for miss distance variation given no maneuver, the investigation for these parameters must include many more factors, including the fact that the pilot or autopilot is executing a conflict resolution maneuver, may be performing a sub-optimal maneuver, or may be executing a wrong maneuver. In the future, aircraft will employ Required Navigation Performance (RNP) equipment standards with higher accuracies and Automatic Dependent Surveillance-Broadcast (ADS-B) methods; these factors must also be taken into consideration. For example, we may need to determine the RNP that will guarantee that an acceptable miss distance of at least 1.5 nmi can be met 99.997% of the time for a typical crossing encounter between two turbojets.

The performance metrics that should be investigated include the conflict detection probabilities of false alarms, missed alarms, and incorrect maneuvers. A false alarm is an erroneous conflict detected even though adequate miss distance (as determined by the PCA) would be achieved without a maneuver. False alarms are annoyances to pilots, cause extra

workload, may cause pilots to disregard actual conflict warnings, and could add additional flight cost since they may cause the pilot to maneuver the aircraft when no maneuver is needed. A missed alarm has an actual conflict present, but because of measurement error or an unknown or unexpected maneuver, a safe PCA is projected. This could cause the conflict resolution maneuver initiation to be delayed so that an economic or safety penalty is incurred. That is, the maneuver could be more severe than if started earlier causing less efficient flight, or the range at PCA could be smaller than the value that has been established to represent adequate safety (acceptable miss distance). Finally, an incorrect maneuver occurs when an actual conflict is present and detected, but because of measurement error or unexpected maneuvering, the conflict resolution maneuver is incorrect (*e.g.*, in the wrong direction). This could cause either an economic or safety penalty.

During a strategic encounter, there is also a need to monitor the situation between aircraft in order to collect the appropriate data for conflict detection and resolution. As the aircraft fly closer together, the errors in the relative state, the relative trajectory's forward projection to the PCA, and the projected miss distance become smaller because (a) more measurements have been processed, and (b) less time-to-PCA is available for the wind field and actuation errors to propagate. Thus, one strategy favors continuing to take data while allowing the aircraft to get closer so as to be more certain that a maneuver is necessary (*i.e.*, the probability of conflict continues to grow). However, if a maneuver is necessary, waiting increases the magnitude of the maneuver required thereby increasing the cost of the maneuver. The other strategy favors maneuvering as soon as a potential conflict is detected to minimize the amount (and cost) of the maneuver required. However, generally the PCA uncertainty is very large at long range, so maneuvering early would cause a high false alarm rate. This problem lends itself to a solution where the two strategies (wait and take more data to potentially become more certain; and maneuver soon to reduce maneuver cost) are blended. The logic would compute and monitor: 1) the time history of probability of conflict (as in Chapter 3); and 2) the maneuver cost as a function of time-to-go to PCA (as in Chapter 5). These two functions can be combined using, for instance, fuzzy logic, and if their combination exceeds a preset threshold, then a maneuver would be activated. Fuzzy logic would also allow aircraft to include other conditions for initiating a maneuver.

### **6.3 Mechanization of Conflict Detection Logic**

As previously discussed in this report, probability maps, Strategic and Tactical Alert Zones, and maneuver charts provide the means for summarizing the conflict detection and

resolution logic. While these summarize many initial conditions, only the particular initial condition relevant to the two aircraft in a conflict are appropriate in the mechanization. Only the equations and logic relevant to handle a conflict situation need to be implemented onboard in real-time. Furthermore, once the conflict resolution logic is determined, the coordination and communication of data need to be established. These issues were not discussed in the algorithmic development in previous chapters.

For the 2-aircraft encounter, where it is assumed that both aircraft are equipped for conflict detection and resolution, a “Master-Slave” coordination may be established. One aircraft A (the “Master”) plans and commands the maneuvers and the other aircraft B (the “Slave”) concurs with the plan and executes the maneuver delegated to it. Various rules need to be set into logic to determine which aircraft is “Master”, and if this role would ever change or be over-ridden. We can refer to this logic as “Rules-of-the-Road” regarding conflict detection and resolution management. For example, Free Flight policy might adapt the rules used at sea whereby the starboard vessel has right of way. Or we might adapt the hemispherical altitude rule, for example, such that the more westbound aircraft has the “Master” role. This establishment of “Rules-of-the-Road” requires further study to determine the best policy.

The aircraft have limited maneuver choices – turn right (R) or left (L), climb up (U) or descend (D), accelerate (Ac) or decelerate (Dc) – followed by a period of holding the velocity vector constant until PCA. Thus, the cooperative turn combinations to be examined are simply RR, RL, LR, or LL; climb/descend options are UD or DU; acceleration combinations are AcDc or DcAc. The logic which tries each of these maneuver combinations, as appropriate, for any encounter initial conditions is easily implementable in software. The dynamic part of the maneuver is stopped when the result of continuing along a straight line path yields greater than the required miss distance with sufficient probability. The software logic would compute the relative trajectories from each combination, determine if an acceptable solution exists for that combination, and compute the cost of that solution. The minimum cost solution would be chosen to be displayed to the pilots. However, sub-optimal solutions should be retained for contingencies.

One contingency would be needed when the conflict resolution maneuver puts both aircraft into a deadlock condition. For example, a deadlock would exist if A turns right, B turns left, and both end up going along parallel paths, side by side and away from their intended courses. In this case, the second best maneuver pair could be chosen instead to avoid the deadlock. Note that if an altitude maneuver or a maneuver combining heading

and altitude were used for conflict resolution, then both aircraft could proceed with any horizontal return to track maneuver without a deadlock, since the vertical separation requirement would be satisfied during the recovery maneuver.

A second contingency would be needed when a 2-aircraft conflict resolution maneuver is constrained by a third aircraft C. Here, one possible outcome is that aircraft A and B have a second maneuver choice that does not conflict with C. Another possibility is that the algorithm determine a conflict resolution strategy using an optimal 3-aircraft maneuver. This will require more study than what has been investigated in this report to determine all the conflict avoidance maneuver choices available and how to establish which aircraft is “Master”. For the multiple aircraft (three or more) encounters, reverting control to the ground-based ATM system might be the best choice.

A third contingency would be needed when there are maneuvering constraints such as airspace restrictions, terrain, or weather that eliminate certain maneuver options. For example, climb/descend to a different altitude might not be desirable because of known turbulence or icing conditions at the new altitude. Turning might take the aircraft into restricted Special Use Airspace (SUA), into a region with very congested traffic so that Free Flight is severely limited, or into a different ATC sector where the aircraft would be taken into a less desirable TRACON feeder fix leading to a less desirable runway. Each aircraft conflict detection and resolution system/pilot would need to have veto power in order to self limit such maneuver options.

The final part of the maneuver implementation logic is the recovery maneuver, directed at returning the aircraft back to course after the PCA has been passed. Exactly what the desired aircraft return maneuver consists of depends on where the aircraft is relative to the original destination. In some cases, the preference will be to return, within some time period or range, to the original 3D flight plan after passing the PCA. In other cases, the preference will be to create a new plan starting from the PCA and proceeding directly to the intended destination. Both options will have their utility, so both should be allowed for in the mechanization.

#### **6.4 Coordination and Communications Requirements**

Good information is a pre-requisite for good decision making. The nature of coordinating and communicating the information available for conflict detection and resolution affects how, when, where, and what decisions are made. Important questions related to handling and communication of data include:

- (i) *Types*: What types of information need to be communicated between conflict detection and resolution algorithms? This includes position, velocity, aircraft identification, aircraft type, time, intent, destination, and vehicle capabilities (equipment).
- (ii) *Accuracy*: How accurate do these data need to be?
- (iii) *Transport*: What is required to get the data to the appropriate place for processing? What kinds of communications protocols are necessary? What are the data latencies? How does data latency impact candidate solutions? What nominal data update rates should be used?
- (iv) *Integrity*: What precautions must be taken to assure data integrity (error detection and correction, and/or forward error corrected communications)? How does an implemented system check itself? How does the system respond to violations of data integrity? For example, depending upon back-up modes of operation, GPS drop-outs can result in an increased position and velocity uncertainty. How can GPS or other information drop-outs be discerned, handled, and reported?
- (v) *Completeness*: Information about the local air traffic scenario may vary in content and in regularity/availability due to equipment levels, ground support, aircraft density, etc. What considerations arise as data content varies?
- (vi) *Adaptability*: Technological advances are likely to improve the quantity and quality of data available for conflict detection and resolution algorithms. How should the algorithms and data structures be designed to allow for future changes in the quantity and quality of data, enhancements to the conflict detection and resolution logic, and evolution from non-equipped to fully equipped fleets?
- (vii) *Coordination Method*. What type of coordination is required for timing and selection of conflict resolution maneuvers? Is a "Master/Slave" system necessary, and will one on board computer determine the movement of both aircraft or will the second aircraft solve for and/or negotiate its own action?
- (viii) *Data Flow within System Elements*. Data flow and latency requirements also exist between system elements. Data flow requirements are associated

with sensor, alert, display, command/resolution, and pilot input data. Delays are associated with data acquisition, communications, algorithm processing, display processing, and pilot interfacing. What are the effects of these delays on conflict detection and resolution, and what is needed to ensure that the system appropriately accounts for these delays?

Finally, the conflict detection and resolution system imposes communications requirements, not necessarily dedicated solely to solving conflict problems, but perhaps contributing to an overall communications network. To address implementation issues, the overall air-air and/or air-ground data and voice communications needs, including data content, integrity, and data broadcast rate need to be understood and specified. Furthermore, a mechanism for handling lost data and addressing the effects of lost data must be investigated.

## **6.5 Displays and Human Factors**

The means of presenting conflict detection and resolution information to pilots and air traffic controllers will play a crucial role in the effectiveness of an operational system. Existing human-computer interfaces may become insufficient as Free Flight introduces more complex conditions with potentially less-ordered traffic patterns than today. Today's controller plan view displays use flat, 2D, monochrome displays with trackball inputs. Cockpit traffic displays (*e.g.*, TCAS II) have color 2D displays with knob controls. In the future, highly interactive, real-time systems with 2D multi-layered moving map displays or 3D stereoscopic views from both the controller's as well as the pilot's perspective, color and texture, touch-screen, and spatialized sound are possibilities.

Studies in display design indicate that there are tradeoffs and benefits to both 2D and 3D displays for conflict detection and resolution and ATC/ATM. The study by [SEL82] indicates that when a display does not show the third spatial dimension as readily apparent as the other two, pilots tend to solve conflict avoidance problems in the displayed two dimensions, rather than exploiting all three dimensions. For conflict resolution, this implies that a 2D plan view display may bias conflict resolution solutions to heading maneuvers even though the altitude maneuver might be a better choice. In a related study [EMH87], pilots were more likely to chose a conflict resolution maneuver with a vertical component when using a perspective display. Further studies by [HW93, Ma93, MCW95, PG93, WTS89] explore 2D and 3D displays to aid specific ATC/ATM tasks.

To illustrate the potential of multi-modal human-computer interfaces for ATC/ATM and Free Flight, [ADK96] investigated a virtual reality system. Conflict detection and resolution advisories were displayed in a multi-modal system engaging the visual, auditory, and vocal channels. As shown in previous chapters, 3D perspective views of the Protected Airspace Zone and Tactical Alert Zone can be overlaid around an aircraft's current position or some future position (using intent data). Using these zones as alerting cues, an air traffic controller or pilot can preview conflict resolution strategies prior to engagement, and select appropriate actions. Egocentric views allow the user to travel along with a particular aircraft; exocentric views allow the user to view the situation from any point in this virtual space. Using multiple viewpoints, the air traffic controller or pilot can thoroughly investigate and accept or reject conflict resolution advisories, and can coordinate and/or negotiate actions between aircraft. Guidance maneuvers can be performed using tunnels-in-the sky (Figure 96) or by following a trace of the conflict resolution trajectory into the future (Figure 97). Feedback from pilots and air traffic controllers differed for this system. Pilots tended to like how the visualization of future paths helped them to locate neighboring aircraft and precondition them for conflict resolution maneuvers. Pilots also like the egocentric viewpoint, since they typically use displays centered around the motion of their own aircraft. Controllers, on the other hand, traditionally have fixed plan view type displays that help them to estimate separation distances. Moving around in a virtual space presented in a perspective view created problems with judging distances and performing their analysis.

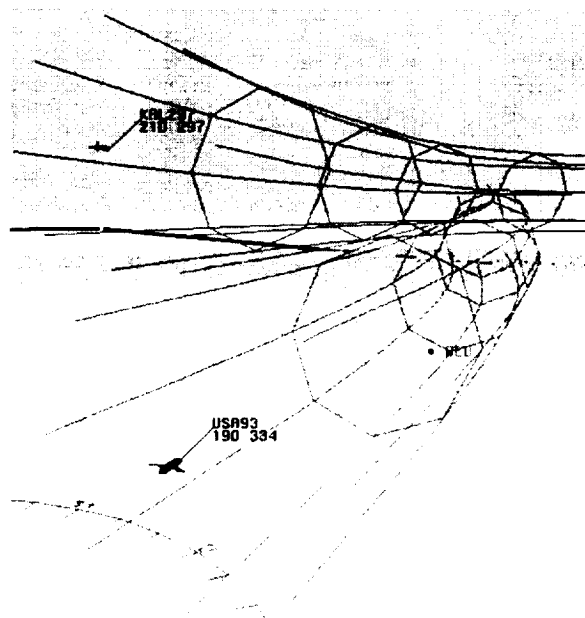


Figure 96. A 3D perspective display showing tunnels-in-the-sky for intent data (taken from [ADK96] with permission from the authors).

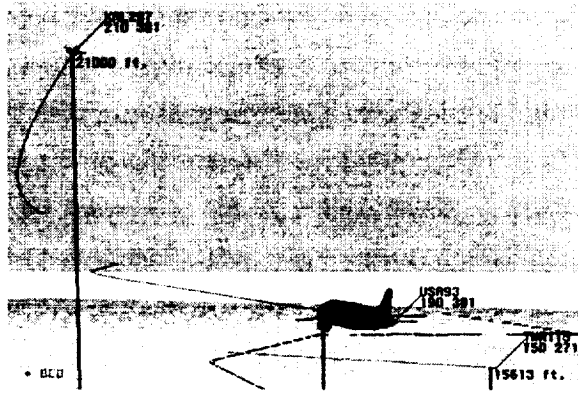


Figure 97. A 3D perspective display showing intent data from trajectory prediction results (taken from [ADK96] with permission from the authors).

Further research is necessary to evaluate the human factors issues for both 2D and 3D types of displays and the process of performing conflict detection and resolution. Important issues include determining the times required to: preview and negotiate a conflict resolution advisory with another aircraft, activate the maneuver guidance logic to perform a maneuver, and alert controllers and AOC dispatchers (if desired) to inform them of the situation. Other issues include: display symbology effectiveness, passenger comfort, information requirements for pilot and/or air traffic controller situation awareness, and workload analysis. Towards this end, an overview of such human factors issues related to human-centered aviation automation is presented in [Bi96].

## 6.6 Real-Time Testing

Both real-time cockpit simulator and flight tests will play an important role in the system mechanization by providing real-world calibration and feedback about conflict detection and resolution algorithms and interfaces. Real-time cockpit simulation would be done using piloted cockpit simulators with possibly inclusion of the air traffic manager/controller and/or the AOC dispatcher at appropriate workstations. Flight tests would be done with one or more aircraft collecting real data for conflict detection and resolution. Required technologies include processors, displays, GPS receivers, and digital radio communications equipment. These hardware technologies, in tandem with the software algorithms that drive them, promise to be central elements of the operational conflict detection and resolution functionality envisioned for Free Flight. Early manned simulation of a conflict detection and resolution system will help reveal real-world considerations early in the process, provide for human-factors experimentation and feedback, and allow for rapidly prototyping of such a system. While analyses of algorithms, fast-time Monte-Carlo

simulations, and real-time cockpit simulations are valuable tools for understanding many of the issues associated with complex matters like real-time conflict detection and resolution, they remain only approximations of the actual flight environment. Thus, flight testing will also be needed to reveal the final operational considerations.

Among the matters that should be investigated in real-time simulation and flight testing are:

- (i) *Latencies*: What latencies exist in the various elements of the system, including displays, GPS, communications equipment, processed information, pilot reactions, etc.? What are the properties of these latencies? How do they affect system performance?
- (ii) *Integrity*: Are there weak links in the proposed solutions? What are the system's fault tolerance properties? Does the system degrade gracefully? What communications integrity is sufficient?
- (iii) *Communications*: Are the update rates set by simulation testing sufficient for data/communications and displays, and under what circumstances? What confirmations for actions are desired and when?
- (iv) *Pilot Interface*: What are effective means to communicate conflicts and resolutions to pilots? What symbologies and audibles are expected at what times? How difficult are the alerts and displays to learn? Does the pilot understand and/or believe the data being presented? How does the pilot work when in an environment characterized by varied queues, disturbances, and work loads? How quickly can pilots be expected to identify alerts and/or address them?

There are several motivations and advantages of the real-time testing. First, a real-time simulation of two or more interacting aircraft requires thoughtful development of the conflict detection and resolution implementation logic to a form similar to what would be mechanized in actual avionics. This process would begin with a high-level block diagram such as shown in Figure 94 and proceed to add functional detail. Completing this process insures that the conflict detection and resolution logic, software and hardware are realizable for all points in the envelope of possible aircraft encounters; this modeling and code development process insures technical feasibility of the design.

A real-time simulation is the test bed in which the displays, avionics technology, and other input/output devices for pilot (and controller and/or AOC dispatcher) interaction with the conflict detection and resolution system can be investigated. Displays cannot be developed fully without testing them in a dynamic environment with the humans who will be using them in the loop. Real-time testing is necessary to establish the timing requirements of information exchange between aircraft-to-aircraft and aircraft-to-ground.

Real-time testing is also necessary to establish the procedures for pilots, controllers, and AOC dispatchers in using a conflict detection and resolution system. This includes the transition process of going from a complete air-to-air solution to an Alert Zone violation for which ground-based ATM takes over. This testing is necessary to establish the operational viability of the system.

Next, real-time simulation allows for an investigation into un-modeled error sources that affect the dynamics of the encounter. As a simulation is run, the effects of these errors can be directly measured with respect to performance metrics of the conflict detection and resolution system. With repeated runs, stochastic distributions of miss distance, probability of false alarm, etc. can be quantitatively evaluated.

Finally, real-time testing is useful for planning subsequent flight tests of the system, since simulation testing is much less expensive than conducting flight tests and field trials. Also, simulation testing allows the engineer to set the conditions and environment of the flight test; in contrast, during field trials you literally take what you get. Flight testing will clarify real-world considerations and address issues associated with the actual flight condition mechanization. Flight test investigations can perform a real-world check of the validity of assumptions and address the practicality of conflict definitions, conflict determinations, and resolution algorithms.

## 7. SUMMARY, CONCLUSIONS, AND RECOMMENDATIONS

In this chapter, we summarize our research, state conclusions, and list recommendations for future investigations.

### 7.1 Summary and Conclusions

For conflict detection, we performed both 2-dimensional and 3-dimensional analyses for conflicts based on the penetration of the Protected Airspace Zone of one aircraft by a second aircraft. Assuming that both aircraft hold constant velocities, analytic equations were derived to identify the point-of-closest-approach and the time to the point-of-closest-approach. Both deterministic (where trajectories are error free) and non-deterministic analyses (where sensor, actuation, and wind perturbation errors may exist) were performed.

In the deterministic analysis, several methods for detecting a tactical conflict were compared. These methods include warnings prior to penetrating the Protected Airspace Zone, generic TCAS logic, and methods based on the reachability space overlap of both aircraft. The warning prior to penetrating the Protected Airspace Zone is tailored to and most appropriate for Free Flight. The TCAS logic was shown to be ineffective at guaranteeing that the Protected Airspace Zone will be avoided. Finally, the reachability conflict detection mechanism is quite conservative, but may be applicable in multi-aircraft short range tactical conflicts where the actions of another aircraft might be extreme.

In a non-deterministic analysis, we showed how a conflict probability map can be constructed. Both a Monte Carlo technique and an analytic technique for constructing conflict probability maps were investigated. The analytic technique has the advantage of not requiring repeated simulations. We showed how this conflict probability map can form the basis for a Strategic Alert Zone definition for long range strategic conflict detection.

An aircraft proximity management system was also described. A Delaunay Triangulation formulation provides a mathematically precise representation for the trajectory data management of all aircraft in a flight level. Such a system provides a means for analyzing the neighbor relationships between aircraft and the nearby free space around air traffic which can be utilized in multi-aircraft conflict detection and resolution. As recommended in the next section, this Delaunay Triangulation formulation may be extended to three dimensions.

Conflict resolution maneuvers were investigated for the horizontal plane with either heading or speed control, and in the vertical plane with altitude control. Optimal conflict resolution maneuvers were developed for tactical close-range as well as strategic far-range cases.

The tactical analysis optimizes safety by maximizing the distance at the point-of-closest-approach. The tactical conflict resolution strategy was found to be the result of an optimization problem: Determine the control as a function of the relative motion state such that the range at closest approach is maximized. Solutions are obtained by applying Euler-Lagrange equations for optimal control, and are best illustrated using maneuver charts. Maneuver charts were generated for cooperative (both aircraft maneuver) and non-cooperative cases (only one aircraft maneuvers) and for heading, speed, and altitude control cases. These maneuver charts concisely illustrate the tactical collision avoidance "rules-of-the-road" indicating the turn directions, acceleration signs, or climb/descent rates that each aircraft should select for any arbitrary initial relative state of conflict. Additionally, the maneuver charts identify a Tactical Alert Zone, the locus of points for which a maneuver must be started in order to avoid penetrating the Protected Airspace Zone of another aircraft.

The strategic analysis optimizes the economical cost of the maneuver while maintaining safety as the constraint. The strategic conflict resolution strategy analyzes the geometry of heading, speed, and altitude maneuvers that safely avoid the Protected Airspace Zone, and estimates the Direct Operating Cost DOC (fuel and time costs) for these maneuvers. Maneuvers can be chosen to minimize the total DOC for all aircraft involved or to minimize the individual DOC of each aircraft; these conditions will not necessarily result in the same maneuver. In general, altitude maneuvers are the most economical, followed by heading maneuvers, and finally speed change maneuvers. For non-cooperative heading maneuvers where only one aircraft maneuvers, it is generally more economical to turn the aircraft to the backside of the non-cooperating aircraft. For cooperative cases where both aircraft maneuver, it is generally better to let the faster aircraft bear more of the burden for the strategic maneuver. The cost and range required for speed control maneuvers usually make this an ineffective means of conflict resolution.

An economics analysis was also performed to investigate the benefit from a reduction of horizontal separation standards. The cost of heading and speed maneuvers can be reduced 3-fold for reducing the separation standard from 5 to 3 nmi. Reducing the horizontal separation standard from 5 to 1 nmi reduces the cost of a maneuver by roughly 10 times. No significant change occurs in the cost of altitude maneuvers due to reducing

the horizontal separation standard; they are relatively inexpensive for all cases. With the reduction of separation standards, it is important to note that the effects of wake vortices behind aircraft may become the limiting factor.

Finally, the mechanization of a conflict detection and resolution system was analyzed. We proposed the necessary components for a conflict detection and resolution system and discussed each component and their interconnectivity. The system sources of error and uncertainties were identified, including measurement and trajectory prediction uncertainty, actuation uncertainties, flight technical errors, and wind uncertainty. Performance metrics were identified for the purpose of evaluating the safety, reliability, and efficiency of the system. These metrics include parameters for collision, near miss, acceptable miss, and excessive miss distances. Suitable values for these parameters should be determined in future research. The need for an analysis of the probability of false alarms, missed alarms, and incorrect maneuvers was also discussed; these are also mentioned in our list of recommendations.

Coordination and communication requirements, human factors issues, displays, and simulation testing were also discussed. A “Master/Slave” type logic was considered for coordination, and for coordination options, we discussed an algorithmic implementation incorporating contingency plans. Contingency plans may be necessary for deadlock conditions, avoiding third aircraft conflicts, or avoiding airspace constraints. The need for pilot, ATM, and AOC dispatcher displays and human factors research was also briefly discussed. Suggestions for displays and human factors research are given in the list of recommendations. Finally, there is a need for real-time testing through simulations and actual flights to provide real-world calibration and design feedback for the conflict detection and resolution algorithms, interfaces, related technologies, and operating procedures.

## 7.2 Recommendations

The following recommendations are identified for further research into the problem of conflict detection and resolution for Free Flight. These recommendations generally fall into three categories: analysis, simulation, and mechanization.

### Analysis:

- 7.2.1 **Conflict Detection.** For conflict detection, we performed both 2D and 3D analyses based on the assumption that both aircraft hold constant velocities. Further analysis should be performed to extend this analysis to consider either aircraft having 1) a constant turn rate, 2) a constant acceleration vector, or 3) intent data (*e.g.*, imbedded in an ADS-B message) indicating a future

heading, speed, or altitude change. Furthermore, analysis is necessary to assess effects of state measurement uncertainty, trajectory prediction errors, and wind field perturbations on far range strategic conflict detection. Wind data provided by real-time measurements onboard aircraft that have previously flown through the airspace near a conflict may be used to model the wind. The application of fuzzy logic may be useful in dealing with the trade-off that exists between using early maneuvers versus processing more data to better assess the expected probability of an actual conflict.

- 7.2.2 **Error Sensitivity Analysis.** The conflict probability maps derived in Chapter 3 propagate position and velocity uncertainty errors, but further error analysis is necessary for conflict detection. The additional errors which are not considered include horizontal wind gradients (the wind field in front of the own aircraft may be different from that of an intruder aircraft), flight technical errors (pilot control errors), and guidance errors. The last involves the errors the system makes in computing an optimum resolution flight profile based on uncertainties in measured aircraft states.
- 7.2.3 **Altitude Maneuver Analysis.** Altitude maneuvers were shown to be more economical compared to heading and speed maneuvers. Consequently, future air traffic control and air traffic management may involve a far greater percentage of altitude maneuvers compared to today's fixed route, fixed flight level system. A further, more detailed investigation should be performed to look at the feasibility of multiple aircraft performing altitude maneuvers in Free Flight. Altitude constraints for terrain, turbulence, and weather should be included in the analysis.
- 7.2.4 **Constrained Conflict Resolution.** In this report, 2-aircraft encounters were investigated without any constraints due to sector boundaries, restricted airspace zones, weather, neighboring traffic, or terrain. For instance, the type of conflict resolution strategy could be influenced by *where* the aircraft are located relative to sector boundaries. These types of constraints on conflicts should be included into the conflict resolution analysis in further research.
- 7.2.5 **Rules-of-the-Road.** The notion of a combined maneuver chart was introduced in this report to combine the analysis of probability of missed and false alarms with strategic and tactical conflict resolution strategies. Further research should be performed to determine the best partitioning of this combined maneuver chart and a mechanism for coordination of aircraft maneuvers (e.g., the "Master/Slave" method). In addition, an analysis should be performed to define the near miss, acceptable miss, and excessive miss distances, as discussed in Chapter 6, based on following the "rules-of-the-road".
- 7.2.6 **Multi-Aircraft Conflicts and the Domino Effect.** In this report, 2-aircraft encounters were investigated for tactical and strategic conflicts. Encounters which include three or more aircraft should be investigated in the same detail. Such an investigation would extend the results derived for the 2-aircraft scenarios. Also, the domino effect needs to be investigated. The domino effect occurs when a conflict resolution maneuver for two aircraft propagates into a conflict with a third (or more) aircraft. The Delaunay Triangulation of all aircraft provides nearest neighbor information that might be

combined with conflict resolution analysis to investigate the domino effect. A mathematical criterion should be established to identify when the domino effect will happen.

- 7.2.7 ***Proximity Management.*** The Delaunay Triangulation of all aircraft in a flight level is a computationally efficient mechanism to maintain proximity information. A comparison should be made between a method using layers of 2D Delaunay Triangulations, a method using a full 3D Delaunay Triangulation, and a method of using grid-based sorting of aircraft for the purpose of proximity management. Experiments should be performed to investigate the utility of these techniques for providing ATM with a robust and distributed system for monitoring and tracking all aircraft, for AOC dispatchers with proximity management of their fleets, and for aircraft with proximity management of nearby traffic.

#### Simulation:

- 7.2.8 ***Detailed System Modeling.*** A high fidelity simulation capability can be developed by expanding the system block diagram components in Figure 94 into functional details of environmental models, aircraft dynamics, communications elements, sensors, algorithms, and displays. Mathematical models need to be developed for each system component with realistic error characteristics, parameter options, and environmental disturbances. Encounters between aircraft with different equipment and in well modeled environmental conditions should be investigated with this type of high fidelity simulation capability.
- 7.2.9 ***Fast Time Simulations.*** Fast time algorithm simulations are needed to provide Monte Carlo results investigating: effects of errors on the statistics for final miss distance, false, and missed alarms; sensitivity of performance to the variations of system parameters; and performance of the “rules-of-the-road” and trigger mechanisms for conflict detection.
- 7.2.10 ***Manned Simulations.*** Manned simulations are needed to provide the real-world calibration and human factors feedback about a conflict detection and resolution system under Free Flight scenarios. Issues to be investigated with such a simulation capability include system latencies, communications, interfaces, and system effectiveness. These simulations and the preparations of the algorithms and hardware components for these simulations will help setup follow-on flight tests.

#### Mechanization:

- 7.2.11 ***Displays.*** Candidate displays should be developed for conflict detection and resolution for not only the pilot, but for ATM as well as AOC dispatchers. This work should be performed with NASA human factors experts providing guidance in a human-centered design approach [Bi96]. 3D perspective, 2D plan view, and 2D profile view displays should be compared.

- 7.2.12 ***Communications/Coordination.*** Cooperative conflict resolution strategies require good communications/coordination between the two aircraft involved. Further investigations should be performed to identify the complexities of hand shaking, "Master/Slave" coordination, time delays, data dropouts, and update rates. This analysis should include manned simulations to evaluate the best parameter selections.
- 7.2.13 ***Transfer of Control to Ground-Based ATM.*** An investigation into the transfer of control from an air-to-air flight-deck-based solution for the conflict resolution problem to a ground-based ATM positive control solution is needed. This research will affect parameters chosen for Alert Zone sizing and conflict detection. This research will also need to investigate the relationship between dynamic density in Free Flight and the transition to ground-based control.
- 7.2.14 ***Multi-Modal Visualization.*** Several 3D perspective views of the conflict detection and resolution scenarios were presented in this report based on an investigation performed by [ADK96]. This visualization may be extended to include combined Protected Airspace Zone, Alert Zone, intent, traffic, weather, terrain, wake vortex, and wind field information. Also, this visualization should be expanded to include multi-modal human-computer interaction techniques, that is, voice commands, audible warnings, 3D spatialized sound, data gloves inputs, etc. (see [ADK96]). Human factors issues related to such human-computer interaction techniques should be investigated to identify the utility of presenting information this way to either a pilot, air traffic manager, or AOC dispatcher. This may require further development of multi-modal visualization environments specifically designed for the pilot, air traffic manager, or AOC dispatcher.

## 8. REFERENCES

- [AIM95] *Airman's Information Manual / Federal Aviation Regulations*, TAB/Aero Staff, McGraw-Hill Pub., 1995.
- [AMGR91] Albers, G., Mitchell, J.S.B., Guibas, L.J., and Roos, T., "Voronoi Diagrams of Moving Points", *17th Workshop on Graph-Theoretic Concepts in Computer Science*, 1991.
- [An89] Anderson, J.D., *Introduction to Flight*, McGraw Hill, New York, NY, 1989.
- [A95] Aviation Week Special Report on Free Flight, *Aviation Week and Space Technology*, July 31, 1995.
- [ADK96] Azuma, R., Daily, M., and Krozel, J., "Advanced Human-Computer Interfaces for Air Traffic Management and Simulation," *AIAA Flight Simulation Technologies Conf.*, San Diego, CA, Aug., 1996.
- [BAW94] Ball, D.W., Altman, S.I., and Wood, M.L., "TCAS: Maneuvering Aircraft in the Horizontal Plane", *The Lincoln Lab. Journal*, Vol. 7, No. 2, pp. 295-312, 1994.
- [BE96] Ballin, M.G. and Erzberger, H., "Benefits Analysis of Terminal-Area Air Traffic Automation at the Dallas/Fort Worth International Airport", *AIAA Guidance, Navigation, and Control Conf.*, San Diego, CA, July, 1996.
- [Bi96] Billings, C.E., *Human-Centered Aviation Automation: Principles and Guidelines*, NASA Tech. Memorandum TM-110381, Feb., 1996.
- [BH75] Bryson, A.E. and Ho., Y.-C., *Applied Optimal Control*, Hemisphere Pub., Washington D.C., 1975.
- [CBB92] Cardosi, K.M., Burki-Cohen, J., Boole, P.W., Hourihan, J., Mengert, P., and DiSario, R., *Controller Response to Conflict Resolution Advisory*, Dept. of Transportation Tech. Report, DOT/FAA/NA-92/2, Volpe National Trans. Systems Center, Cambridge, MA, Dec., 1992.
- [CD95] Couluris, G. and Dorsky, S., *Advanced Air Transportation Technologies (AATT) Potential Benefits Analysis*, Final Report, NASA Contract NAS2-13767, Seagull Technology, Inc., Cupertino, CA, Sept., 1995.
- [Cr83] Cross, S.E., *Qualitative Reasoning in an Expert System Framework*, Ph.D. Thesis, Univ. of Illinois at Urbana-Champaign, Urbana, IL, May, 1983.
- [Da92] Davis, G.A., *AERA2 APR Knowledge Base*, MITRE Tech. Report MTR-89W00120, The MITRE Corp., McLean, VI, Jan., 1992.
- [DEG91] Davis, T.J., Erzberger, H., and Green, S.M., "Design and Evaluation of an Air Traffic Control Final Approach Spacing Tool," *Journal of Guidance, Control, and Dynamics*, Vol. 14, No. 4, pp. 848-854, 1991.

- [DAC95] Durand, N., Alliot, J-M, and Chansou, O., "Optimal Resolution of En Route Conflicts", *Air Traffic Control Quarterly*, Vol. 3, No. 3, pp. 139-161, 1995.
- [Eb94] Eby, M.S., "A Self-Organizational Approach for Resolving Air Traffic Conflicts," *The Lincoln Laboratory Journal*, Vol. 7, No. 2, 1994.
- [EMH87] Ellis, S.R., McGreevy, M.W., and Hitchcock, R.J., "Perspective Traffic Display Format and Airline Pilot Traffic Avoidance," *Human Factors*, Vol. 29, No. 4, pp. 371-382, Aug., 1987.
- [Er92] Erzberger, H. *CTAS: Computer Intelligence for Air Traffic Control in the Terminal Area*, NASA TM-103959, Ames Research Center, Moffett Field, CA, July, 1992.
- [Er95] Erzberger, H., "Design Principles and Algorithms for Automated Air Traffic Management", *Knowledge-Based Functions in Aerospace Systems*, AGARD-LS-200, Nov., 1995.
- [F86] Ford, R.L., "The Protected Volume of Airspace Generated by an Airborne Collision Avoidance System," *Journal of Navigation*, Vol. 39, No. 2, pp. 139-158, 1986.
- [FAA93] *National Airspace System Configuration Management Document: Oceanic Display and Planning System (ODAPS) Conflict Probe*, Federal Aviation Administration Technical Center, Tech. Report NAS-MD-4319, July, 1993.
- [FF95] Free Flight URL <[http://www.orlab.faa.gov/freeflit/ff\\_home.html](http://www.orlab.faa.gov/freeflit/ff_home.html)>
- [FP93] Fang, T-P and Pieg, L.A., "Delaunay Triangulation Using a Uniform Grid", *IEEE Computer Graphics and Applications*, pp. 36-47, May, 1993.
- [Ga96] Gazit, R.Y., *Aircraft Surveillance and Collision Avoidance Using GPS*, Ph.D. Dissertation, Stanford University, Stanford, CA, Aug., 1996.
- [GS85] Guibas, L. and Stolfi, J., "Primitives for the Manipulation of General Subdivisions and the Computation of Voronoi Diagrams", *ACM Transactions on Graphics*, Vol. 4, No. 2, pp. 74-123, April, 1985.
- [Ha89] Harman, W.H., "TCAS: A System for Preventing Midair Collisions", *The Lincoln Lab. Journal*, Vol. 2, No. 3, pp. 437-457, 1989.
- [HW93] Haskell, I.D. and Wickens, C.D., "Two and Three-Dimensional Displays for Aviation: A Theoretical and Empirical Comparison", *Intern. Journal of Aviation Psychology*, Vol. 3, No. 2, pp. 87-109, 1993.
- [HGT83] Hauser, S.J., Gross, A.E., and Tornese, R.A., *En Route Conflict Resolution Advisories: Functional Design Specification*, Tech. Report MTR-80W137, The MITRE Corp., McLean, VI, Feb., 1983.
- [HM70] Holt, J.M. and Marner, G.R., "Separation Theory in Air Traffic Control System Design", *Proc. of the IEEE*, Vol. 58, No. 3, pp. 369-376, March, 1970.

- [Ku96] Kuchar, J.K., "Methodology for Alerting-System Performance Evaluation", *Journal of Guidance, Control, and Dynamics*, Vol. 19, No. 2, pp. 438-444, March-April, 1996.
- [LS80] Lee, D.T., and Schacter, B.J., "Two Algorithms for Constructing a Delaunay Triangulation", *International Journal of Computer and Information Sciences*, Vol. 9, No. 3, pp. 219-242, June, 1990.
- [Ma93] Mahlich, S.E., "Interactive Analysis and Planning Tools for Air Traffic and Airspace Management", *AGARD Conf. Proc. 538, Machine Intelligence in Air Traffic Management*, Berlin, Germany, May, 1993.
- [MCW95] May, P. A., Campbell, M., and Wickens, C.D., "Perspective Displays for Air Traffic Control: Display of Terrain and Weather", *Air Traffic Control Quarterly Journal*, Vol. 3, No. 1, pp. 1-17, 1995.
- [Mer73] Merz, A.W., "Optimal Aircraft Collision Avoidance," *Joint Automatic Control Conf.*, Columbus, OH, pp. 449-454, June, 1973.
- [Mi86] Mitchell, J.S.B., *Planning Shortest Paths*, Ph.D. Dissertation, Stanford University, Dept. of Operations Research, Aug., 1986.
- [Mo58] Morrel, J.S., "The Mathematics of Collision Avoidance in the Air", *Journal of Navigation*, Vol. 11, No. 1, pp. 13-28, Jan., 1958.
- [Ni89] Niedringhaus, W.P., "A Mathematical Formulation for Planning Automated Aircraft Separations for AERA 3", MITRE Tech. Report PB89-233902, Dept. of Transportation Tech. Report DOT/FAA/DS-89/20, Advanced System Design Service, FAA, Washington, DC, 20591, April, 1989.
- [No94] Nolan, M.S., *Fundamentals of Air Traffic Control*, Wadsworth Pub. Comp., Belmont, CA, 1994.
- [OBS92] Okabe, A., Boots, B., and Sugirara, K., *Spatial Tessellations: Concepts and Applications of Voronoi Diagrams*, John Wiley and Sons, New York, 1992.
- [PM89] Pozesky, M.T. and Mann, M.K., "The US Air Traffic Control System Architecture," *Proc. IEEE*, Vol. 77, No. 11, pp. 1605-1617, Nov., 1989.
- [PG93] Pruyn, P.W., and Greenberg, D.P., "Exploring 3D Computer Graphics in Cockpit Avionics", *IEEE Computer Graphics and Applications*, pp. 28-35, May, 1993.
- [PS85] Preparata, F.P. and Shamos, M.I., *Computational Geometry*, Springer Verlag, New York, NY, 1985.
- [RTCA94] RTCA, Final Report of RTCA Task Force 3, *Free Flight Implementation*, Nov., 1994.
- [Ra92] Raymer, D.P., *Aircraft Design: A Conceptual Approach*, American Inst. of Aeronautics and Astronautics, Washington, DC, 1992.

- [SW95] Sacher, B.H. and Winokur, D.J., Operational Concept for the User Request Evaluation Tool (URET), MITRE Tech. Report, May, 1995.
- [SEL82] Smith, J.D., Ellis, S.R., and Lee, E., *Avoidance Manuevers Selected while Viewing Cockpit Traffic Displays*, NASA Ames Research Center Tech Report TM-84269, Oct., 1982.
- [SM73] Sorensen, J.A., Merz, A.W., Cline, T.B., Karmarkar, J.S., Heine, W., and Ciletti, M.D., *Horizontal Collision Avoidance Systems Study*, Final Report, FAA-RD-73-203, Systems Control, Inc., Palo Alto, CA, Dec., 1973.
- [Ste93] Stengel, R.F., "Toward Intelligent Flight Control", *IEEE Trans. on Systems, Man, and Cybernetics*, Vol. 23, No. 6, pp. 1699-1717, Nov./Dec., 1993.
- [SuI92] Sugihara, K. and Iri, M., "Construction of the Voronoi Diagram for "One Million" Generators in Single-Precision Arithmetic", *Proc. of the IEEE*, Vol. 80, No. 9, pp. 1471-1484, Sept., 1992.
- [WaS94] Wangermann, J.P. and Stengel, R.F., "Principled Negotiation Between Intelligent Agents: A Model for Air Traffic Management", *19th ICAS Congress*, Anaheim, CA, Sept., 1994.
- [WaS95] Wangermann, J.P. and Stengel, R.F., *Technology Assessment and Baseline Concepts for Intelligent Aircraft/Airspace Systems*, Tech. Report No. MAE-2016, Princeton Univ., Dept. of Mechanical and Aerospace Engr., Princeton, NJ, Feb., 1995.
- [WaS96] Wangermann, J.P. and Stengel, R.F., "Optimization and Coordination of Multi-Agent Systems Using Principled Negotiation", *AIAA Guidance, Navigation, and Control Conf.*, San Diego, CA, July, 1996.
- [WTS89] Wickens, C.D., Todd, S., and Seidler, K., *Three-Dimensional Displays: Perception, Implementation, and Applications*, Tech. Report ARL-89-11, Univ. of Illinois at Urbana-Champaign Aviation Research Lab., 1989.
- [WiS89] Williamson, T. and Spencer, N.A., "Development and Operation of the Traffic Alert and Collision System (TCAS)", *Proc. of the IEEE*, Vol. 77, No. 11, pp. 1735-1744, Nov., 1989.
- [YaK97] Yang, L.C. and Kuchar, J.K., "Prototype Conflict Alerting System for Free Flight", to appear, 35th Aerospace Sciences Meeting, Reno, NV, Jan., 1997.